Melt Processable Poly(acrylonitrile)-based Precursors for Carbon Fiber Production and Advanced Polymeric Membranes for Gas Separation and Water Electrolysis Applications

Gregory C. Miller, Jr.

Dissertation submitted to the Faculty of the Virginia Polytechnic Institute and State University in partial fulfillment of the requirements for the degree of

Doctor of Philosophy

in

Macromolecular Science and Engineering

Judy S. Riffle, Chair

Robert Moore

S. Richard Turner

Richey M. Davis

Sue Mecham

May 1, 2017

Blacksburg, Virginia

Keywords: Carbon Fiber, Melt-processing, Polyacrylonitrile, Gas separation, Water Electrolysis

Abstract

An effort concerned with the feasibility of achieving melt-processable polyacrylonitrile copolymer system precursors for producing high modulus carbon fibers is detailed. High molecular weight poly(acrylonitrile-ran-methyl acrylate) (PAN-MA) copolymer with high acrylonitrile content were mixed with various water containing binary melting point modifiers to produce systems that formed stable melts at temperatures below the temperature corresponding to the onset of PAN-MA crosslinking. The structure of the copolymer was found to be 96.5 ± 0.13 mole % acrylonitrile and 4.40 ± 0.13 mole % methyl acrylate by ^{1}H-NMR with an M_w = 238 kDa and dispersity of 1.9 determined by size exclusion chromatography. A reduction in the T_m of the copolymer of 200°C was established for a copolymer/melting point modifier system containing copolymer mixed with water and acetonitrile with the following composition: PAN-MA/ACN/H_2O 55/25/20 wt:wt:wt. This corresponds to the greatest reduction in a PAN-based copolymer melting temperature yet reported. From isothermal DSC and pressurized capillary rheometry experiments it was found that the stability of the resulting melts shows a strong temperature dependence, but does not show a strong dependence on shear rate. Copolymer mixtures with H_2O and acetonitrile or H_2O and adiponitrile were found to be suitable for melt-extrusion at 170°C with viscosities ranging from 1800-2000 Pa*s with stabilities ≥ 1 hour.

The modification of membranes to improve gas separation properties is of considerable interest. Crosslinking is one route to modify membranes, but the

resulting effects on thin membranes have yet to be investigated to understand the impact of such modification at thicknesses that are relevant to industrial membranes. In this study, the influences of UV irradiation and physical aging on O_2 and N_2 gas permeation properties of thin (~ 150 nm) glassy poly(arylene ether ketone) (PAEK) films at 35°C and 2 atm were investigated. Thin PAEK films prepared from tetramethyl bisphenol A and 4,4'-difluorobenzophenone were UV irradiated on both sides in air or N_2 at wavelengths of 254 nm or 365 nm. This induced crosslinking and, in some cases, photooxidation. Gas permeability decreased and O_2/N_2 selectivity increased as UV irradiation and aging time were increased. At 254 nm, samples irradiated in air had lower permeability coefficients and higher selectivities than samples irradiated in N_2, and this was ascribed to additional decreases in free volume due to photooxidation in air-irradiated samples. Additionally, air-irradiated samples at 254 nm exhibited less physical aging than non-crosslinked and N_2-irradiated samples at 254 nm, possibly due to interactions among photooxidative polar products that may restrict polymer chain mobility, thereby lowering the aging rate. The influence of water vapor on physical aging of air-irradiated samples was examined. Finally, irradiation at 254 nm leads to more extensive crosslinking and/or photooxidation than irradiation at 365 nm, possibly due to greater UV absorption by the polymer and the higher probability of radical formation at the lower wavelength.

Poly(2,6-dimethyl-1,4-phenylene oxide) (PPO) is utilized for gas separation membranes. It has a relatively high free volume with high gas permeabilities but

suffers from low selectivities. PPO polymers with M_n's from 2000-22,000 g/mole were synthesized and blended with a poly(arylene ether ketone) derived from bisphenol A and difluorobenzophenone (BPA-PAEK). DSC showed that the blends with all but the lowest molecular weight PPO had two T_gs, thus suggesting that two phases were present. The ketone carbon and benzylic methyl groups on the BPA-PAEK and the PPO polymers crosslinked upon exposure to UV light. The gel fractions after UV exposure were high and the tensile properties were similar to the PPO control polymer that is currently used as a gas separation membrane. The crosslinked blends had improved gas selectivities over their linear counterparts. The 90/10 wt/wt 22k PPO/BPA PAEK crosslinked blends gained the most O_2/N_2 selectivity and maintained a high permeability.

Two series of high molecular weight disulfonated poly(arylene ether sulfone) random copolymers were synthesized as proton exchange membranes for high temperature water electrolyzers. These copolymers differed based on the position of the ether bonds on the aromatic rings. One series was comprised of fully *para*-substituted hydroquinone comonomer and the other series incorporated 25 mole % of a *meta*-substituted comonomer, resorcinol, and 75 mole % hydroquinone. The influence of the substitution position on water uptake and electrochemical properties of the membranes were investigated and compared to the state-of-the-art membrane, Nafion™. Mechanical properties of the membranes were measured for the first time in fully hydrated conditions at room and elevated temperatures. While submerged in water, these hydrocarbon-based copolymers had moduli an order of magnitude higher than Nafion™

membrane. Selected copolymers of each series showed dramatically increased proton conductivity at elevated temperature and fully hydrated conditions while their H_2 gas permeabilities were well controlled over a wide range of temperatures. These improved properties were attributed to the high glass transition temperature of poly(arylene ether sulfone)s.

General Audience Abstract

In this work, the author is attempting to create precursor material for carbon fiber that is melt-processable. Currently, carbon fibers are produced from precursor fibers which were spun from organic solvent solutions. This method is more expensive and less environmentally friendly than producing the precursor fibers from the melt. The precursor polymer has a tendency to crosslink and degrade at temperatures that are less than its melting point, thus preventing is from being melt-processed. By creating formulations with the precursor polymer and various modifiers, the author was able to produce materials that could be melted without significant degradation and could therefore potentially be used to melt-process carbon fiber precursor fibers.

Acknowledgements

This is written and dedicated in loving memory of my parents, Paula Jane Wheeler Miller who provided me with an insatiable thirst for knowledge and Gregory Charles Miller, Sr. who provided me with the foundation from which I could become the person that I am now. You believed in my when no one else did. Just look at me now, Paula Jane.

Next I must acknowledge my committee, Dr. Moore, Dr. Turner, Dr. Davis, Dr. Mecham, and especially my committee chair, Dr. Judy Riffle who has effortlessly guided me through this perilous journey of graduate school. I want to thank all of them for their guidance and their generous exchange of knowledge and expertise as well as their non-wavering support over the years that I have known them. I would also like to thank Dr. Jack Lesko for agreeing to sit as a substitute on my committee on very short notice. My mentor, Dr. Riffle must be particularly thanked for providing me with the opportunities which allowed me to amplify my abilities and deepen my experience. Her many efforts are very much appreciated and I am truly blessed to have her as an advisor. I must also acknowledge the late Dr. James E. McGrath. I was honored to have known such a great man and brilliant scientist and I feel very fortunate to have been able to learn from such a giant in the field of polymer science.

I would like to thank Dr. Felix Paulauskas and Robert Norris at Oak Ridge National Laboratory who illuminated the path by which much of my research was to travel.

The financial support of the National Science Foundation, the Department of Energy, and Oak Ridge National Laboratory for research as well as the stipend support from the

Macromolecules Innovation Institute and the Macromolecular Science and Engineering Program.

I would like to thank all of my labmates, colleagues and collaborators who have helped me throughout these years. I cannot name them all, but I will attempt to recognize those who were most integral to this research. For characterization assistance I would like to thank Geno Iannoccone and Ken Knot (NMR), Dr. Sue Mecham and Shreya Roy Choudhury (SEC), Dr. Don Baird, Dr. Michael Bortner, and Jianger Yu (Rheometry), Dr. Sharavanan Balasubramaniam (Multi-inlet Vortex Mixer), and Dr. Bruce Orler and Dr. Andrew Shaver (DSC, TGA). I would like to thank my all of my labmates, but I would like to particularly acknowledge Dr. Andrew Shaver, Gurtej Narang Singh, Amin Daryaei, Ran Lui, Matt Joseph, Donald Savacool, Ami Jo, Britannia Vondrasek, and Dr. Jarrett Rowlett for their friendship, research suggestions, and help throughout the years.

My family deserves a great deal of recognition including my brother, Samuel Miller, my step-mother Cheryl Miller, my cousins Jeremy Wheeler, Casie Wheeler, and Robert Miller, my future mother-in-law Tami Mathis, and many others too numerous to name for their love and support. I must also acknowledge the support system of my aunt/uncles Joe/Sharon Miller, Steve/Verena Miller, Mike/Susan Wheeler and especially Don/June Wheeler. Thank you for always being there when I need you Aunt June, you know you are like a second mother to me.

Last but not least, I would like to thank my fiancé, Chelsey Leigh Mathis for sticking with me through the highs and lows all of these years with steadfast love and dedication. I look forward to a lifetime with you, and it has only just begun.

Authors contribution to each chapter:

Chapter 2: Melt-spinnable Polyacrylonitrile Copolymer Precursors for Carbon Fibers

The author is the primary researcher on this topic.

2.2.2 Blending of PAN copolymers and modifiers

The author blended each copolymer/modifier mixture that was used in this chapter.

2.2.3 Structural characterization

The author performed the ^{1}H-NMR used to characterize the copolymer composition in this chapter.

2.2.4 Differential scanning calorimetry (DSC)

The author performed all DSC experiments.

2.2.5 Preparation of polymer/modifier pellets for rheology measurements

The author prepared all of the samples used for rheometry in this chapter.

2.2.6 Pressurized capillary rheometry

The author performed all the rheometry represented in this chapter.

Chapter 3: Effect of UV Irradiation and Physical Aging on O_2 and N_2 Gas Transport Properties of Thin Glassy Polyarylene Ether Films Based on Tetramethyl Bisphenol A and 4,4'-Difluorobenzophenone

3.2.1 TMBPA-BP Synthesis

The author synthesized the monomers and copolymers used in this chapter including the tetramethyl bisphenol-A monomer.

Chapter 4: Poly(2,6-dimethyl-1,4-phenylene oxide) Blends with a Poly(arylene ether ketone) for Gas Separation Membranes

4.2.2 Synthesis of BPA-PAEK

The author synthesized the copolymer used in this chapter.

4.2.6. Film-casting

The author cast selected films used in this chapter, and assisted development of the film-casting procedure.

Chapter 5: Synthesis and Membrane Properties of Sulfonated Poly(arylene ether sulfone) Statistical Copolymers for Electrolysis of Water: Influence of meta and para-Substituted Comonomers

5.2.9 Differential Scanning Calorimetry (DSC)

The author performed the DSC in both the dry and hydrated states that was used in this chapter.

Table of Contents

Table of Figures

Table of Tables

Chapter 1: Introduction

1.1 Polyacrylonitrile

Polyacrylonitrile (PAN) is a homopolymer of 2-propenenitrile repeating units. It is produced commercially as a copolymer with various comonomers including styrene, butadiene, methyl acrylate and vinyl acetate. Polyacrylonitrile is produced for many different applications including carbon fiber precursors and acrylic textiles.

1.2 Acrylonitrile Synthesis

Acrylonitrile is mainly used for the production of polyacrylonitrile for acrylic fiber production, but it is also used for the synthesis of acrylamide, adiponitrile and in high performance plastic resins like ABS (acrylonitrile-butadiene-styrene) and SAN (styrene-acrylonitrile). Acrylonitrile is commercially synthesized via a route developed by Shio known as propylene ammoxidation, in which propylene and ammonia are reacted in stoichiometric amounts in an oxygen-rich environment (Figure 1.1).[1] Acrylonitrile can also be synthesized from propylene or acetylene with nitric oxide in lieu of air.[2]

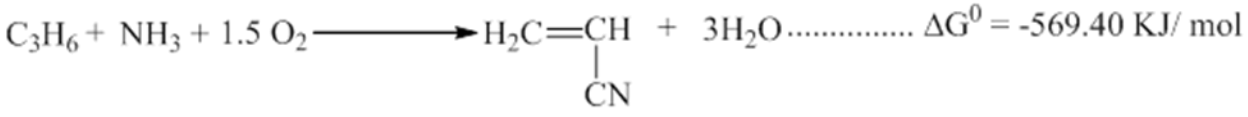

Figure 1.1. Propylene ammoxidation route to synthesize acrylonitrile.

1.3 Polyacrylonitrile chain morphology

Polyacrylonitrile (PAN) has highly polar pendant nitrile groups along its backbone. The highly polar nature of nitrile groups as well as their close proximity in space along a PAN chain, lead to large intramolecular dipolar and steric repulsions. If these repulsive forces were not present, the chain would most likely form a zigzag configuration, but the repulsion along the chain forces a "violent" kinking and twisting of the molecule. Even for a stereoregular polymer the distortion takes on a random nature, as the twisting is sometimes clockwise and other times counterclockwise. Primary valence bonds along the chain serve to restrain the strong repulsive forces, and a stiff, internally braced structure results. Therefore, PAN adopts a symmetrical rod-like structure with a diameter ~6 Å. The randomly kinked molecule has no regular longitudinal repeat distance, which is why it has no off-equatorial x-ray diffraction. The rigid rods pack laterally into a hexagonal pattern, which is the origin of its 5.2 Å equatorial diffraction. There is a contraction along the chain axis relative to the normal length of an extended zigzag chain that is due to the kinking effect. This leads to a higher density (ρ=1.17-1.22) than would be estimated for a polymer with hexagonal lateral packing and 2.54 Å longitudinal repeat distance (ρ=1.13).[3-6]

Polyacrylonitrile is highly crystalline, up to 42%, and has a relatively high crystalline melting point of at least 317°C.[5, 7] PAN tends to degrade via cyclization and crosslinking reactions at a temperature range of 200-300°C, prior to reaching the melting temperature.[8-12] Polyacrylonitrile is insoluble in most

common solvents including water, acetonitrile, and even its own monomer, acrylonitrile. PAN can be dissolved in polar aprotic solvents such as DMSO, DMF, and DMAc and in some inorganic salt solutions such as aqueous zinc chloride solution and sodium thiocyanate solution.[13]

1.4 Polyacrylonitrile copolymers

Polyacrylonitrile is generally copolymerized with comonomers which act as internal plasticizers by increasing the distance between pendant nitrile groups, therefore disrupting the polar repulsion.[14-19] Comonomers can improve the solubility of PAN in solvents and lower the melting point, which help enable the melt-processing of the resulting polymer.[13] Comonomers also have the effect of enhancing the segmental mobility of the polymer chains which can result in better orientation during carbon fiber stabilization processes.[20]

Many applications exist for acrylonitrile based copolymers which range from lower end applications such as acrylic textile fibers, poly(styrene-co-acrylonitrile) plastics, poly(acrylonitrile-butadiene-styrene) rubber to higher end applications such as water and gas separation membranes and carbon fiber precursors.[21] Acrylonitrile based copolymers have attractive and tunable properties such as rigidity, chemical resistance, and gas barrier properties that lend to their versatility in applicable end uses.

As a film, polyacrylonitrile provides excellent barrier properties towards oxygen and carbon dioxide, presumably due to the high crystallinity provided by packing of the chains due to favorable interchain nitrile dipole-dipole

interactions. The high polarity of the polymer also gives the films high water vapor uptake. Copolymers of acrylonitrile and vinylidene chloride are used to make high barrier films, and laminates are used in food containers to provide barrier resistance to oxygen.[22] Acrylonitrile copolymers with 2-dimethylaminoethyl methacrylate are being explored for potential biomedical applications such as ultrafiltration dialysis membranes and adsorbent coatings.[23]

1.5 Polyacrylonitrile copolymer synthesis

PAN-based copolymers are synthesized via free radical routes, generally through solution, bulk, emulsion, or suspension polymerizations.[24] The polymerization of acrylonitrile differs characteristically from other vinyl polymerizations. The monomer is soluble in most organic solvents and water. However, the polymer is insoluble in most common organic solvents, in water, and in its monomer. The polymerizations often become heterogeneous, even at fairly low conversions and monomer concentrations, and the borders between emulsion and suspension polymerization are not sharp.[19] When these heterogeneous polymerization techniques are employed, the kinetics quickly show autoacceleration behavior if an insufficient amount of surfactant is utilized. Among the PAN synthesis literature, there is not a clear consensus in the use of the terms *solution polymerization, dispersion polymerization, and precipitation polymerization,* particularly in aqueous systems.[19] Because the monomer is water soluble and the polymer is water insoluble, some of the differences among solution, suspension, and emulsion polymerization of PAN are not easily

distinguishable. The kinetics differ strongly from those that are expected for normal suspension and emulsion polymerizations.[19]

1.6 Polyacrylonitrile based fibers

The initial commercial development and marketing of polyacrylonitrile was under the tradename Orlon beginning in 1941 by DuPont. Fibers of polyacrylonitrile were first reported in 1938. Commercial production of acrylic fibers did not begin until 1955, and the delay in large scale fiber production is attributed to the lack of suitable solvents for wet/dry spinning. The commercial viability of acrylic fibers really became apparent with the copolymerization of acrylonitrile with vinyl acetate and methyl acrylate, with the fibers being solution spun from *N,N*-dimethylformamide (DMF).[25]

Fibers based on polyacrylonitrile copolymers fall into two categories: acrylic and modacrylic fibers where acrylic fibers are defined as containing ≥ 85 wt% acrylonitrile and modacrylic fibers contain between 35 and 85 wt% acrylonitrile. For PAN-based high performance carbon fibers, acrylic fibers are necessary. Acrylic fibers are the major application of polyacrylonitrile, and the main comonomers used in commercial acrylic fibers are listed in Table 1-1.[26]

Table 1-1. TYPICAL COMONOMERS FOUND IN COMMERCIAL ACRYLIC FIBERS.

Neutral Comonomer	Ionic or Acid Comonomer
Methyl Acrylate	Sodium styrene sulfonate
Vinyl acetate	Sodium methallyl sulfonate
Methyl methacrylate	Sodium 2-methyl-2-acryamidopropane
Acrylamide	Itaconic acid

Modacrylic fibers often contain comonomers such that the resulting fiber has flame retardant or acid-dyeable characteristics. Flame retardant modacrylic fibers generally contain an unsaturated halogen compound like vinyl chloride, vinylidene chloride, or vinyl bromide. These fibers are produced commercially via a wet-spinning process.[26]

The final end-use properties that can be obtained from acrylic fibers depend on a number of parameters, but molecular weight is one of the most important parameters. Textile grade acrylic fibers require polymers with molecular weights in the range of 90,000-170,000 g/mol.[25] The molecular weight and molecular weight distribution are affected by many variables such as initiator type and concentration, comonomer type and concentration, surfactant type and concentration, polymerization temperature and time.[25] Initiating systems such as potassium persulfate combined with sodium metabisulfite are inexpensive, and when used in low concentrations allow for ideal placement of some comonomers such as sulfates or sulfonates which are used for dyeability.[27]

1.7 Carbon Fibers

Carbon is known to have a number of different distinct molecular or crystalline forms, known as allotropes, and these allotropes have distinct properties arising from their unique structure. Some examples of carbon allotropes include diamond, graphite, graphene, and fullerenes. Other forms of carbon include pyrolytic graphite, glass-like carbon, graphite whiskers, vapor-grown carbon fibers, catalytic chemical vapor-deposited filaments, carbon black,

charcoal, coal, coke, soot, carbon nanotubes, and carbon fibers.[24, 28-32] Graphite is a layered structure in which hexagonally arranged carbon atoms are bonded in a planar condensed ring system with bond lengths of 0.1415 nm. The sp^2 hybridized atoms of graphite can participate in coplanar and interplanar bonding, and the layers of graphite are weakly bonded through van der Waal's interactions.[24]

The first documented use of carbon fibers was in the carbonization of cotton and bamboo fibers which were used for filaments in incandescent lamps.[24] Thomas Edison used carbon fiber filaments in his incandescent light bulb experiments as early as 1879, and the use of carbon fibers as filament materials for electric lamps was patented by Edison.[33] Although incandescent bulb filaments were upgraded to tungsten, Edison's use of carbon fibers introduced the scientific community to these magnificent materials and paved the way for carbon fibers' use in fields ranging from transportation (including automotive and aerospace), building construction, marine, electrical and thermal insulation, and other industrial products.[24]

The practical use of carbon fibers as reinforcement materials began in the 1960s. Union Carbide began exploring the use of rayon and polyacrylonitrile for precursors to carbon fibers and developed high-strength (rayon) and high-modulus (PAN) carbon fibers in 1959 and 1962, respectively. Many other carbon fiber precursor materials have been explored since Union Carbide's initial investigations including pitch, polyesters, polyamides, polyvinyl alcohol, polyvinylidene chloride, poly-p-phenylene, and phenolic resins.[34]

Carbon fibers are classified based on the fiber structure and degree of crystallite orientation as ultrahigh-modulus (UHM), high-modulus (HM), intermediate modulus (IM), high-tensile-strength (HT), and isotropic carbon fibers, which are summarized in Table 1-2.[24] The UHM and HM carbon fibers are highly graphitized and are known to have high moduli, where UHM moduli are greater than 500 GPa, and HM moduli are greater than 300 GPa, and both have a strength-to-modulus ratio of less than 1%. The IM and HT carbon fibers have high strength and low modulus because they have undergone lower temperature heat treatments. The IM carbon fiber moduli are up to 300 GPa and their strength-to-modulus ratio is greater than 1×10^{-2}. The HT carbon fibers have moduli greater than 3 GPa and have a strength-to-modulus ratio lying between $1.5\text{-}2 \times 10^{-2}$.[24]

Table 1-2. CLASSIFICATION OF CARBON FIBERS.

Carbon Fiber Type	Heat Treatment temp. (°C)	Crystallite orientation	Long-range order	Abbreviation
Type I high modulus	>2,000	Mainly parallel to the fiber axis	High	UHM HM
Type II high strength	~1,500	Mainly parallel to the fiber axis	Low	IM HT
Type III isotropic	<1,000	Random	Very Low	Isotropic

Carbon fibers may be short or continuous, and the structure may be crystalline, amorphous, or semi-crystalline. The atomic structure of carbon fibers is similar to graphite with a distance between layer planes of 3.35 Å and layers arranged in regular hexagonal patterns. The structure of the crystalline microdomains consists of sp^2 hybridized carbon atoms arranged two-dimensionally in a honeycomb structure, as is pictured in Figure 1.2. The

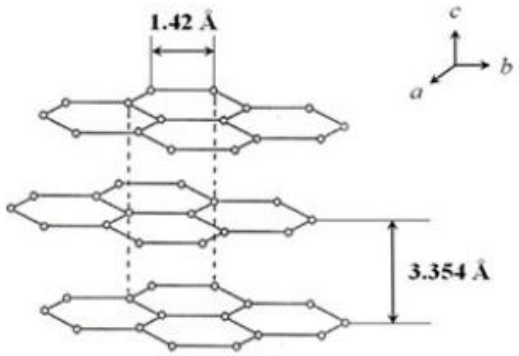

Figure 1.2. Structure of the crystalline microdomains of carbon fibers. (Figure used with permission from Springer).

graphite layer consists of carbon atoms which are bonded both covalently from the overlap of the sp^2 hybridized orbitals and through metallic bonds arising from delocalization of π electrons. The excellent electrical and thermal conductivity of graphite are credited to the delocalization in the *x-y* plane.[24] However, the primary structural unit of most carbon fibers is a stack of turbostratic layers. In this structure, the distance between parallel graphene sheets is greater than in graphite. These turbostratic layers can be irregularly split, tilted, twisted, folded, and conjoined to form microdomains. The structure

of the turbostratic layers is shown in Figure 1.3. The structure of carbon fibers is

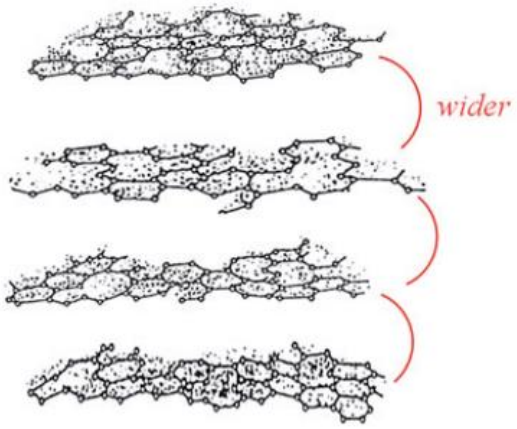

Figure 1.3. Structure of turbostratic carbon. (Figure used with permission from Springer).

not homogeneous, and involves a combination of crystalline, graphitic, and turbostratic domains. An illustration of what the combination of these structural units may look like is shown in Figure 1.4.[24, 35]

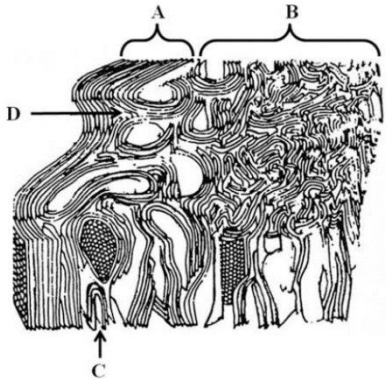

Figure 1.4. Combination of structural microdomains of carbon fiber: *A* skin region; *B* core region; *C* a hairpin defect; and *D* a wedge disclination. (Figure used with permission from Springer).

1.8 Carbon Fiber Production

Carbon fibers are produced from precursor fibers by a combination of heating and stretching treatments which vary depending on the precursor material. Generally, carbon fibers are produced by subjecting a stabilized fiber of the precursor material to controlled pyrolysis in a multi-step process. In the first step, the precursor fibers are stabilized and stretched in the temperature range of 200-400°C. Next, in the carbonization process, non-carbon elements are removed by subjecting the stabilized fiber to temperatures ranging from 800-1,600°C, in an oxygen free environment. The final step, known as graphitization, involves heating the fibers up to 3000°C while stretching at 50-100% elongation in an argon environment. The graphitization step ensures the preferred crystalline orientation, and results in fibers with higher moduli than carbonized fibers. A structural model of carbon fibers during the graphitization process in shown in Figure 1.5. Finally, the resulting carbon fibers are subjected to surface treatments which help to enhance their adhesion to composite matrices.[36-41]

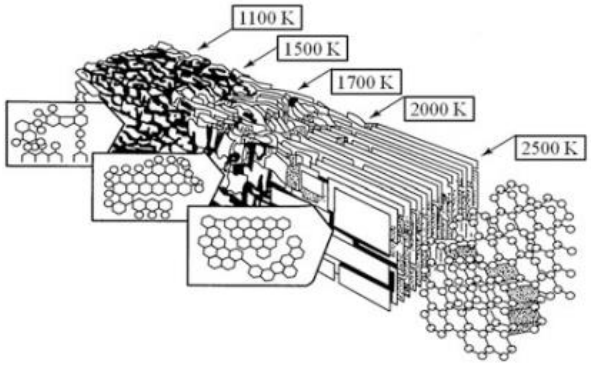

Figure 1.5. Structural model of carbon fibers during graphitization. (Figure used with permission from Springer).

1.9 PAN-based Carbon Fiber

PAN-based polymers are the optimum precursors for carbon fiber production because of the carbon yield, as well as the tensile and compressive properties. The PAN fibers are produced using a solution spinning technique like wet spinning, then subjected to stabilization which produces a flameproof fiber that is stable at high temperatures and can therefore be further transformed through carbonization and graphitization. The typical scheme for the preparation of PAN precursor-based carbon is shown in Figure 1.6.[24] The

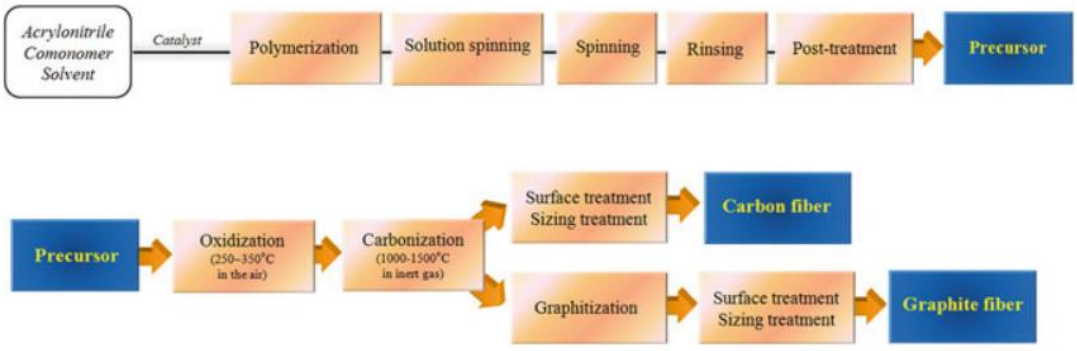

Figure 1.6. Schematic of the process to produce PAN-based carbon fibers. (Figure used with permission from Springer).

thermal stabilization step of PAN-based precursors can require several hours, depending on the temperature and precursor diameter. Conditions such as heating rate, time, and temperature are optimized for each precursor. The stretching of PAN fibers during the stabilization step of carbon fiber production is in a direction parallel to the fiber axis, and a transformation from a linear molecule into a ladder polymer is observed. The mechanism of the cyclization process is a matter of some controversy within the literature, but the most widely accepted reaction mechanism is shown in Figure 1.7.[11, 42] The carbonization and graphitization steps to produce PAN-based carbon fibers are carried out in nitrogen or argon rich inert atmospheres. Argon can be up to eight times more expensive than nitrogen, but is used because the resulting carbon fiber has improved mechanical strength because of the higher density

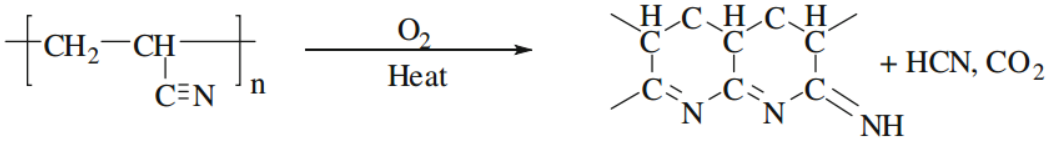

Figure 1.7. Mechanism for the cyclization of PAN to form a ladder structure during thermal stabilization in carbon fiber production.

and viscosity of the gas.[43] The temperature used for carbonization is determined based on the type of application for the carbon fiber. For high strength applications, a temperature of 1,500-1,600°C is preferred as a decrease in tensile strength is observed for fibers produced at temperatures greater than 1,600°C.[42] In contrast, for high modulus applications, an additional graphitization heat treatment is required with temperatures up to 3,000°C. Nitrogen reacts with

carbon to form cyanogen at temperatures above 2,000°C, and therefore graphitization is generally conducted in an Argon rich environment.[24] The scheme for the graphite structure production is shown in Figure 1.8.

PAN-based polymer precursors for carbon fibers fall into two general categories: pure homopolymer and copolymers, and copolymers are widely preferred in commercial production. Homopolymer PAN is too difficult to process due to sudden and rapid heat evolution during the initial stabilization step which makes the process hard to control.[24] Comonomers

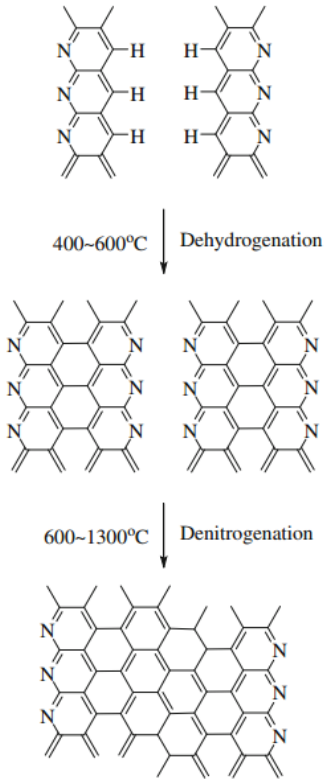

Figure 1.8. Scheme of the graphite structure development during carbon fiber production from PAN-based precursor materials. (Figure used with permission from Springer).

enhance the segmental mobility of the polymer chain which can result in better orientation and mobility during the stabilization step which ultimately provides

better mechanical properties for the carbon fiber. Some comonomers that have been used with AN for carbon fiber precursor material include vinyl acetate (VAc), methyl acrylate (MA), and methyl methacrylate (MMA), but PAN-VAc may not be appropriate as a carbon fiber precursor.[44-47] Comonomers can function as internal plasticizers, spacing out nitrile groups along the polymer chain, and making the polymer more readily soluble in spinning solvents.[45] A nearly exhaustive list of comonomers that have been used for PAN-based carbon fiber precursor materials is shown in Table 1-3.[24]

Table 1-3. Comonomers used in PAN-based carbon fiber precursors.[24]

Class	Comonomer	Structure
Acids	Acrylic acid	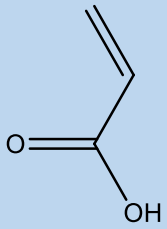
	Itaconic acid	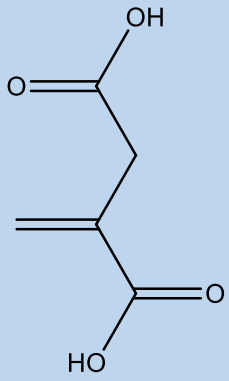
	Methacrylic acid	

		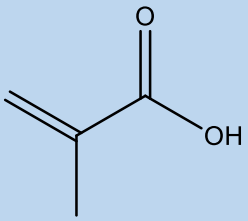
Acrylates/Acetates	Methyl acrylate	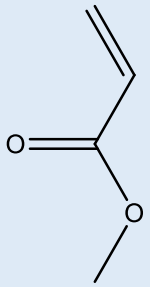
	Ethyl acrylate	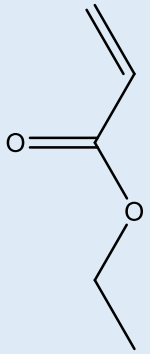
	Butyl acrylate	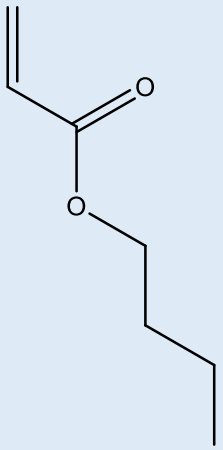
	Propyl methacrylate	

	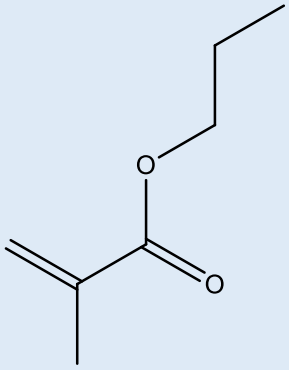
Butyl methacrylate	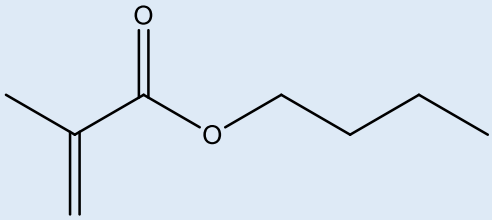
β-Hydroxyethyl methacrylate	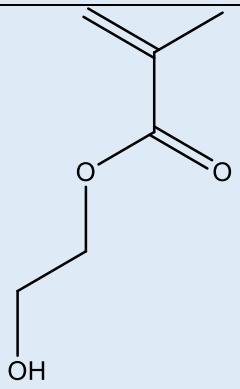
Dimethylaminoethyl methacrylate	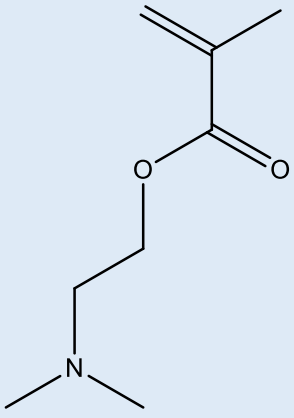

	2-Ethylhexylacrylate	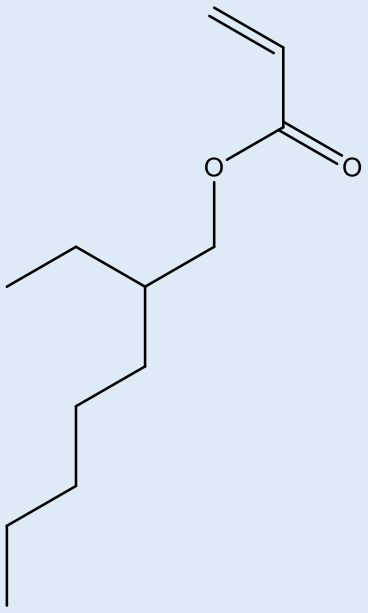
	Vinyl acetate	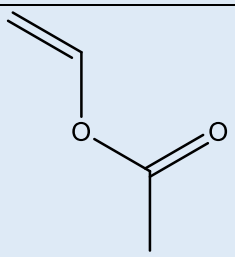
	Vinyl propionate	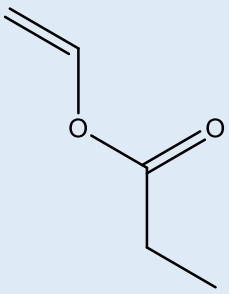
Acrylamides	Acrylamide	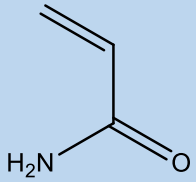

	Diacetone acrylamide	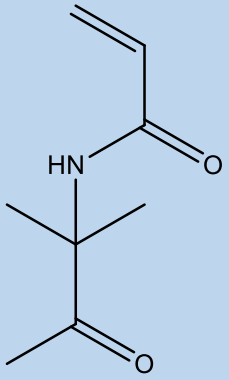
	N-methylolacrylamide	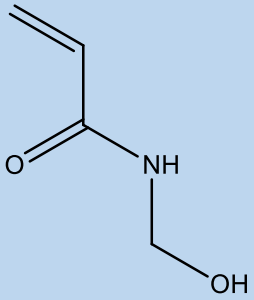
Vinyl halides	Allyl chloride	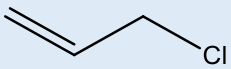
	Vinyl bromide	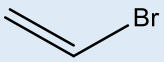
	Vinyl chloride	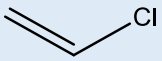
	Vinylidene chloride	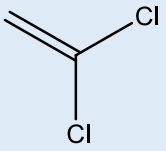
Sodium salts of sulfonic acids	Sodium vinyl sulfonate	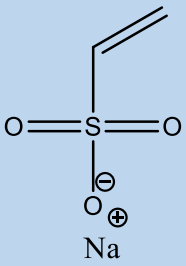

	Sodium p-styrene sulfonate	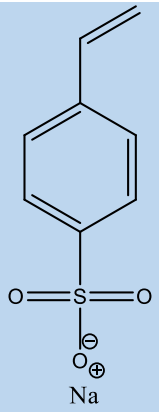
	Sodium methallyl sulfonate	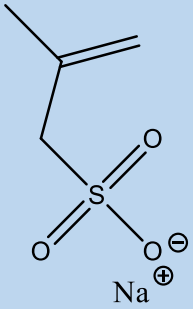
	Sodium-2-acrylamido-2-methyl propane sulfonate	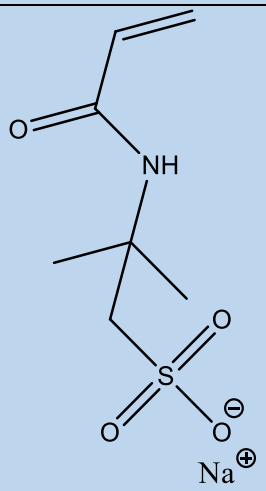
Others	Methacrylonitrile	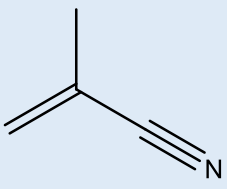

	2(1-Hydroxylalkyl) acrylonitrile or acrylic acid	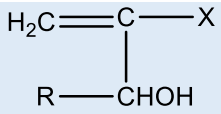 (where R = -CH_3 or -C_2H_5 and X= -CN or -COOH)
	Allyl alcohol	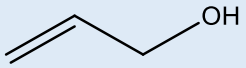
	Methallyl alcohol	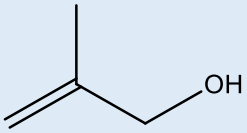
	1-Vinyl-2-pyrollidone	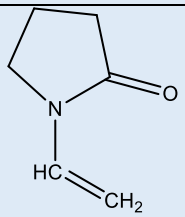
	4-Vinylpyridine	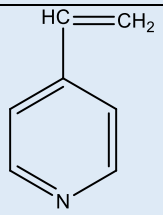
	2-Methylene glutaronitrile	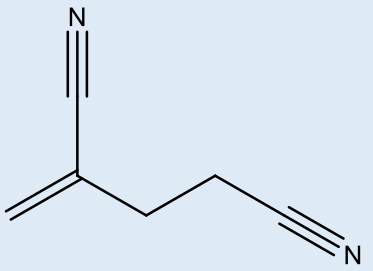

1.10 Pitch-based Carbon Fiber

Pitch is a complex blend of polyaromatic molecules and heterocyclic compounds, and can contain over 80% carbon. Pitch can be obtained from a number of sources including petroleum refining, called bitumen or asphalt,

destructive distillation of coal, natural asphalt, and from the pyrolysis of PVC. The exact composition of pitch can vary quite a bit depending on the source of the tar and processing conditions.[24, 48] Natural pitches, from petroleum and coal sources, are the most common pitches used in the production of carbon fibers, but synthetic pitches, from pyrolysis of synthetic polymers, are also used.[49] In general, pitch can be considered to be composed of the following chemical compounds:[50]

1. Low molecular weight saturated aliphatic compounds
2. Low molecular weight aromatics and saturated ring structures
3. Polar aromatics: Higher molecular weight and primarily heterocyclic aromatics
4. Asphaltenes: Higher molecular weight fractions containing the most aromaticity and these may be the most thermally stable

Asphaltene-rich pitch tends to be the most suitable for carbon fiber production. Table 1-4 lists many of the aromatic components commonly found in natural pitch.[24]

As a precursor to carbon fiber, pitch has the advantage of low material cost, high yield, and a higher degree of orientation relative to PAN.[51] Pitch-based carbon fibers can have higher elastic moduli and higher thermal and electrical conductivity along the fiber direction, but the processing cost to achieve high-performance carbon fibers is higher.[52] Pitch from coal tar or petroleum sources is isotropic, and can be spun into low-cost, low modulus,

and low strength carbon fibers after the low molecular weight fractions are evaporated. High performance pitch-based carbon fibers must be made from anisotropic mesophase pitch. Mesophase pitch is formed either by thermally polymerizing petroleum or coal-tar pitches, or by the catalytic polymerization of pure compounds such as naphthalene. An intermediate phase forms between 400-550°C, and this eventually becomes domains of highly parallel, plate-like molecules.[53, 54]

The production of carbon fibers from pitch-based precursors involves several stages, similar to production from PAN-based precursors. In the first step, precursor fibers are melt-spun by extrusion through a spinneret and then the fibers are drawn as they cool. An appropriate spinning temperature must be implemented, which varies depending on the composition of the pitch.[54] Next, the fibers must be stabilized in a manner that is analogous to the process used for PAN-based precursor fibers. This is generally done between 250-350°C in air, but the temperature must be below the softening point of the fiber in order to maintain the oriented structure. Finally, the stabilized fibers are carbonized and graphitized. Carbonization takes place at 1,500-1,800°C and graphitization is done at temperatures close to 3,000°C to enhance the modulus.[24]

Table 1-4. Aromatic hydrocarbons commonly found in natural pitch.

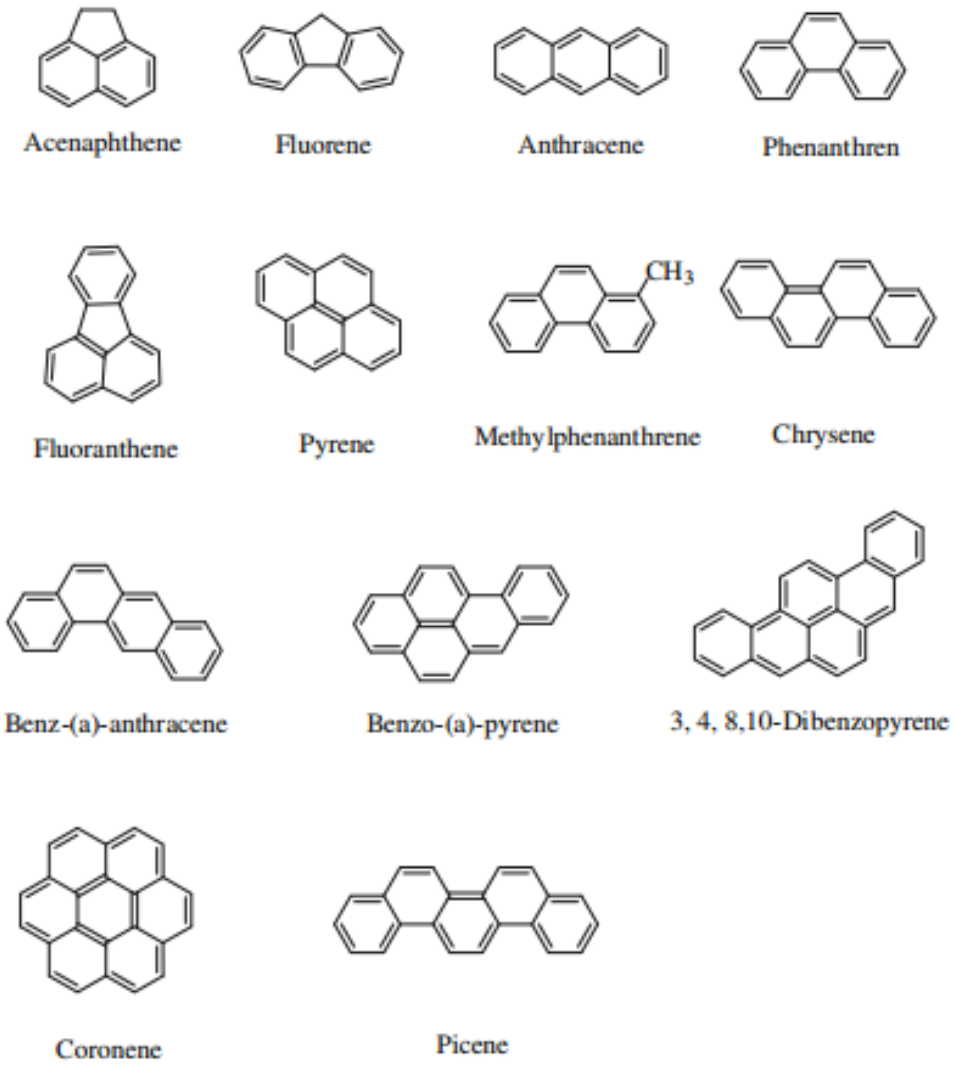

1.11 Melt Processable PAN

It is desirable to melt-process PAN-containing copolymers to produce carbon fiber precursors because of the lower costs as well as the higher quality of fibers produced. PAN begins to crosslink, cyclize, and degrade between 200-300°C, but does not melt until ~317°C.[10] An active area of research involves developing melt-processable PAN by lowering the temperature of melting by addition of either internal or external plasticizers.[18] A plasticizer is defined as a

polymeric additive which has the effect of lowering the glass transition temperature, T_g, by increasing the free-volume of the polymer, generally within the amorphous regimes.[12] In general, when a plasticizing agent is introduced to a semicrystalline polymeric system, it will lower the T_g of the polymer, and subsequent heating results in a lower melting temperature relative to the pure polymer.[55] The following equation describes this behavior,

$$\frac{1}{T_m} - \frac{1}{T_m^0} = \frac{R}{\Delta H_f} x'((1-\phi_2) - \chi_c)(1-\phi_2)^2) \qquad (1.1)$$

where T_m and T_m^0 are the experimental and equilibrium melting temperatures, respectively; ΔH_f = heat of fusion/ mole of repeat unit; x' = ratio of partial molar volumes of the polymer repeating unit to the diluent; ϕ_2 = the volume fraction of polymer in the mixture; χ_c = the Flory-Huggins interaction parameter; and R is the universal gas constant. This can be physically described by the increase in entropy due to the presence of the plasticizing agent.[55]

1.11.1 Internal Plasticization of PAN to Depress the Melting Temperature

Internal plasticization of PAN is primarily realized by incorporation of a second or third comonomer during polymerization which acts to disrupt long range order along the chain.[56] McGrath *et al.* reported a melt-processable PAN-MA copolymer, but found that no polymer flow could be achieved until at least 10% comonomer was incorporated.[14, 15] Ogale *et al.*[57] have reported a melt-processable carbon fiber precursor based on a terpolymer of acrylonitrile, methyl

acrylate, and acryloyl benzophenone. However, the precursor has to be stabilized with UV light, which only achieves ~65% gel fraction and adds an additional cost to production. Other approaches have been the incorporation of methacrylic acid and itaconic acid, with some success.[58] The approach of incorporating internal plasticizers into PAN to render it melt-processable is still an active research field, but many efforts have found that the high comonomer percentages that are needed tend to make a fiber which softens or fuses during the stabilization step, which is undesirable.

A series of high acrylonitrile containing copolymers were developed in the 1990's by British Petroleum which the authors claimed could be made melt-processed by using a starved monomer feed strategy during polymerization.[59, 60] Although the resulting polymers were made melt-processable by the manipulation of the comonomer incorporation, the rate of extrusion was too slow for cost effective commercial viability.

1.11.2 External Plasticization of PAN for Melting Temperature Depression

Another approach towards melt-processable PAN-based carbon fibers is external plasticization which is realized by incorporation of small molecule plasticizing additives, usually with a PAN-copolymer such as PAN-MA.[18] These plasticizers tend to disrupt the strong polar interactions between nitrile groups along the polymer chain, thus lowering the glass transition and melting

temperatures of the polymer.[61] The choice of additive is based on ease of removal from the spun fibers, toxicity, boiling point, and flash point, all of which can contribute to the overall cost of fiber production as well as to the quality of the resulting fibers.

Coxe[62] first reported using water as a melting point depressant with PAN in 1952, but his attempts were never commercialized due to an apparent foaming problem with the extruded fibers. Coxe's method was improved upon by Porosoff,[63] who developed a pressurized chamber for the melt-spinning apparatus, but the resulting fibers were found to contain voids. Min *et al.* found that a maximum melting point reduction of PAN copolymers with water was achieved at 23 wt% water. The results showing the melting temperature from DSC with various water percentages is shown in Figure 1.9. The authors found that when excess water was added (>27 wt%), foaming of the melt-extruded fibers occurred.

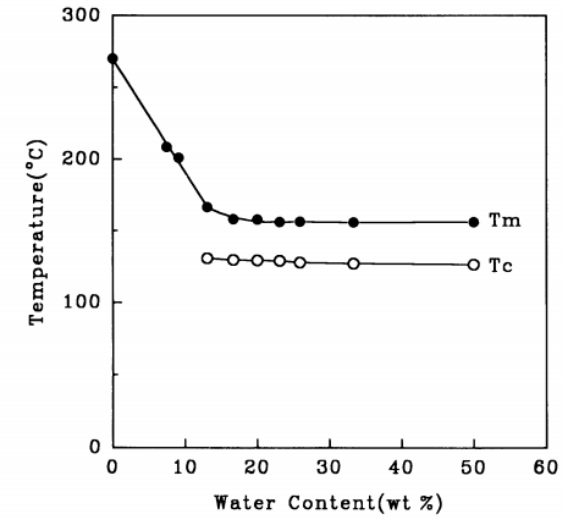

Figure 1.9. Melting point reduction of PAN copolymer with various wt. percentages of water.

Min *et al.* found that by incorporating ethylene carbonate in addition to ~23% water, a greater reduction in melting point of PAN copolymers could be achieved.[61] Bashir[5, 6, 64] has reported that melt extrusion of PAN copolymers without the use of a pressure chamber could be achieved by incorporation of propylene carbonate as a plasticizing melting point reducing agent. However, the resulting fibers lacked the chain orientation necessary for good mechanical properties in the resulting carbon fiber.

Min[65] *et al.* reported that by incorporation of DMF in addition to ~23 wt% water into PAN-copolymers, a very attractive reduction in melting point could be achieved. Figure 1.10 shows the DSC thermograms of a PAN-copolymer

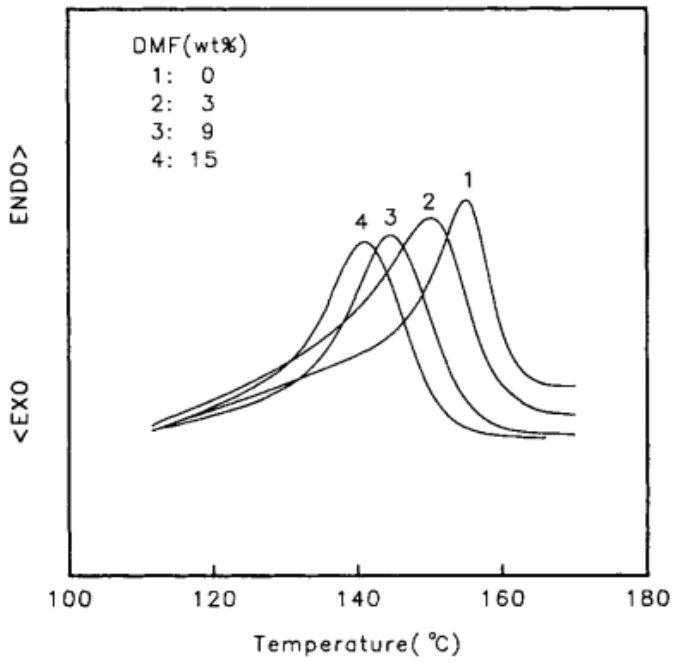

Figure 1.10. DSC thermograms of PAN copolymer mixed with 23 wt% water and various percentages of DMF.

mixed with 23 wt% water and various percentages of DMF. One of the more effective melting point depression agents is acetonitrile, and much effort has been spent towards melt-spinnable PAN copolymers mixed with water and acetonitrile. However, there are concerns with the toxicity of acetonitrile as well as the fairly low flash point.[66-68] Recent efforts to incorporate melting point depressing agents have included the use of ionic liquids[56, 69], γ-butyrolactone[70], and an oligomer of AN and methyl-2-(1H-imidazol-1-yl) acrylate[18] with varying degrees of success.

1.12 Summary and Conclusions

In summary, carbon fibers are integral reinforcing agents for composites that find application with high performance demands. At present, carbon fibers are relatively expensive materials, and much of the cost is driven by the high processing costs associated with solution spinning of PAN-based precursor fibers. One approach to reducing the cost of carbon fibers is to devise a scheme to melt process the precursor fiber, which often involves reducing the T_m of the PAN copolymer and subverting the crosslinking side reactions that the copolymer undergoes between 200-300°C.

1.13 References

1. *US Pat.*, 2904580, to James D. Idol, Jr. of The Standard Oil Co., 1959.
2. C. A. Finch, *British Polymer Journal*, 1985, **17**, 321-321.
3. V. F. Holland, S.B. Mitchell, W.L. Hunter, P.H. Lindenmeyer, *J. Polymer Sci.*, 1962, **62**, 145.
4. C. R. Bohn, J.R. Schaefgen, W.O. Statton *Journal of Polymer Science*, 1961, **55**, 531-549.

5. Z. Bashir, *Journal of Polymer Science Part B: Polymer Physics*, 1994, **32**, 1115-1128.
6. Z. Bashir, *Polymer*, 1992, **33**, 4304-4313.
7. W. R. Krigbaum, N. Tokita, *Journal of Polymer Science*, 1960, **XLIII**, 467-488.
8. A. Mustafa, *Polymer Degradation and Stability*, 2007, **92**, 1421-1432.
9. A. F. Ismail, *Journal of Analytical and Applied Pyrolysis*, 2012, **93**, 1-13.
10. V. G. Hinrichsen, *Die Angewandte Makromoleckulare Chemie*, 1971, **20**, 121-127.
11. G. Henrici-Olive, S. Olive, *Polymer Bulletin*, 1981, **5**, 457-461.
12. L. Allcock, *Contemporary Polymer Chemistry*, Prentice Hall, 2 edn., 1990.
13. M. Chanda, S.K. Roy., *Plastics Technology Handbook*, Marcel Dekker, Inc., United States of America, Third edn., 1998.
14. P. Rangarajan, V. Bhanu, D. Godshall, G.L. Wilkes, J.E. McGrath, D.G. Baird, *Polymer*, 2002, **43**, 2699-2709.
15. P. Rangarajan, J. Yang, V. Bhanu, D. Godshall, J.E. McGrath, G. Wilkes, D. Baird, *Journal of Applied Polymer Science*, 2002, **85**, 69-83.
16. M. J. Bortner, V. Bhanu, J.E. McGrath, D.G. Baird, *Journal of Applied Polymer Science*, 2004, **93**, 2856-2865.
17. V. A. Bhanu, P. Rangarajan, K. Wiles, M. Bortner, M. Sankarpandian, D. Godshall, T.E. Glass, A.K. Banthia, J. Yang, G. Wilkes, D. Baird, J.E. McGrath, *Polymer*, 2002, **43**, 4841-4850.
18. B. L. Batchelor, S. F. Mahmood, M. Jung, H. Shin, O.V. Kulikov, W. Voit, B. M. Novak, D.J. Yang, *Carbon*, 2016, **98**, 681-688.
19. H. R. Kricheldorf, ed., *Handbook of Polymer Synthesis: Part A*, Marcel Dekker, New York, NY, 1992.
20. Y. Furushima, M. Nakada, H. Takahashi, K. Ishikiriyama, *Polymer*, 2014, **55**, 3075-3081.
21. *US Pat.*, 8017050 B2, to B.D. Freeman et al. of The University of Texas, 2010.
22. S. M. Allen, M. Fujii, V. Stannett, H.B. Hopfenberg, J.L Williams, *Journal of Membrane Science*, 1977, **2**, 153-163.
23. J. M. Courtney, G.B. Park, I.A. Fairweather, R.M. Lindsay, *Biomaterials, Medical Devices, and Artificial Organs*, 1976, **4**, 263-275.
24. S. J. Park, *Carbon Fibers*, 2015, **210**.
25. J. C. Masson, *Acrylic fiber technology and applications*, M. Dekker, New York, 1995.
26. J. E. McIntyre, *Synthetic fibres: nylon, polyester, acylic, polyolefin*, CRC Press, Boca Raton; Cambridge, England, 2005.

27. J. R. Ebdon, T.N. Huckerby, T.C. Hunter, *Polymer*, 1994, **35**, 4659-4664.
28. J. B. Donnet, R.C. Bansal, *Carbon Fibers*, Marcel Dekker, New York, 1984.
29. J. B. Donnet, R.C. Bansal, *Carbon Blacks: Physics, Chemistry, and Elastomer Reinforcement*, Marcel Dekker Inc., New York, 1976.
30. H. Kroto, *Science*, 1988, **242**, 1139.
31. S. Iijima, *Nature* 1991, **354**, 56.
32. A. K. Geim, K.S. Novoselov, *Nat. Mater.*, 2007, **6**, 183.
33. *US Pat.,* 223898, to T. A. Edison, 1879.
34. A. Kelly, C. Zweben, *Journal*, 2000, **1**.
35. S. C. Bennet, D.J. Johnson, London, 1978.
36. A. R. Bunsell, *Fibre Reinforcements for Composites Materials*, Elsevier Science Publishers, Amsterdam, The Netherlands, 1988.
37. T. Ma, Z.H. Chen, *Ceramic. Int.*, 2012, **38**, 4229.
38. F. Vautard, S. Ozcan, H. Meyer, *Appl. Sci. Manufac.*, 2012, **43**, 1120.
39. P. Tsotra, K. Friedrich, *Appl. Sci. Manufac.*, 2003, **34**, 75.
40. M. A. Montes-Moran, A. Martinez-Alonso, J.M.D. Tascon, M.C. Paiva, C.A. Bernardo, *Carbon*, 2001, **39**, 1057.
41. S. Wei, G. Aijuan, L. Guozheng, Y. Li, *Appl. Surf. Sci.*, 2011, **257**, 4069.
42. L. H. Peebles, *Carbon Fiber-Formation, Structure, and Properties*, CRC Press, Los Angeles, 1995.
43. M. S. A. Rahaman, A.F. Ismail, A. Mustafa, *Polym. Degrad. Stab.*, 2007, **92**, 1421.
44. O. P. Bahl, in *Carbon Fibers,* ed. J. B. Donnet, Wang, T.K., Rebouillat, S., Peng, J.C.M., Marcel Dekker, New York, 1998, pp. 1-84.
45. V. A. Bhanu, Rangarajan, P., Wiles, K., Bortner, M., Sankarpandian, M., Godshall, D., Glass, T. E., Banthia, A. K., Yang, J., Wilkes, G., Baird, D., McGrath, J. E., *Polymer*, 2002, **43**, 4841.
46. B. N. Frushover, Marcel Dekker, New York, 1995, ch. 7, pp. 197-258.
47. G. T. Sivy, M.M. Coleman, *Carbon*, 1981, **19**, 127.
48. C. Berrueco, P. Alvarez, N. Diez, M. Granda, R. Menendez, C. Blanco, R. Santamaria, M. Millan, *Fuel*, 2011.
49. T. Matsumoto, *Pure and Appl. Chem.*, 1985, **57**, 1553.
50. D. M. Riggs, R.J. Shuford, R.W. Lewis, *Handbook of Composites*, Van Nostrand Reinhold Co., New York, 1982.
51. E. Mora, C. Blanco, V. Prada, R. Santamaria, M. Granda, R. Menendez, *Carbon*, 2002, **40**, 2719.

52. *High-Performance Synthetic Fibers for Composites*, National Academy Press, Washington, DC, USA, 1992.
53. M. Z. Ozel, K.D. Bartle, *Turk. J. Chem.*, 2002, **26**, 417.
54. *US Pat.,* 4,032,430, to I. C. Lewis of Union Carbide Corporation, 1977.
55. E. Piorkowska, G.C. Rutledge, ed., *Handbook of Polymer Crystallization*, Wiley, Hoboken, NJ, 2013.
56. S. Lui, K. Han, L. Chen, Y. Zheng, M. Yu, *Polymer Engineering and Science*, 2015, DOI: 10.1002/pen.24121, 2722-2728.
57. A. K. Naskar, R.A. Walker, S. Proulx, D.D. Edie, A.A. Ogale, *Carbon*, 2005, **43**, 1065-1072.
58. P. Bajaj, T.V. Sreekumar, K. Sen, *Polymer*, 2000, **42**, 1707-1718.
59. *CA Pat.,* CA2134825A1, to R. C. Smierciak et al. of The Standard Oil Co., 1995.
60. *US Pat.,* US5618901A, to R. C. Smierciak et al. of The Standard Oil Co., 1997.
61. B. G. Min, T.W. Son, B.C. Kim, C.J. Lee, W.H. Jo, *Polymer Journal*, 1992, **24**, 841-848.
62. *US Pat.,* 2,585,444, to Charles D. Coxe of E. I. du Pont de Nemours & Co., 1952.
63. *US Pat.,* 4,163,770, to H. Porosoff of American Cyanamid Co., 1979.
64. S. A. Atureliya, Z. Bashir, *Polymer*, 1993, **34**, 5117.
65. B. G. Min, T.W. Son, B.C. Kim, C.J. Lee, W.H. Jo, *Journal of Applied Polymer Science*, 1994, **54**, 457-462.
66. *US Pat.,* 5,168,004, to G. P. Daumit of BASF, 1992.
67. *US Pat.,* 3,634,575, to G. A. Serad of Celanese Corp., 1968.
68. P. E. Slade, *Themochimica Acta*, 1970, **1**, 459-463.
69. Y. Wang, S. Wang, J. Liu, *Key Engineering Materials*, 2014, **575-576**, 151-155.
70. *US Pat.,* 2,706,674, to G. M. Rothrock of E. I. du Pont de Nemours & Co., 1955.

Chapter 2: Melt-spinnable Polyacrylonitrile Copolymer Precursors for Carbon Fibers

Gregory C. Miller,[a,c] Jianger Yu,[b,c] R. M. Joseph,[a,c] Shreya Roy Choudhury,[a,c] S. J. Mecham,[a,c] D. G. Baird,[b,c] M. Bortner,[b,c] F. L. Paulauskas,[d] R. Norris,[d] J. S. Riffle[a,c*]

[a]Department of Chemistry, [b]Department of Chemical Engineering, [c]Macromolecules Innovation Institute, Virginia Polytechnic Institute and State University, Blacksburg, VA 24061 and [d]Oak Ridge National Laboratory, Oak Ridge, TN

2.1 Introduction

Polyacrylonitrile (PAN) is an acrylic polymer with a very high crystalline melting point (~317°C) and limited solubility in most common solvents with the exception of ethylene carbonate,[1] propylene carbonate,[2, 3] concentrated aqueous solutions of inorganic salts,[4] and some dipolar aprotic solvents including dimethylformamide (DMF), dimethylsulfoxide (DMSO), and dimethylacetamide (DMAc).[5] The high melting point of PAN has been attributed to dipolar forces among polar nitrile groups adjacent to one another along the polymer backbone that restrict bond rotation leading to a stiff rod-like polymer.[4, 6] Strong repulsive dipole-dipole intramolecular interactions between parallel nitrile neighbors along the polymer backbone lead to an irregular helical conformation, and attractive

dipole-dipole intermolecular interactions between anti-parallel nitrile groups of neighboring chains lead to a parallel orientation of the helices relative to one another.[7]

Carbon fibers are exceptional materials due to their high strength, chemical inertness, and low density relative to glass. More than 50% of the carbon fibers produced are utilized in air and spacecraft applications to save on weight and fuel without sacrificing structural integrity, but they are increasingly finding applications in shipping, sporting and medical fields.[8, 9] The structural unit of a carbon fiber is a planar network of connected benzene rings, similar to the planar hexagonal honeycomb arrays found in graphite.[8, 10] The two most common precursor sources for the commercial production of carbon fibers are a mesophase pitch produced by the destructive distillation of coal and synthetic polymeric fibers of polyacrylonitrile copolymers (PAN).[11] Most carbon fibers are of the latter variety, produced from a PAN copolymer-based precursor[9] in a multi-step method. First, the precursor fiber is subjected to a thermo-oxidative so-called stabilization procedure in which the fiber is heated to ~220-280°C under tension in air for long times.[12] This stabilization process results in crosslinking and cyclization reactions that form a ladder-type structure. The process most likely occurs via a combination of intra- and inter-molecular reactions between pendant CN groups. Next, in a process known as carbonization, the fiber is heated to ~1300°C in an unstressed state and inert atmosphere to yield a fiber with at least 97% carbon content.[10, 11, 13] Finally, in a graphitization step, the

filament is further heated to ~3000°C to increase the modulus of the carbon fiber.[10-17]

More than 300 million pounds of acrylic PAN-based fibers are produced annually.[18] Polyacrylonitrile fibers are generally spun in a wet-spinning process that includes drawing in such a way that the polymer chains become oriented parallel to the fiber axis. Comonomers such as methyl acrylate and vinyl acetate are often incorporated into PAN to increase the solubility of the polymer in solvents that are used in the spinning process as well as to mediate the kinetics of crosslinking during the exothermic thermo-oxidative step.[8, 11, 14] High production costs associated with the organic solvent and its recovery are inherent in all of the current carbon fiber production processes.[14] It would be desirable to melt-spin the PAN copolymer fibers for both economic and environmental reasons. However, the polymer undergoes a thermal crosslinking reaction prior to reaching the melting temperature.[9, 19-21]

Research into melt-spinning processes for PAN involve two general approaches: internal and external modification. Several examples of internal modification exist. This is generally achieved by adding one or more comonomers during the free radical polymerization.[9, 14, 22-25] In 1952, Coxe [26] pioneered the field of external PAN modification when he observed that high pressure mixtures of PAN with water could be melt-extruded. However, foaming of the fibers as they exited the spinneret and the water evaporated prevented this method from being widely adopted. Much research has been conducted building on Coxe's initial findings including exploring different techniques involving pressurized mixtures

of PAN and water,[20, 27, 28] pressurized mixtures of PAN, ethylene carbonate, and water,[19] pressurized mixtures of PAN, dimethylformamide and water,[21] pressurized mixtures of PAN, acetonitrile and water,[29, 30] pressurized mixtures of PAN and carbon dioxide,[31] and mixtures of PAN with ionic liquids.[32] It has been shown that the modification effect of water on a poly(acrylonitrile-*ran*-vinyl acetate) copolymer comprised of 88 wt % of acrylonitrile with a M_v = 82,000 g/mole reached a maximum potential at 23 wt % water, and additional water past this critical concentration had no added benefit.[19] Min et al. [21] found that by adding DMF in addition to the critical 23 wt % of water, both the melting point and the crystallization temperature of a poly(acrylonitrile-*ran*-vinyl acetate) copolymer (88 wt % acrylonitrile, 12 wt % vinyl acetate) could be decreased further, even achieving melting points as low as 140°C.

This study details effects of incorporating binary systems of polar additives as modifiers on the melting temperatures of high molecular weight PAN-MA copolymers with well-defined compositions and molecular weights. The melt rheological behavior of the modified PAN-MA copolymer is described as a function of temperature, time, and shear-rate to assess whether the selected mixtures would be appropriate for melt-spinning.

2.2 Experimental

2.2.1 Materials

Poly(acrylonitrile-*ran*-methyl acrylate) (PAN-MA) was purchased from Fisipe and used as received. *N*-methyl-2-pyrrolidone (NMP), *N,N*-

dimethylformamide (DMF), and acetonitrile (ACN) were purchased from Spectrum Chemicals and used as received. 1,6-Hexanedinitrile (adiponitrile) (ADPN) and 2-ethyl-2-oxazoline (EtOx) were purchased from Sigma-Aldrich and used as received.

2.2.2 Mixing of PAN copolymers and modifiers

DMF (0.5 g), polymer powder (3.5 g) and DI water (1 g) were incorporated thoroughly by mixing the components with a spatula in until a consistent paste-like mixture was produced. This produced 5 g of a copolymer mixture containing 10 wt % of DMF and 20 wt % of water [70:10:20 wt:wt:wt]. This process was repeated for each copolymer/melting point modifier composition. Melting point modifiers used in this study included deionized water, NMP, DMF, 2-ethyl-2-oxazoline, acetonitrile, and hexanedinitrile (commonly referred to as adiponitrile).

2.2.3 Structural characterization

Proton nuclear magnetic resonance (^{1}H NMR) spectroscopy was performed on an Agilent MR4 spectrometer operating at 400 MHz. All ^{1}H spectra were obtained from 15% (w/v) 1-mL solutions in deuterated dimethylsulfoxide (DMSO-d_6) using a 30° pulse angle, 5s relaxation delay, and 64 scans and was performed in triplicate to obtain quantitative results. Molecular weights of the copolymer were obtained by size exclusion chromatography (SEC). The SEC system consisted of an isocratic pump (Agilent 1260 infinity, Agilent Technologies, Santa Clara, CA) with an online degasser (Agilent 1260, Agilent

Technologies, Santa Clara, CA), autosampler and column oven used for mobile phase delivery and sample injection, and three Agilent PLgel 10-μm Mixed B-LS columns 300 x 7.5 mm (polystyrene/divinylbenzene) connected in series with a guard column as the stationary phase. A system of multiple detectors connected in series was used for the analysis. The columns and detectors were maintained at 50°C. A multi-angle laser light scattering (MALS) detector (DAWN-HELEOS II, Wyatt Technology Corporation, Goleta, CA), operating at a wavelength of 658 nm, and a refractive index detector operating at a wavelength of 658 nm (Optilab T-rEX, Wyatt Technology Corporation, Goleta, CA) provided online results. The system was corrected for interdetector delay, band broadening, and the MALS signals were normalized using a 21,720 g/mole polystyrene standard obtained from Agilent Technologies or Varian. Data acquisition and analysis were conducted using Astra 6 software (Wyatt Technology Corporation, Goleta, CA). The mobile phase was DMAc, which was vacuum distilled over CaH_2 before use. A solution of 0.1 M LiCl, dried at 120°C *in vacuo* for 2 h, in DMAc was prepared, and the solvent solution was degassed and filtered before use. The sample solutions were prepared in a concentration range of 2~3 mg/mL and were filtered to remove any dust or insoluble particles using 0.22-μm PTFE filters. Molecular weights were calculated from the light scattering data.

Differential refractive index increment (dn/dc) measurements of the PAN-MA copolymer were made using an Agilent 1260 infinity multidetector SEC equipped with a Wyatt T-rex differential RI detector at 30°C and with a flow rate of 0.3 mL/min. The following representative procedure was used: 400 mg of the

sample was weighed into a vial and dissolved in 20 mL of DMAc containing 0.1 M LiCl (dried as described previously). The solution was stirred for approximately 12 h. The sample solution was then diluted to 50 mL in a volumetric flask. This stock solution was used to make 7 new dilutions that were filtered through 1-μm PTFE filters. The refractive index for each of 8 concentrations was measured and the data points were fitted to a straight line. The dn/dc was determined by the slope of the line.

2.2.4 Differential scanning calorimetry (DSC)

The glass transitions, melting temperatures and the relative stabilities of the copolymer/modifier mixtures were investigated with a TA Instruments DSC Q200 using high volume DSC pans with O-rings. For determining the copolymer T_m's, the copolymer/modifier mixtures were heated under nitrogen at a rate of 10°C min^{-1} to 200°C, cooled at a rate of 10°C min^{-1} to 0°C, and heated again at a rate of 10°C min^{-1} to 240°C. For determining the T_g's of the copolymer/modifier mixtures containing acetonitrile, a modified experimental procedure was developed. The mixtures were heated at a rate of 10°C min^{-1} to 200°C, cooled at a rate of 20°C min^{-1} to 0°C, then heated again at a rate of 5°C min^{-1} to 240°C. The reported DSC transitions were from the second heating scans. For determining the relative stabilities of the copolymer/modifier mixtures, an isothermal DSC experiment was employed in which the mixtures were heated under nitrogen at a rate of 10°C min^{-1} to 110°C, cooled at a rate of 10°C min^{-1} to 40°C, heated to ~10°C below the target temperature, equilibrated at the target temperature, then held isothermally for 4 h at the desired temperature.

2.2.5 Preparation of polymer/modifier pellets for rheology measurements

The copolymer powder was first mixed thoroughly with the modifier(s) to obtain the desired composition, as detailed in *Section 2.2.2*, then the mixture was press molded at room temperature with a hydraulic press into a metal die to obtain a cylindrical pellet with a uniform diameter of 9.5 mm. The copolymer pellet helped to prevent voids in the samples as well as make it easier to load the copolymer/modifier mixture into the capillary rheometer with minimal solvent loss. For mixtures containing acetonitrile, an additional heating step was necessary to suitably press the pellets. The mixture was heated in a sealed resin kettle for ~1 h above the mixture's T_g (42 °C), then it was allowed to cool overnight before preparing the pellets. It is believed that heating the copolymer mixture above its T_g allowed better incorporation of the solvent mixture into the copolymer due to the increased chain motion and free volume at the elevated temperature. It is anticipated that this treatment will be necessary to prepare PAN-MA/ACN/H_2O samples for melt-extrusion as well. A sample pellet of approximately 10 grams was required for each set of rheological measurements.

2.2.6 Pressurized capillary rheometry

Viscosity measurements were conducted on an Instron model 3211 capillary rheometer with modifications and using a procedure similar to that reported by Bortner and Baird.[31] The rheometer was modified by adding a sealed chamber at the capillary exit to create a static pressure that maintained a homogeneous single melt phase and minimized macrophase separation or

volatilization of the modifiers from the copolymer. The pressure assembly also enabled collection of the extrudate during the viscosity measurements for subsequent analysis. Nitrogen was used with a constant pressure of 1.38 MPa to apply a static pressure to the capillary exit. This pressure is above the calculated saturation pressure for the additives at the test temperatures. Nitrogen was used because prior work had verified that nitrogen does not exert a plasticizing effect on PAN polymers.[31] Teflon O-rings were employed on the plunger and Teflon spacers were used between the pressure chamber assembly and the capillary to seal the pressurized system. A detailed schematic diagram of the modified capillary rheometer is provided in Figure 2.1.

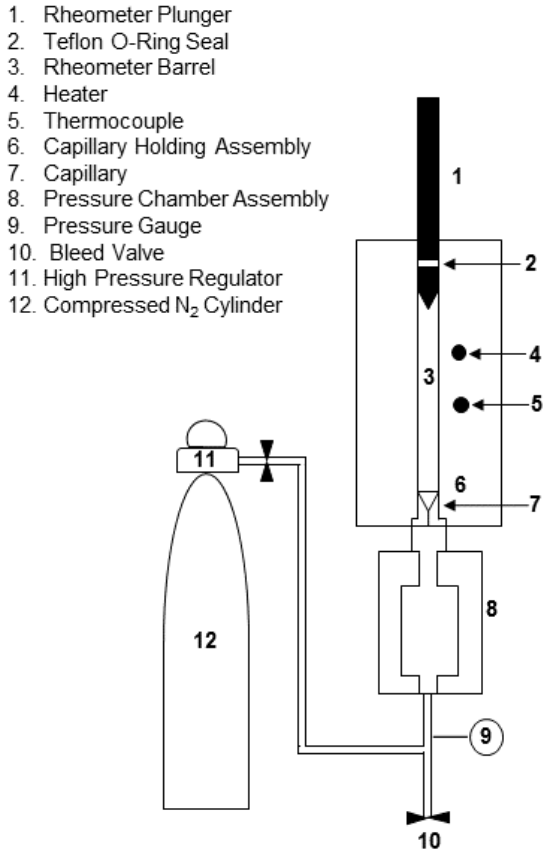

Figure 2.1. Schematic diagram of the modified capillary rheometer to operate under pressure

The following procedure was implemented to prevent the loss of melting point modifiers that would normally occur if loaded into a preheated rheometer. Copolymer/modifier pellets were loaded into the rheometer at room temperature with a chamber diameter of 9.53 mm, a capillary diameter of 0.0356 mm, and an entry angle of 90°. The system was sealed with a piston and static pressure was applied to the capillary exit. The rheometer was heated to the experimental temperature, with the system pressurized. The copolymer pellet was initially held

at the experimental temperature for 10-12 min to allow complete melting of the pellet in the rheometer prior to performing the rheological tests. To quickly compact the sample following heating, a high plunger speed of 2 cm/min was used until a quasi- steady state force was reached, at which time the plunger speed was decreased to 0.06 cm/min and the melt was allowed to relax to steady-state. The pressure gradient was calculated using the force measured by the load cell at the top of the plunger. Corrections were made by subtracting the contribution of applied static pressure at the capillary exit (1.38 MPa) and the frictional force from the Teflon O-rings used to seal the space between the plunger and barrel. A capillary with L/D of 88 was used to minimize the impact of entry effects.

Steady shear viscosity measurements were performed at a constant apparent shear rate of 161.3 s^{-1} to analyze the time dependence of viscosity. Further measurements were performed at apparent shear rates ranging from 80-10,755 s^{-1} until a steady-state viscosity was achieved for each shear rate. Viscosities were calculated by known methods from plunger speeds and force measurements.[33] The apparent shear rate, $\dot{\gamma}_a$, was calculated based on the volumetric flow rate of the polymer through the capillary, Q, and the radius of the capillary, R, as defined by Eq. (2.1):

$$\dot{\gamma}_a = \frac{4Q}{\pi R^3} \tag{2.1}$$

The wall shear stress, τ_R, was calculated using Eq. (2.2):

$$\tau_R = \frac{\Delta P R}{2L} \quad (2.2)$$

where ΔP is the pressure gradient, R is the radius of the capillary, and L is the length of the capillary. The apparent viscosity was calculated from Eq. (2.3).

$$\eta_a = \frac{\tau_R}{\dot{\gamma}_a} \quad (2.3)$$

The power law fluid model was used for comparing the relative shear thinning behavior between samples according to Eq. (2.4):

$$\log \eta_a = \log m + (n-1) \log \dot{\gamma}_a \quad (2.4)$$

where m is the flow consistency index and n is the flow behavior index.

2. 3 Results and Discussion

The feasibility of melt extrusion of a PAN-MA copolymer relies upon melting of the copolymer, a sufficiently low viscosity of the resulting melt, as well as the stability of the melt against competing cyclization and crosslinking reactions under the extrusion conditions. During melt extrusion, the viscosity is expected to increase as a result of crosslinking in addition to cyclization, which depends on the processing temperature and residence time in the extruder [14]. It is prudent to describe quantitatively the changes in viscosity as a function of temperature, time, and shear rate so that proper melt-extrusion parameters can be identified.

2.3.1 Composition and stability of PAN-based copolymers

From prior literature,[9] it is known that PAN-MA copolymers containing more than 10 mole % of MA have improved melt processability, but this comes at the expense of lower carbon content and compromised mechanical properties in the resulting carbon fibers after conversion. Therefore, the copolymer used to make a precursor fiber for a carbon fiber should ideally contain less of the comonomer to achieve carbon fibers with good mechanical properties. The composition of the copolymer used for this investigation was determined by ^{1}H-NMR. The spectrum had well-resolved peaks that confirmed that the copolymer consisted of methyl acrylate and acrylonitrile repeat units. Methyl acrylate is a desirable comonomer for PAN-based carbon fiber precursors because the reactivity ratios of AN with MA in DMF at 62°C have previously been found to be 1.29 and 0.96, respectively. Therefore, the copolymer that is produced is a predominately random copolymer.[34] A representative spectrum is shown in Figure 2.3.2. The signal at 3.2 ppm (b,d) corresponds to the backbone methine (CH) protons from acrylonitrile and methyl acrylate. The signal at 2.1 ppm (a,c) corresponds to the backbone methylene (CH_2) protons from both acrylonitrile and methyl acrylate. The signal at 3.7 ppm (e) corresponds to the methyl ester (CH_3) protons of the methyl acrylate units. The copolymer composition was calculated from the integral values of the methylene protons according to the following equations:

$$Moles\ MA\ \alpha\ \left(\frac{\int CH_3}{3}\right)$$

$$(Moles\ MA)\ \times\ \left(86.04\ \frac{g}{mole}\right) = relative\ weight\ MA$$

$$Moles\ AN\ \alpha \left[\left(\frac{\int X}{2}\right) - \left(\frac{\int CH_3}{3}\right)\right]$$

$$(Moles\ AN)\ \times \left(53.06\ \frac{g}{mole}\right) = relative\ weight\ of\ AN$$

$$Weight\ Percent\ AN = \frac{relative\ weight\ AN}{relative\ weight\ AN\ + relative\ weight\ MA} \times 100$$

$$Weight\ Percent\ MA = 100 - weight\ percent\ AN$$

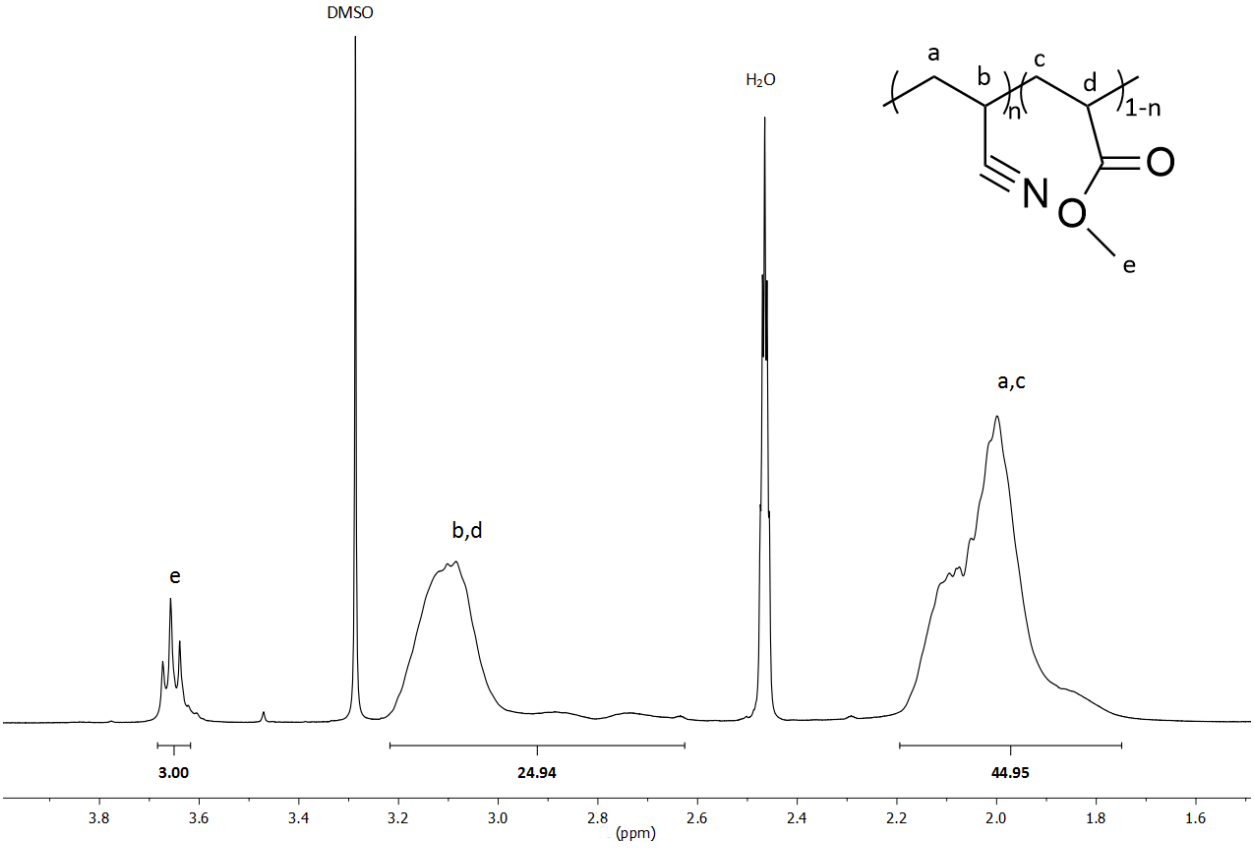

Figure 2.2. ^{1}H NMR Spectrum of PAN-MA

From analysis of the ^{1}H-NMR spectra, the copolymer was found to be 95.6 ± 0.13 mole % acrylonitrile and 4.40 ± 0.13 mole % methyl acrylate.

2.3.2 Molecular weight of the PAN-MA copolymer

Molecular weight of the PAN-MA precursor copolymer has been shown to exert an effect on the mechanical properties of the resulting carbon fiber produced from solution-spun precursor fibers. Very high molecular weight copolymers yield carbon fibers with higher tensile strengths, elastic moduli, and ultimate elongations than carbon fibers produced from lower molecular weight copolymers.[35, 36] The precursor fiber produced from a high molecular weight PAN-MA produced filaments of smaller diameter than filaments produced from low molecular weight PAN-MA due to lower solids content in the spinning dope and higher drawability. It is hypothesized that the smaller diameter of the precursor filaments allows better diffusion of oxygen throughout the carbon fiber as it forms, thus resulting in a homogeneous microstructure across the diameter of the carbon fibers and that this contributes to significantly higher moduli and tensile strengths.[36]

SEC was used to analyze the molecular weight and molecular weight distribution of the PAN-MA copolymer in this study. The light scattering and refractive index curves are shown in Figure 2.3. The results show a smooth light scattering curve, without any high or low molecular weight shoulders, indicative of a normal Gaussian distribution. The dn/dc value for this copolymer composition was measured offline and used in the calculation of molecular

weights. This is necessary since the molecular weights calculated from the light scattering data depend on the square of the refractive index increment, and thus, this provides confidence in the molecular weight values.

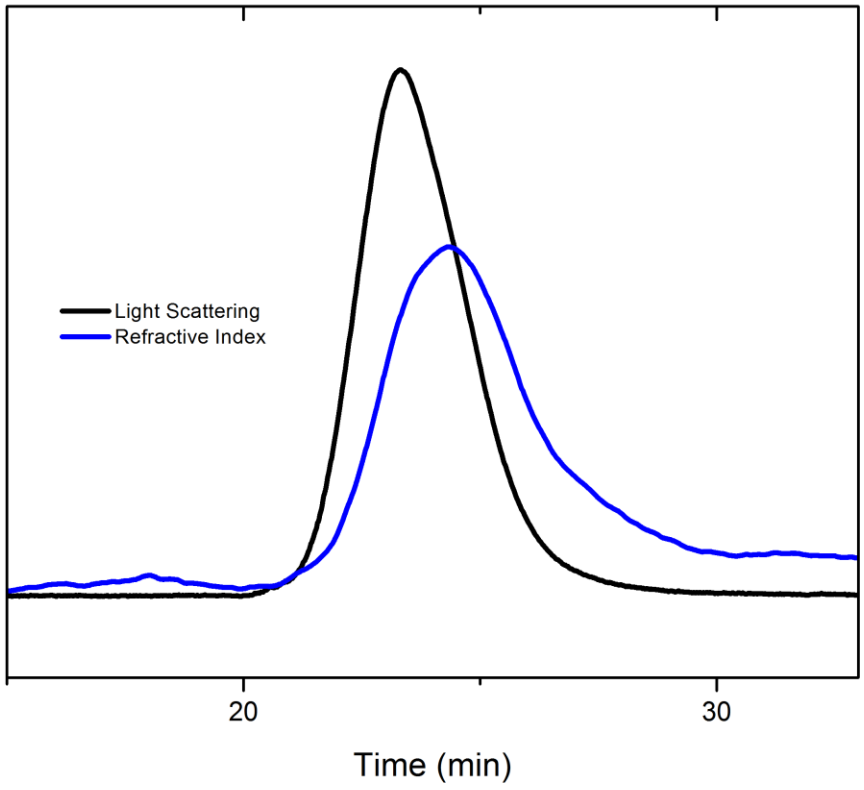

Figure 2.3. Size Exclusion Chromatograms for PAN-MA Copolymer where the M_n = 123 kDa, M_w = 238 kDa, polydispersity = 1.9, and dn/dc = 0.0855 mL/g.

2.3.3 Thermal transitions of polymer/modifier blends

DSC was used to determine the melting points of PAN-MA compounded with a binary mixture consisting of H_2O and various melting point modifiers. Analysis of the DSC experiments was performed using TA Universal Analysis software. The T_m of each composition was assigned as the peak of the endotherm

of the second heat of each experiment. Prior literature has shown that the maximum melting point depression of a PAN-vinyl acetate copolymer (88 wt % acrylonitrile and 12 wt % vinyl acetate) solely from modification with H_2O occurs at 20 wt % of H_2O. This yielded a melting point of ~155°C [19], and additional modifiers had to be added into the mixture to depress the melting point further.[21] The melting point depression effect of H_2O is not well understood, but it is thought that the water molecules are able to interact with the pendant nitrile groups of the copolymer in a hydrogen bonding motif. This is most likely in the amorphous component of the copolymer, and weakly shields the nitrile from the repulsive dipole-dipole interactions which give the copolymer its characteristic rigid helical morphology.[2, 3, 37, 38] For the data depicted in Figure 2.4, all compositions included 20 wt % of H_2O with increasing amounts of a second melting modifier. The ratio of water molecules relative to nitrile substituents on the copolymer at 20 wt% of water is approximately 0.87:1. Figure 2.4 shows a curve of T_m vs percentage of the second modifier. It shows that the two nitrile containing modifiers, acetonitrile (ACN) and adiponitrile (ADPN), are more efficient at depressing the melting points relative to the other modifiers when used in combination with the water.

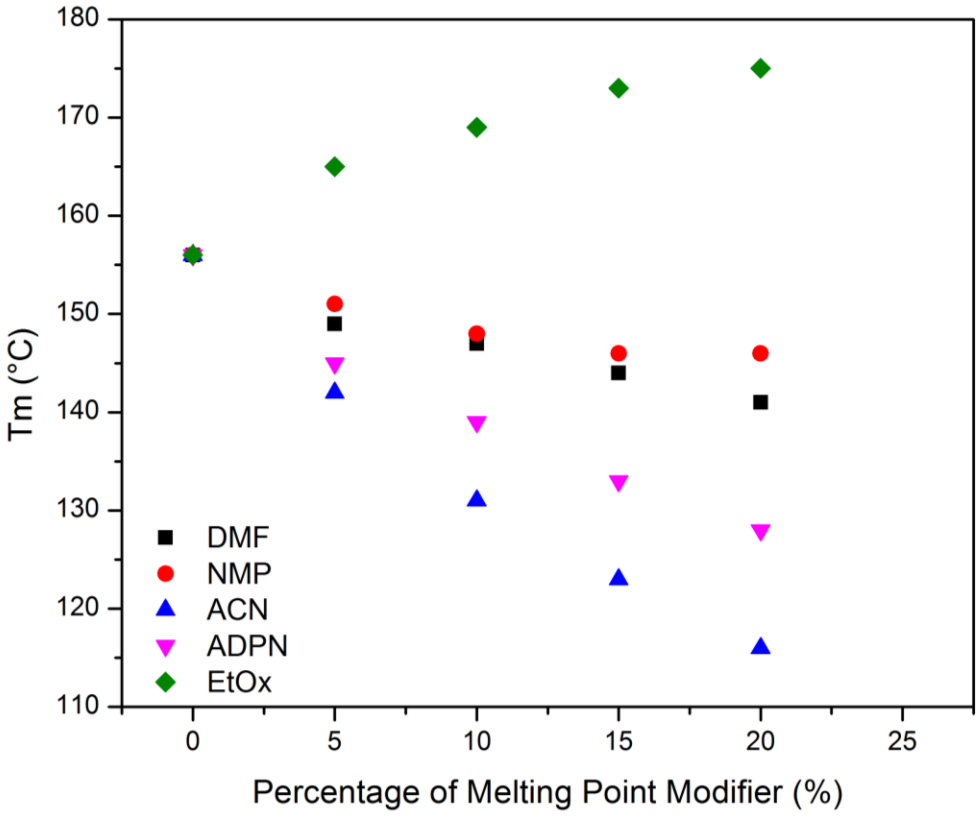

Figure 2.4. Melting points vs percentage of modifier in the PAN-MA mixtures. Each composition contains 20 wt % of water in addition to the denoted modifiers.

It is hypothesized that the mechanism for this pronounced effect of the nitrile-containing modifiers arises from the modifier nitrile group maintaining complementary dipole interactions with the nitrile groups along the PAN-MA backbone, thereby disrupting some of the interchain nitrile-nitrile interactions between neighboring PAN-MA chains. This may penetrate somewhat into the crystalline domains, thereby allowing the ingress of water into those regions which may have otherwise been inaccessible. Complementary interchain nitrile-nitrile polar interactions are thought to be the mechanism by which acrylonitrile based polymers form lamellae for crystallization.[3, 37-41] One composition, PAN-

MA/ACN/H_2O 55:25:20 wt:wt:wt, showed a depressed melting point of 116°C, which is a depression of over 200°C from the neat copolymer. DMF and NMP also have a synergistic effect with H_2O to depress the melting point of PAN-MA. Unlike ACN and ADPN, DMF and NMP are good solvents for the copolymer at room temperature. It is hypothesized that these two materials depress the melting point of the copolymer by a similar mechanism as the one in which they dissolve the copolymer. We postulate that such modifiers are able to disrupt the crystallinity of the polymer and allow the H_2O to penetrate into these domains, thereby lowering the melting point. In contrast to all of the other materials used in this study, EtOx had an antagonistic effect in combination with H_2O on the melting point of the copolymer. As more EtOx was added to the PAN-MA/20 wt % H_2O blends, the melting point of the system increased systematically. This was a somewhat surprising result, since EtOx is an isomer of NMP. This affords some insight into the mechanism by which these modifiers mediate the melting points, and strongly supports the assertion that the water is necessary to achieve the desired melting point depression. EtOx is a monomer for a very hydrophilic polymer [42], and is quite hydrophilic itself. Some melting point depression is achieved just by the addition of 20 wt % of H_2O, but as EtOx is added to the system, it is believed that a competition results between the polymer and EtOx for interaction with the H_2O molecules, thereby reducing the efficacy of the effect of H_2O hydrogen bonded to the copolymer.

Since the two nitrile-functional melting point modifiers used in this study yielded the best melting point depressant properties when used in combination

with H_2O, these two materials were chosen for a further study in which the wt % of water was varied and the resulting T_m's were determined by DSC. The results are tabulated in Table 2-1, and indicate that many compositions of PAN-MA mixed with water and a nitrile-containing melting point modifier show promise as potential melt-processable carbon fiber precursor materials.

Table 2-1. T_m of PAN-MA/ACN/H_2O or PAN-MA/ADPN/H_2O compositions.

MP Mod.	PAN-MA (%/wt.)	MP Mod. (%/wt.)	H_2O (%/wt.)	T_m (°C)
ACN	55	25	20	116
	60	20	20	123
	65	15	20	131
	70	10	20	142
	70	15	15	134
	70	20	10	135
	70	25	5	146
	70	30	0	165
	75	10	15	139
	80	10	10	150
	85	10	5	168
ADPN	55	25	20	128
	60	20	20	133
	65	15	20	139
	70	10	20	145
	70	15	15	136
	70	20	10	136
	70	25	5	161
	70	30	0	185
	75	10	15	148
	80	10	10	158
	85	10	5	181

2.3.3 Thermal stability of polymer/modifier blends against crosslinking

PAN-based polymers are known to undergo crosslinking reactions in the presence of oxygen and at elevated temperatures. This results in the desired ladder polymer formation during carbon fiber production. However, it is important for the carbon fiber precursor to undergo this reaction at the appropriate time in the stabilization process. Therefore, it was judicious to determine whether the melts that resulted from mixing PAN-MA with water and the synergistic melting point modifiers resisted crosslinking for an amount of time that was adequate to extrude precursor fibers. An isothermal DSC experiment was designed to probe the relative stabilities of melts of PAN-MA compounded with a binary mixture consisting of H_2O and various melting point modifiers. Each experiment was performed at a temperature above the melting point of the mixture. During the isothermal DSC experiment, the evolution of an exotherm was attributed to crosslinking reactions, and the time required for the exotherm to begin was recorded. Some of the most promising candidates from Figure 2.4 were chosen for this experiment.

Conventional wisdom dictates that a melt should remain stable against crosslinking for at least an hour to be a suitable candidate for melt extrusion. Figure 2.5 shows the times for onset of an exotherm vs temperature for various PAN-MA/melting point modifier/H_2O mixtures. It was observed that all of the compositions studied were stable for at least an hour at temperatures ≤ 200°C. The general trend from Figure 2.5 is that the stability of PAN-MA/melting point

modifier/H_2O compositions are as follows: ADPN>ACN>DMF with the nitrile-containing melting point modifiers producing mixtures that were significantly more stable than when using DMF. This is most likely due to the fact that the nitrile modifiers are better able to disrupt the nitrile-nitrile interchain forces which are necessary for the crosslinking reaction. It is also worth noting that there was little difference in stability between the two ACN containing mixtures that were studied.

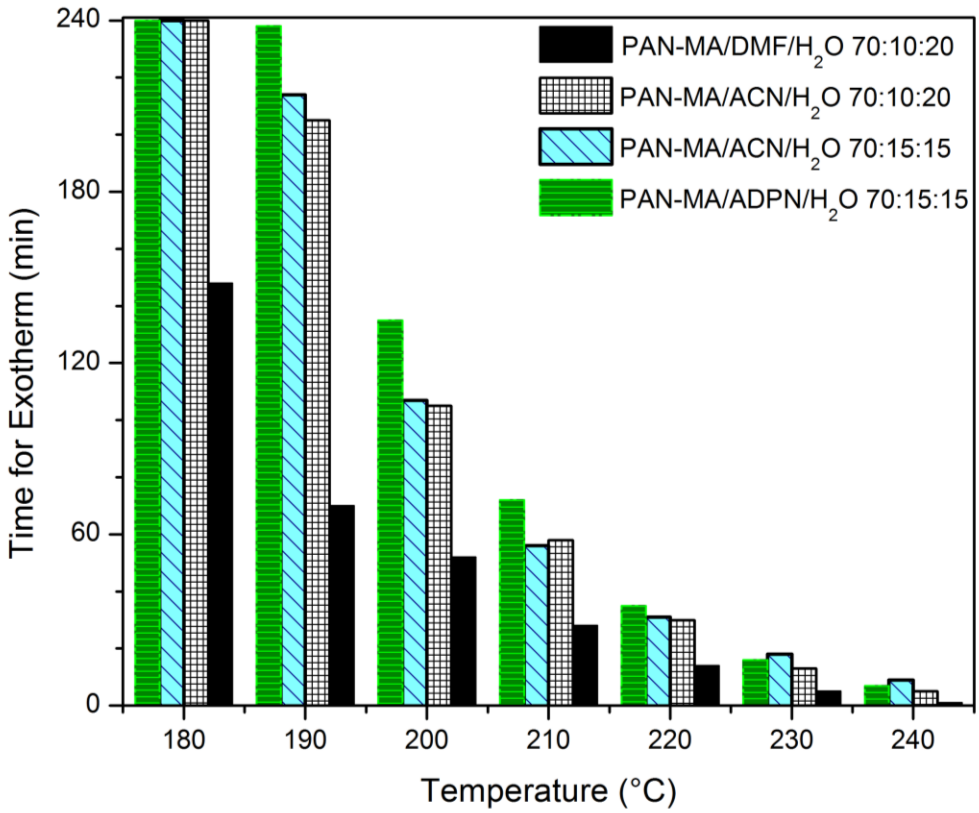

Figure 2.5. Times for onset of an exotherm vs temperature in isothermal DSC experiments.

2.3.4 Time and shear dependent melt rheology

Melt viscosities are key to understanding potential melt extrusion conditions that are suitable for melt processing of copolymer/melting point modifier mixtures. Specifically, we wish to understand the relationship between melt viscosity and shear rate as a function of time and temperature to establish practical limitations on extrusion flow rate, die geometry, and residence time. Temperatures were chosen above the melting points of the mixtures. Steady shear viscosity was measured as a complementary experiment to analyze the thermal stability of the copolymer/modifier mixtures under shear, and for comparison to the static thermal stability analysis performed using isothermal DSC.

Results of the time-dependent steady shear measurements are illustrated in Figure 2.6. A relative low apparent shear rate of 161.3 s^{-1} was used in all measurements to enable the longest possible measurement time at a low volumetric flow rate. Figure 2.6A shows the apparent viscosity for a PAN-MA/ACN/H_2O 70:15:15 wt:wt:wt blend at temperatures ranging from 170-190°C. The data show an increase in the viscosity at 170 and 180°C that occurs at different times during the experiment. Following the pre-conditioning step at high plunger speed that was employed to compress the sample at the beginning of the experiment, the copolymer mixtures require time to relax to steady-state viscosity. At the higher temperature of 190°C, the melt quickly relaxes to steady-state viscosity. As temperature is decreased to 180 and then to 170°C, the relaxation time increases as expected, as less thermal energy and corresponding

thermal motion increase the characteristic relaxation time.[43] However, in all cases, the polymer mixture relaxes to a steady state viscosity plateau prior to observation of significant crosslinking, which is typically observed as a sharp increase in viscosity from the steady state plateau.

The results in Figure 2.6A suggest that the activation energy for flow is relatively small for the copolymer mixtures, with relatively small differences in viscosity observed as a function of temperature at the measured shear rate.[43] However, the thermal stability is drastically impacted by changes in measurement temperature. At 170°C, the composition maintained a stable viscosity of approximately 2000 Pa*s for 116 minutes under shear. The times that are reported are limited by the amount of sample that can be loaded into the rheometer, but the sample was stable during the whole course of the experiment. At 180°C, the mixture reached a stable viscosity of approximately 2000 Pa*s, which it maintained for approximately 87 minutes, after which the viscosity increased at a moderate rate. The viscosity at 190°C showed a mixture that maintained a stable viscosity of approximately 1300 Pa*s for approximately 47 minutes, after which the viscosity sharply decreased and then quickly increased. It is hypothesized that the crosslinking kinetics increase substantially as temperature increases. As the kinetics increase, contraction of the system during the crosslinking step occurs faster than the rheometer can push the material through the capillary. As a result, there is a period of time before the plunger completely compacts the contracted copolymer prior to observation of

the very sharp, almost discontinuous increase in viscosity that is indicative of a crosslinked system.

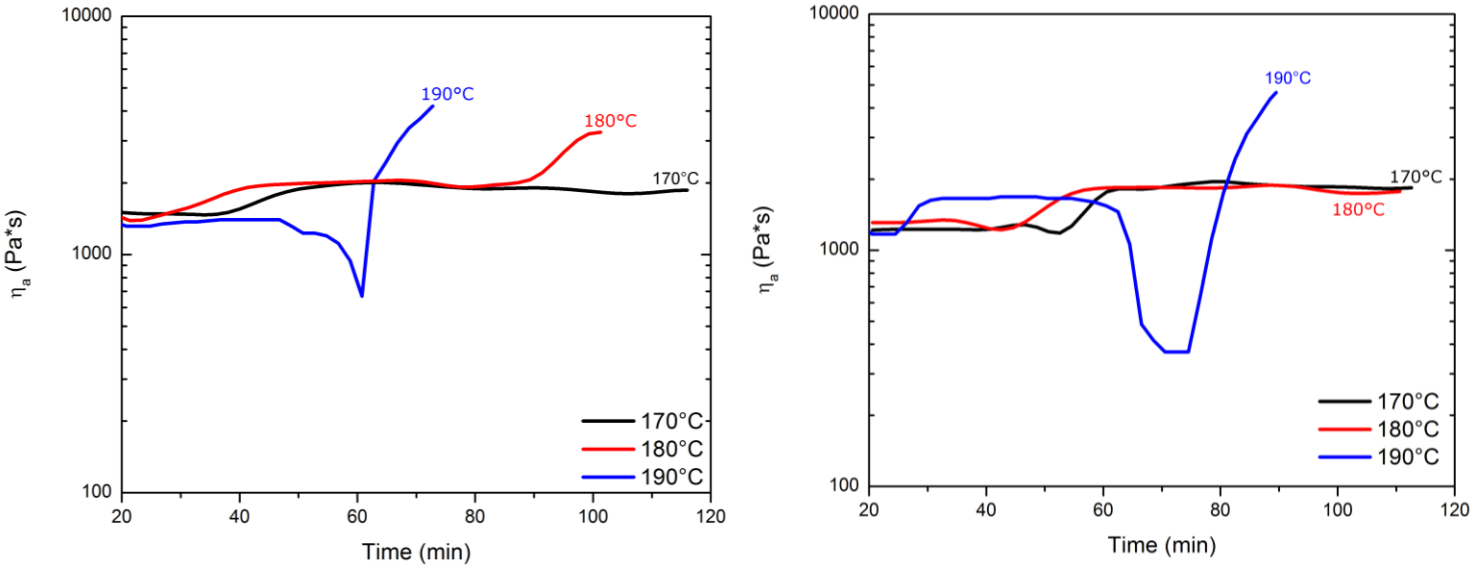

Figure 2.6. (A) Log Viscosity as a function of Time for PAN-MA/ACN/H_2O 70:15:15 wt:wt:wt mixtures. (B) Log Viscosity as a function of Time for PAN-MA/ADPN/H_2O 70:15:15 wt:wt:wt mixtures

Figure 2.6B shows the analogous time dependent apparent viscosity results for PAN-MA/ADPN/H_2O 70:15:15 wt:wt:wt blends at temperatures ranging from 170-190°C. This mixture exhibits similar trends in response to the PAN-MA/ACN/H_2O 70:15:15, except that the relaxation to steady state requires a longer time to reach a viscosity plateau. Additionally, the mixture exhibits a comparable stable time relative to the ACN mixture at 170°C, and a longer stable time than the ACN mixture at both 180 and 190°C. This result confirms the results from isothermal DSC measurements that indicate that PAN-MA mixtures containing ADPN are more stable against thermally induced crosslinking than

mixtures that contain ACN. However, the times observed via capillary viscosity measurements are substantially shorter than isothermal DSC results. DSC measures thermal stability under static flow conditions, while rheometry imposes a constant shear and high pressures. The combined effects of shear and pressure assist in introducing thermally metastable functionalities during the crosslinking reaction, effectively increasing the rate at which the reaction takes place and resulting in an equivalent reduction in stable time.

Overall, time-dependent capillary rheometry indicated that mixtures of PAN-MA, ACN or ADPN, and H_2O can maintain a stable viscosity for over an hour at both 170°C and 180°C. Mixtures containing ADPN prove to be slightly more stable than their ACN counterparts. At 190°C, PAN-MA mixtures containing either ACN or ADPN are thermally metastable and have limited potential extrusion residence time prior to crosslinking. The stability times can be found in Table 2-2.

In order to process polymer melts, one needs knowledge of the shear rate dependence of viscosity to analyze multiple potential processing conditions. Figure 7 illustrates the shear rate dependence of viscosity for mixtures of PAN-MA/H_2O with ACN and ADPN at temperatures ranging from 170-190°C. Residence time was limited based on the results in Figure 6 to ensure that minimal thermally induced crosslinking occurred during the course of the measurements.

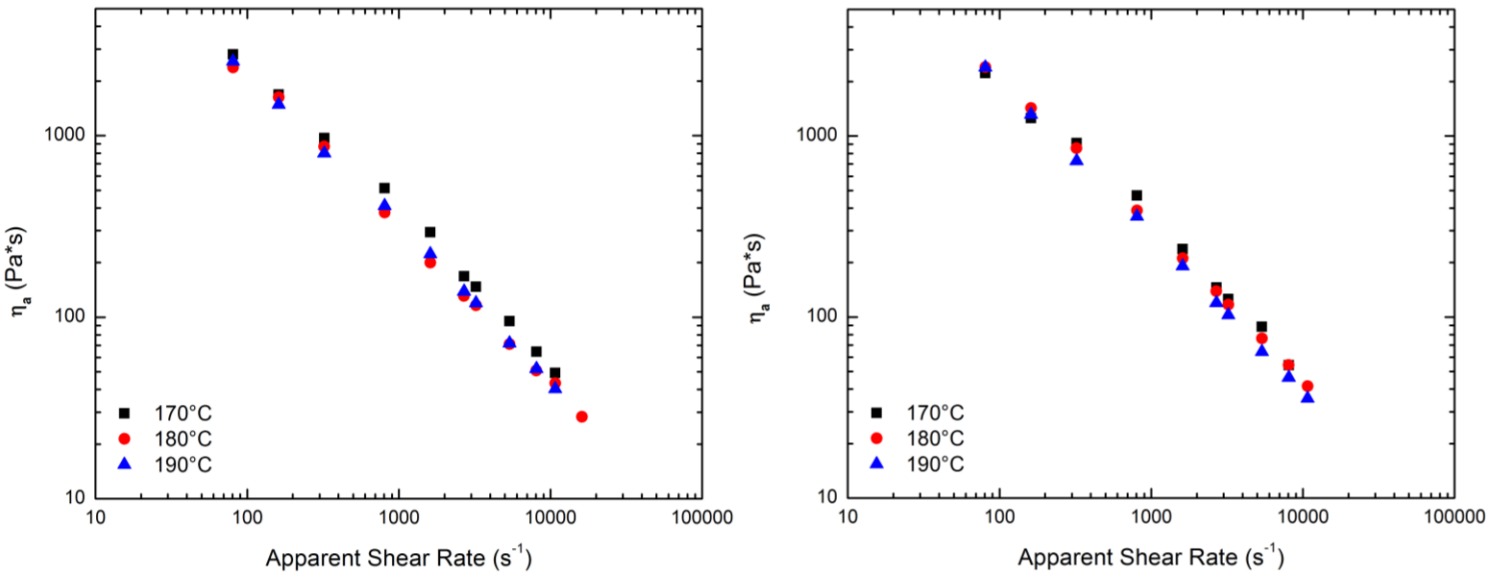

Figure 2.7. (A). Viscosity as a function of Apparent Shear Rate for PAN-MA/ACN/H_2O 70:15:15 wt:wt:wt mixtures. (B) Viscosity as a function of Apparent Shear Rate for PAN-MA/ADPN/H_2O 75:10:15 wt:wt:wt mixtures.

For both materials, the data in Figure 2.7 indicate shear-thinning behavior for these copolymer mixtures at all of the measurement temperatures. Furthermore, in all cases, the data can be fitted by a linear regression with excellent fit; R-squared values are all >0.99. The flow consistency index, m, and the flow behavior index, n, were calculated for both mixtures at all three temperatures using a power law fluid model (equation 2.5) for comparison of the effect of the additives on viscosity at multiple shear rates and temperatures (Table 2-2). The results indicate that the ADPN modifier/H_2O mixture induces more change in the degree of shear thinning as temperature is increased, which is desirable and advantageous for extrusion and increased throughput compared to the ACN modifier/H_2O mixture. However, at 180°C, the ACN/H_2O mixture has a higher degree of shear thinning. Thus the benefit of the temperature-dependent

shear response of ADPN/H_2O is not realized until the mixture is processed above 180°C.

Table 2-2. Stability Times of Melts and Power Law Model Parameters

Copolymer Mixture	Temperature	Stability Time (min)	m	n
PAN-MA/ACN/H_2O 70:15:15	170°C	≥116	115202	0.17
	180°C	87	113611	0.15
	190°C	47	112769	0.15
PAN-MA/ADPN/H_2O 70:15:15	170°C	≥113	81072	0.20
	180°C	≥111	100249	0.16
	190°C	63	106064	0.14

2.4 Conclusions

Properties of blends of multiple small molecule melting point modifiers with a high molecular weight, high acrylonitrile content PAN-MA copolymer have been investigated to assess the potential for melt spinning. Melting point modifiers that contain nitrile functionality, when used synergistically with water, showed the most promise as they lower the T_m of the copolymer most effectively. The resulting melt is stable for ample time to allow melt extrusion as confirmed by isothermal DSC and time-dependent capillary rheometry. Copolymer mixtures containing nitrile melting point modifiers, in combination with water, show a strong time dependence for remaining stable, but do not show a strong temperature dependence on shear-dependent melt viscosity. By fitting the shear-dependent viscosity results to a power law fluid model, the flow consistency index and flow behavior index were determined at temperatures ranging from 170-190°C to compare the impact of the different compositions on rheology and

enable estimation of viscosity at shear rates above those measured via pressurized capillary rheometry. The model results indicate that the ADPN/H_2O mixture has a stronger influence on the temperature dependence of shear thinning, but that the benefit is not realized unless the mixture is processed above 180°C. However, the stability times may be marginal above 180°C and thus, both the ACN/H_2O and ADPN/H_2O mixtures are likely good candidates for further investigations of melt-spinning. The results overall suggest that multiple compositions of the PAN-MA copolymer mixed with water and nitrile-containing melting point modifiers are potentially suitable for melt spinning to produce economical precursor fibers for carbon fiber production.

ACKNOWLEDGMENT OF FUNDING

This research at Virginia Tech and Oak Ridge National Laboratory, managed by UT Battelle, LLC, for the U.S. Department of Energy (DOE) under contract DE-AC05-00OR22725, was sponsored by the Office of Energy Efficiency and Renewable Energy (EERE) Fuel Cell Technologies Office (FCTO) Hydrogen Storage Program.

2.5 References

1. L. H. Peebles, *Journal of Polymer Science Part A: General Papers*, 1965, **3**, 341-351.
2. Z. Bashir, *Polymer*, 1992, **33**, 4304-4313.

3. Z. Bashir, *Journal of Polymer Science Part B: Polymer Physics*, 1994, **32**, 1115-1128.
4. M. Chanda, S. K. Roy., *Plastics Technology Handbook*, Marcel Dekker, Inc., United States of America, Third ed., 1998.
5. M. M. Iovleva, V.N. Smirnova, G. A. Budnitskii, *Fibre Chemistry*, 2001, **33**, 262-264.
6. V. G. Hinrichsen, *Die Angewandte Makromolekulare Chemie*, 1971, **20**, 121-127.
7. H. R. Kricheldorf, *Handbook of Polymer Sythesis: Part A*, Marcel Dekker, Inc., United States of America, 1992.
8. G. Odian, *Principles of Polymerization*, Wiley, United States of America, Fourth ed., 2004.
9. P. Rangarajan, J. Yang, V. Bhanu, D. Godshall, J. E. McGrath, G. Wilkes, D. Baird, *Journal of Applied Polymer Science*, 2002, **85**, 69-83.
10. M. S. Dresselhaus, K. Dresselhaus, Sugihara, I. L. Spain, H. A. Goldberg, *Graphite Fibers and Filaments*, Springer-Verlag, Germany, 1988.
11. *Polymers and polymer composites in construction*, Thomas Telford, Ltd., Great Britain, 1990.
12. D. M. Riggs, R. J. Shuford, R. W. Lewis, *Handbook of composites*, Van Nostrand, New York, 1982.
13. J. B. Donnet, R. C. Bansal, *Carbon Fibers*, Marcel Dekker, New York, 1984.
14. M. J. Bortner, V. Bhanu, J. E. McGrath, D. G. Baird, *Journal of Applied Polymer Science*, 2004, **93**, 2856-2865.
15. J. B. Donnet, R. C. Bansal, *Carbon Blacks: Physics, Chemistry, and Elastomer Reinforcement*, Marcel Dekker Inc., New York, 1976.
16. A. F. Ismail, *Journal of Analytical and Applied Pyrolysis*, 2012, **93**, 1-13.
17. A. Mustafa, *Polymer Degradation and Stability*, 2007, **92**, 1421-1432.
18. A. Carmichael, Man-Made Fibers Continue To Grow, http://www.textileworld.com/textile-world/fiber-world/2015/02/man-made-fibers-continue-to-grow/, (accessed 3/8/2017, 2017).
19. B. G. Min, T. W. Son, B. C. Kim, C. J. Lee, W. H. Jo, *Polymer Journal*, 1992, **24**, 841-848.
20. W. R. Krigbaum, N. Tokita, *Journal of Polymer Science*, 1960, **XLIII**, 467-488.
21. B. G. Min, T. W. Son, B. C. Kim, C. J. Lee, W. H. Jo, *Journal of Applied Polymer Science*, 1994, **54**, 457-462.
22. P. Rangarajan, V. Bhanu, D. Godshall, G. L. Wilkes, J. E. McGrath, D. G. Baird, *Polymer*, 2002, **43**, 2699-2709.
23. T. Mukundan, V. A. Bhanu, K. B. Wiles, H. Johnson, M. J. Bortner, D. G. Baird, A. K. Naskar, A. A. Ogale, D. D. Edie, J. E. McGrath, *Polymer*, 2006, **47**, 4163-4171.

24. B. L. Batchelor, S. F. Mahmood, M. Jung, H. Shin, O. V. Kulikov, W. Voit, B. M. Novak, D. J. Yang, *Carbon*, 2016, **98**, 681-688.
25. V. A. Bhanu, P. Rangarajan, K. Wiles, M. Bortner, M. Sankarpandian, D. Godshall, T. E. Glass, A. K. Banthia, J. Yang, G. Wilkes, D. Baird, J. E. McGrath, *Polymer*, 2002, **43**, 4841-4850.
26. *US Pat.,* 2,585,444, to Charles D. Coxe of E I du Pont de Nemours and Co., 1952.
27. *US Pat.,* 4,163,770, to Harold Porosoff of American Cyanamid Co., 1979.
28. *US Pat.,* 3,984,601, to Robert Alan Blickenstaff of E I du Pont de Nemours and Co., 1976.
29. *US Pat.,* 3,634,575, to George Allibone Serad of Celanese Corp., 1972.
30. *US Pat.,* 5,168,004, to G. P. Daumit, Y. S. Ko, C. R. Slater, J. G. Venner, C. C. Young or BASF SE, 1992.
31. M. J. Bortner, D. G. Baird, *Polymer*, 2004, **45**, 3399-3412.
32. S. Liu, K. Han, L. Chen, Y. Zheng, M. Yu, *Polymer Engineering and Science*, 2015, 2722-2728.
33. C. W. Macosko, *Rheology: principles, measurements, and applications*, VCH, New York, NY, 1994.
34. K. B. Wiles, Master of Science, Virginia Polytechnic Institute and State University, 2002.
35. E. A. Morris, M. C. Weisenberger, S. B. Bradley, M. G. Abdallah, S. J. Mecham, P. Pisipati, J. E. McGrath, *Polymer*, 2014, **55**, 6471-6482.
36. E. A. Morris, M. C. Weisenberger, M. G. Abdallah, F. Vautard, H. Grappe, S. Ozcan, F. L. Paulauskas, C. Eberle, D. Jackson, S. J. Mecham, A. K. Naskar, *Carbon*, 2016, **101**, 245-252.
37. C. R. Bohn, J. R. Schaefgen, W. O. Statton *Journal of Polymer Science*, 1961, **55**, 531-549.
38. V. F. Holland, S. B. Mitchell, W. L. Hunter, P. H. Lindenmeyer, *Journal of Polymer Science*, 1962, **62**, 145-151.
39. R. Chiang, *Journal of Polymer Science: Part A: Polymer Chemistry*, 1963, **1**, 2765-2775.
40. Y. Furushima, M. Nakada, H. Takahashi, K. Ishikiriyama, *Polymer*, 2014, **55**, 3075-3081.
41. R. M. Gohil, K. C. Patel, R. D. Patel, *Colloid & Polymer Sci.*, 1976, **254**, 859-867.
42. O. Celebi, C. H. Lee, Y. Lin, J. E. McGrath, J. S. Riffle, *Polymer*, 2011, **52**, 4718-4726.
43. G. L. Wilkes, *Journal of Chemical Education*, 1981, **58**, 880-892.

1992, **33**, 4304-4313.

Chapter 3: Effect of UV Irradiation and Physical Aging on O_2 and N_2 Gas Transport Properties of Thin Glassy Polyarylene Ether Films Based on Tetramethyl Bisphenol A and 4,4'-difluorobenzophenone

Qiang Liu,[1] Andrew T. Shaver,[2] Yu Chen,[2] Gregory Miller,[2]

Donald R. Paul,[1] J. S. Riffle,[2] James E. McGrath,[2] and Benny D. Freeman[1]*

[1]Department of Chemical Engineering, Texas Materials Institute, Center for Energy and Environmental Research, The University of Texas at Austin, 10100 Burnet Road, Bldg. 133, Austin, TX 78758, USA

[2]Department of Chemistry, Macromolecules Innovation Institute, Virginia Tech, Blacksburg, VA 24061, USA

Liu, Q.; Shaver, A. T.; Chen, Y.; Miller, G.; Paul, D. R.; Riffle, J. S.; McGrath, J. E.; Freeman, B. D., Effect of UV irradiation and physical aging on O_2 and N_2 transport properties of thin glassy poly(arylene ether ketone) copolymer films based on tetramethyl bisphenol A and 4,4'-difluorobenzophenone. *Polymer* **2016,** *87*, 202-214.

3.1 Introduction

Polymers with high permeability, high selectivity, and long term stability are desired for gas separation applications. However, the inherent non-equilibrium state of glassy polymers causes physical properties, including gas transport properties, to drift with time towards a seemingly unattainable equilibrium in a process known as physical aging.[1, 2] As polymer chains undergo self-retarding reorganization in the glassy state, polymer segmental mobility decreases due to free volume reduction.[2] Consequently, gas permeability

generally decreases and selectivity increases with aging.[3-5] Several studies have demonstrated the influence of physical aging on gas transport properties of thick films (> 1 μm).[6-9] Interestingly, as film thickness decreases into the range (~0.1 μm[10-12]) relevant for commercial gas separation membranes, gas permeability decreases more rapidly, suggesting accelerated aging in thin films relative to that in thick films.[3, 13, 14] This phenomenon is still not completely understood, but it is believed to be connected to differences in polymer chain mobility at the surface versus that in the bulk of the films. As thickness decreases, from the tens of microns often used in initial screening of gas transport properties to 100 nm or less, surface to volume ratio increases enormously, so the influence of surface properties of such thin films becomes much more important.

One route to modifying existing polymers to achieve better gas separation properties is via crosslinking. Introducing crosslinks into some polymers can improve selectivity without a significant loss in permeability.[15] Crosslinking reactions may occur by either step-growth polymerization, such as reaction of an amine reactant with an epoxy reagent at elevated temperature [16, 17], or by chain-growth polymerization, which can be activated thermally or by irradiation, such as exposure to UV light.[18, 19] For example, Kita et al. studied the effect of UV irradiation on gas transport properties of a benzophenone-containing polyimide prepared from 3,3′, 4,4′-benzophenone tetracarboxylic dianhydride (BTDA) and 2,4,6-trimethyl-1,3-phenylene-diamine (TMPD).[15] After 30 minutes of irradiation in air, the H_2/CH_4 selectivity of BTDA-TMPD increased by a factor of 50, whereas the H_2 permeability decreased by a factor of only 5. Kita et al.

concluded that the selectivity increase upon UV exposure was mainly due to changes in gas diffusion coefficients.[15] Similar observations were reported in a study involving polyarylates.[20] In these studies, polymer film thicknesses on the order of tens of microns were used. However, the UV penetration depth of thick aromatic polymer films may be small, thereby promoting crosslinking at and near the film surface. This may lead regions of varying crosslinking in the films with little or no crosslinking in the center, yielding non-uniform crosslinking throughout the film.[20, 21] McCaig et al. investigated the influence of UV irradiation in N_2 and physical aging on gas transport properties of thin polyarylate films (≤ 1 μm). Both crosslinking and aging decreased gas permeability and increased selectivity, but the gain in selectivity from crosslinking was more pronounced than that due to aging. In addition, crosslinked samples exhibited slower aging than uncrosslinked samples, and this effect was attributed to the lower free volume of the crosslinked samples.[22] From a fundamental perspective, it is of interest to study uniformly irradiated samples, but the thicknesses required (~ <1 μm) are be in the range where physical aging effects become significant. Careful experimental design must be implemented to differentiate these effects.

The irradiation environment can also influence gas transport properties. Meier et al. investigated the effect of UV irradiation in air or N_2 on permeation properties of a non-crosslinkable polyimide.[23, 24] Pure-gas O_2/N_2 selectivity increased by 80% after the sample was irradiated in air for 30 minutes. However, the O_2/N_2 selectivity did not change after UV irradiation in N_2. FTIR analysis

revealed that photooxidation products, such as hydroxyl and carbonyl groups, formed in the sample irradiated in air, but not in the N_2-irradiated sample. Meier et al. concluded that photooxidation induced polymer densification and polar group introduction at the surface. These polar groups can interact via hydrogen bonding, lower polymer free volume, and increase gas selectivity. Similar photooxidative effects were observed in other studies involving both non-crosslinkable and crosslinkable polyimides.[25-27]

This study investigated the influence of UV irradiation and physical aging on gas transport properties of ultra-thin glassy poly(arylene ether ketone) (PAEK) films (l ~ 150 nm) prepared from tetramethyl bisphenol A (TMBPA) and 4,4'-difluorobenzophenone (DFBP). The chemical structure and bulk properties of TMBPA-BP are presented in Table 1. This polymer was chosen because the tetramethyl substitution helps to reduce the efficiency of polymer chain packing, thereby increasing the polymer free volume and improving gas permeability and provide an abundant source of benzylic methyl groups useful in crosslinking reactions.[28] In addition, the benzophenone moiety is a well-known photosensitizer that can be excited upon irradiation at 250-370 nm to initiate crosslinking between polymer chains.[29, 30] The uniformity of crosslinking throughout the sample depth was estimated using UV-Vis spectroscopy, and the progress of crosslinking and photooxidation was monitored using Fourier transform infrared spectroscopy (FTIR). The effects of irradiation time, irradiation environment (air vs. N_2), and irradiation wavelength (254 nm vs. 365 nm) on gas transport properties and aging behavior were explored.

Table 3-1. Bulk material properties of uncrosslinked TMBPA-BP.

Polymer	T_g (°C)	Density (g/mL)	FFV	Permeability (Barrer)[1]		Selectivity O_2/N_2[1]
				O_2	N_2	
TMBPA-BP 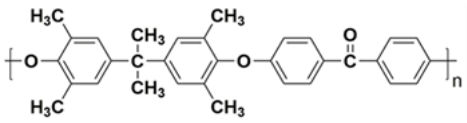	215	1.092	0.167	4.5	0.84	5.4

(Table used with permission from Elsevier).

[1]Gas transport properties measured at 35°C and 10 atm.

3.2 Experimental

3.2.1 TMBPA-BP Synthesis

Sulfuric acid, acetic acid and acetone were purchased from Spectrum (New Brunswick, NJ, USA) and used as received. N-methyl-2-pyrrolidone (NMP) was also purchased from Spectrum and was vacuum distilled over calcium hydride before use. 4,4′-Difluorobenzophenone (DFBP) was kindly donated by Solvay and recrystallized from 2-propanol. Methylene chloride and potassium carbonate were purchased from Fisher Scientific (Pittsburg, PA, USA) and dried at 150°C under vacuum before use. Toluene and 2,6-dimethylphenol (2,6-xylenol) were purchased from Sigma-Aldrich (St. Louis, MO, USA) and used as received.

The synthesis of tetramethyl bisphenol A (TMBPA) was adapted from the synthesis procedure for tetramethyl bisphenol F.[31] Acetone (7.103 g, 122 mmol)

and 2,6-xylenol (18.92 g, 155 mmol) were added to a two-neck 250 mL round bottom flask fitted with a mechanical stirrer and an addition funnel. The solution was well stirred and cooled to 15°C in an ice bath. A solution of sulfuric acid (16.304 g, 0.163 mol) and acetic acid (17.392 g, 0.290 mol) was mixed, chilled to 15°C, and added dropwise to the reaction flask via the addition funnel. The reaction mixture was maintained at room temperature overnight, diluted with 100 mL of water and 150 mL of methylene chloride, and then transferred to a separatory funnel. The organic layer was washed with deionized water three times before collection. The methylene chloride layer was dried over magnesium sulfate overnight and then evaporated to yield the crude product. The product was recrystallized from toluene. Yield was 70%. This synthesis procedure was performed twice to provide sufficient amounts of monomer for TMBPA-BP synthesis.

TMBPA (29.362 g, 103.2 mmol) and DFBP (22.527 g, 103.2 mmol) were added to a three-neck 500 mL round bottom flask equipped with a mechanical stirrer, a condenser, a nitrogen inlet and a Dean-Stark trap. NMP (300 mL) was added to the flask, and the mixture was stirred to obtain a clear solution. Afterwards, K_2CO_3 (16.408 g, 118.7 mmol) was added, followed by 150 mL of toluene. The reaction bath was heated at 155°C for 4 h to azeotropically remove the water and toluene, kept at 150°C for 12 h, and then cooled to room temperature. The reaction mixture was filtered to remove any excess K_2CO_3 or by-product salts and precipitated in 1000 mL of deionized water. The resulting polymer was stirred in deionized water at 80°C overnight and then dried under

vacuum at 110°C for at least 48 h. The yield of TMBPA-BP was 81%. At 35°C, which is the temperature used for both aging and permeation experiments in this study, TMBPA-BP is deep within its glassy state (about 180°C below its T_g, as shown in Table 3-1).

3.2.2 Film Preparation

In general, to avoid rapid evaporation of solvent during spin coating, solvents with high boiling points (>100°C) and low vapor pressures are preferred [3, 4, 32]. For this reason, toluene was used in this study. Film thickness was controlled by varying the solution concentration, typically between 2 and 3 wt%. About 15 mL of polymer solution was prepared and filtered through 5 μm, 0.45 μm, and 0.1 μm Puradisk™ PTFE syringe filters (Whatman, Pittsburg, PA, USA) in that order to remove dust or particulates. Afterwards, the solution was sonicated for 30 min to remove dissolved air bubbles, since air bubbles can introduce pinhole defects in thin films [32].

Thin films were prepared by spin coating the polymer solution onto silicon wafers (Nova Electronics Materials, Flower Mound, TX, USA) at 1000 rpm for 3 min. Next, the silicon wafer was placed on a hot plate and heated at 130°C for 3 min to remove residual solvent. To avoid dust and particulates in the environment, spin coating was performed inside a class 100-1000 clean room. Film thickness was measured using a variable angle spectroscopic ellipsometer (VASE) (M2000D, J. A. Woollam Co., Lincoln, NE, USA), and the Cauchy model

was used to fit the psi (ψ) and delta (δ) parameters taken at three different angels (65, 70, and 75 degrees) over a wavelength range of 450 nm – 1000 nm.[4, 12, 14, 32]

A primary challenge in fabricating thin films is the presence of microscopic pinhole defects, which can compromise gas selectivity and render the film useless for gas separation characterization.[14, 33] To mitigate this problem, a second layer of highly permeable polymer, such as PDMS, is often coated onto the selective layer to block the pinholes and, thus, the selectivity-destroying convective flow.[14, 34-36] This practice of "caulking" the defects was initially employed in industry to treat hollow fiber membranes [34-37], and only recently was used to study the influence of physical aging on gas transport properties of ultra-thin (<400 nm) films.[12, 14, 33, 38] At the aging temperature used for this study, PDMS is about 150 °C above its T_g.[14] Therefore, it will not undergo physical aging.[13, 14] In addition, the PDMS layer, with a thickness typically in the range of 5-6 μm, can also provide mechanical support to the relatively fragile selective layer. Rowe et al. [14] and Cui et al. [12] demonstrated that PDMS does not significantly change the gas transport properties of the thin glassy polymers under study.

A PDMS solution was prepared by mixing Wacker Silicones Corporation Dehesive 944 and cyclohexane in a 2:3 ratio by mass and then adding a crosslinking agent (V24) and proprietary catalyst (OL) as described elsewhere [32, 33]. After the glassy polymer thickness was measured using an ellipsometer, the PDMS/cyclohexane solution was spun onto the glassy polymer at 1000 rpm for 1 min. The wafer was then heated to 115°C for 15 min to fully crosslink the

PDMS. The PDMS layer thickness was measured using a Dektak 6M stylus profilometer (Veeco, Plainview, NY, USA).

The bilayer film was lifted from the wafer using deionized water and transferred to a thin rectangular copper wire (Cat# 2781345, Radioshack, Austin, TX, USA). The free-standing thin film was then annealed at 233°C (~ 15°C above T_g) for 5 min in a HP 5890 gas chromatograph (GC) oven under an ultra-high purity nitrogen purge to erase thermal history and orientation effects.[4] The start of the aging process (t = 0) is defined as the time when the thin film was removed from the GC oven and rapidly quenched to ambient conditions.

3.2.3 UV-Vis Spectroscopy

Ultraviolet-visible spectroscopy (UV-Vis) was performed using an Agilent Cary 5000 UV-Vis-NIR spectrophotometer (Santa Clara, CA, USA). Free-standing films were attached to a sample holder and covered an aperture through which light at various wavelengths passed through. Absorbance was measured at wavelengths ranging from 200-800 nm at 600 nm/min.

3.2.4 FTIR

FTIR was performed using a Thermo Nicolet 6700 spectrometer equipped with a DTGS detector. Samples were tested in the transmission mode with a resolution of 4 cm^{-1} and 256 scans per sample.

3.2.5 UV Irradiation

Thin film samples were irradiated in air or N_2 for various amounts of time on each side using either a UV crosslinker (XL-1000, Spectronics, Westbury, NY, USA) equipped with 254 nm light filter bulbs or a 100W high pressure mercury arc UV lamp (Blak-Ray B-100, UVP, Upland, CA, USA) equipped with a 365 nm light filter bulb. Samples were placed 12 cm from the bulbs in the UV crosslinker and 4 cm from the bulb of the UV lamp. The UV intensity, monitored using a radiometer (Part# 97-0015-02, UVP, Upland, CA, USA), was 6.55 mW/cm^2 for the UV crosslinker and 16.7 mW/cm^2 for the UV lamp. For irradiation in N_2, both the crosslinker and the UV lamp were placed inside a glove box (Cat# 50601-00, Labconco, Kansas City, MO, USA). Prior to UV irradiation, the glove box was purged with N_2 (UHP grade, Airgas, Austin, TX, USA) until the O_2 level was below 0.1% by volume, which was monitored using an oxygen sensor (Part# 9452, Nuvair, Oxnard, CA, USA). At 254 nm, films were irradiated up to 10 min (5 min/side) in air and 20 min (10 min/side) in N_2. Samples irradiated for longer times were not mechanically stable for any characterization experiments.

3.2.6 Gas Permeation

The influence of physical aging (up to approximately 1000 hours) on O_2 and N_2 permeation properties of uncrosslinked and UV-irradiated thin films was investigated. Permeability coefficients were measured at 35°C and an upstream

pressure of 2 atm using a constant-volume, variable-pressure permeation apparatus built in house.[39] Thin films were supported on a 0.02 μm AnoPore membrane disc (Cat# 6809-5502, Whatman, Maidstone, England) and masked on both sides with aluminum tape, as described previously [33]. The mass transfer resistance from the PDMS layer can be accounted for using the series resistance model as follows [14, 40]:

$$\frac{l_{composite}}{P_{composite}} = \frac{l_{PDMS}}{P_{PDMS}} + \frac{l_{Glassy}}{P_{Glassy}} \quad (3.1)$$

where l_{PDMS}, l_{Glassy}, and $l_{composite}$ are the thicknesses of the PDMS layer, the underlying selective layer, and the overall composite (l_{PDMS} + l_{Glassy}), respectively. Accordingly, P_{PDMS}, P_{Glassy}, and $P_{composite}$ are the permeability coefficients of PDMS, the glassy polymer, and the composite structure, respectively. Permeability coefficients of gases in PDMS do not change with time, and these permeability coefficients were obtained from the literature.[14] Permeability of gases in both the uncrosslinked and UV-irradiated TMBPA-BP thin films was calculated using Equation (3.1). When polymer samples were not installed in the gas permeation systems for permeation experiments, they were shielded from light and allowed to age inside a dark gas chromatograph (GC) oven at 35°C.

3.3 Results and Discussion

3.3.1 UV Irradiation Uniformity

One general question with UV crosslinking is the crosslinking uniformity through the sample. In the thin films considered in this study, we cannot

directly measure the extent of crosslinking as a function of depth into the sample. However, we can estimate the uniformity of UV irradiation throughout the sample. Presumably, more uniform irradiation throughout the sample will contribute to more uniform crosslinking. The UV intensity at any point in a film, *I*, can be estimated using the Beer-Lambert law [20]:

$$I = I_0 \times 10^{-ECD} = I_0 \times 10^{-A} \qquad (3.2)$$

where I_0 is the incident UV intensity, E is the extinction coefficient, C is the concentration of photoactive species in the film, D is the path length, and A is the absorbance. As UV irradiation penetrates deeper into a film, its intensity will decrease due to absorption. If there is a sharp gradient of UV intensity between the surface and the center of a film, the resulting crosslinking may not be uniform. For such non-uniformly crosslinked material, the measured gas permeability does not represent the intrinsic property of a homogeneously crosslinked polymer and, therefore, cannot be directly compared with the permeability of homogeneously uncrosslinked samples or other non-uniformly crosslinked samples.

Fig. 3.1 A presents the UV-VIS spectra of TMBPA-BP films of different thicknesses. A strong band at ~200 nm represents the π→π* transition associated with the benzophenone excitation, and a weaker band at ~280 nm represents the n→π* transition.[29] As film thickness decreases, the absorbance at 254 nm (i.e., one of the crosslinking wavelengths considered) decreases. Because the product of EC is a material property and is, therefore, independent

of film thickness, absorbance should be linearly correlated with film thickness, as shown in Fig. 3.1 B. Using Equation (3.2), relative UV intensity at any depth in a film can be calculated. Fig. 3.1 C shows a calculated profile of relative UV intensity for TMBPA-BP films of different thickness. Normalized film thicknesses of 0 and 1 correspond to the two surfaces of a film. Because each film was irradiated on both sides, the calculated UV intensity profile has a parabolic shape. To obtain a uniformly irradiated sample, the film needs to be thin enough so that the UV intensity at the center of the film is similar to that at the surface. As shown in Fig. 3.1 C, the profile becomes more uniform as film thickness decreases. For example, for a 259 nm TMBPA-BP film, there is a 32% difference between the UV intensity at the surface and center of the film. For a 145 nm film, there is only a 14% difference between the UV intensity at the surface and center of the film. Hypothetically, films thinner than 145 nm would have even more uniform irradiation, but to consistently make defect-free films at such thicknesses is very difficult. As a result, films of around 145 nm were used for this study to balance the competing needs for relatively uniform

irradiation and the practicality of making defect-free films.

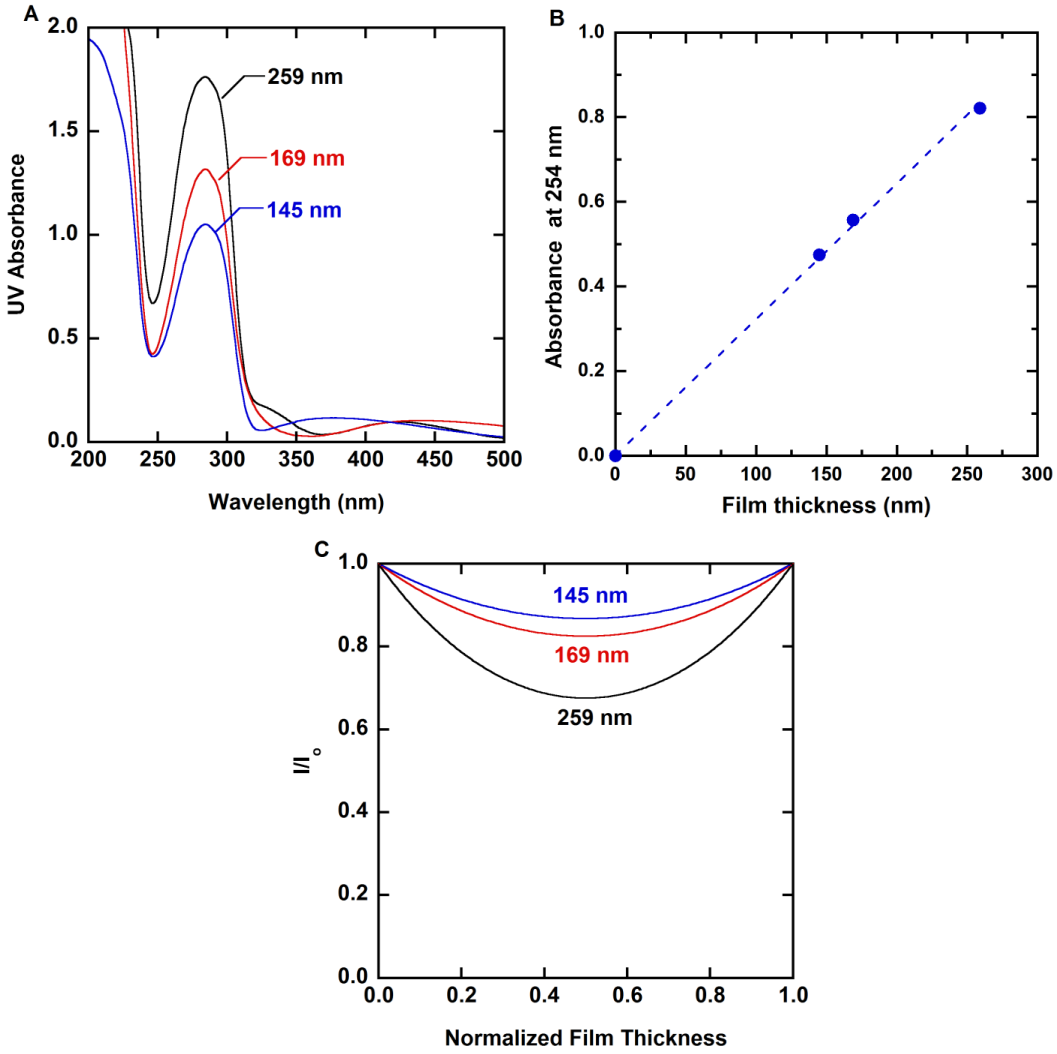

Fig. 3.1. (A) Effect of film thickness on UV-Vis spectra of TMBPA-BP films. (B) Effect of film thickness on UV absorbance at 254 nm. (C) Calculated UV intensity profile at 254 nm in TMBPA-BP films of various thicknesses. (Figure used with permission from Elsevier).

Because PDMS is coated onto the glassy polymer to prevent pinhole formation, one question is whether the PDMS layer may significantly shield the UV light from the underlying glassy polymer, thereby affecting the irradiation uniformity in the glassy polymer. Fig. 3.2 A presents the UV-Vis spectrum of a

TMBPA-BP film (l=145 nm) and a crosslinked PDMS film (l = 6 μm). The absorbance for PDMS is very low at wavelengths above 250 nm. At an irradiation wavelength of 254 nm, the PDMS absorbance (0.069) is 85% lower than that of the TMBPA-BP thin film (0.475). Fig. 3.2 B presents the calculated

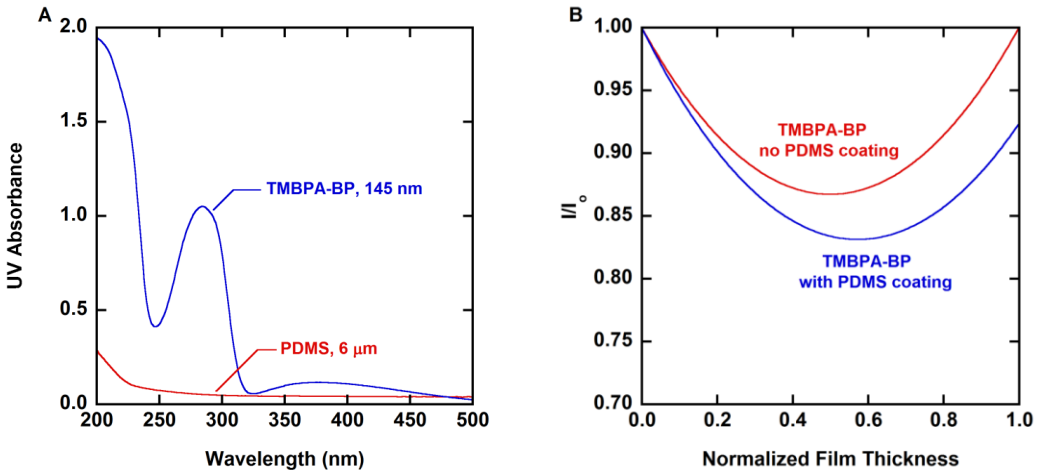

Fig. 3.2. (A) UV-Vis spectra for TMBPA-BP and PDMS. (B) Calculated UV intensity profile at 254 nm in TMBPA-BP films (l = 145 nm) with and without a PDMS coating. (Figure used with permission from Elsevier).

UV intensity profile at 254 nm for TMBPA-BP films with or without PDMS coating. Because the PDMS coating is applied to only one side of the film (at normalized film thickness = 1 in Fig. 3.2 B), the addition of PDMS skews the UV profile slightly away from the center. The maximum difference in UV intensity between the film surface and the interior is 14% for the TMBPA-BP film without a PDMS coating and 17% for the film with a PDMS coating. Therefore, the influence of the PDMS layer on UV irradiation uniformity is believed to be small.

Additionally, UV treatment at 254 nm and 365 nm is not expected to change the physical and gas transport properties of PDMS. PDMS is generally stable against UV irradiation at wavelengths above 200 nm.[41, 42] Below 200 nm, UV irradiation in air can promote ozone formation, which may induce polymer chain scission and oxidation of PDMS to SiO_2 at the polymer-air interface, thereby affecting PDMS physical properties.[42-44] However, at irradiation wavelengths considered in this study (i.e., 254 nm and 365 nm), UV absorbance in PDMS is small (c.f., Fig. 3.2 A). Because light must be absorbed for photochemical reaction to take place (i.e., the Grotthuss-Draper law),[45] little photochemical activities, and thereby physical property changes, are expected at 254 nm and 365 nm.

Because UV absorbance at 365 nm is much lower than that at 254 nm (cf., Fig. 3.1 A), irradiation at 365 nm is more uniform than that at 254 nm. For example, the absorbance of a 145 nm thick TMBPA-BP film at 365 nm (0.112) is 76% lower than that at 254 nm (0.475). As a result, at 365 nm, the difference between UV intensity at the surface and center of a 145 nm thick film is less than 1%, resulting in a uniformly irradiated sample.

3.3.2 Crosslinking and Photooxidation Mechanism

Crosslinking and photooxidation reactions via UV irradiation of benzophenone-containing polymers have been reported.[23, 24, 46] Based upon these literature studies, Fig. 3.3 presents the expected mechanism of these reactions. Upon irradiation at 250-370 nm, benzophenone (BP) can be excited

and undergoes hydrogen abstraction to yield carbon-centered radicals and benzylic radicals (1). If oxygen is present, benzylic radicals (**D**) can rapidly react with oxygen to form peroxy radicals (**E**), which can then abstract another hydrogen to form peroxides (**F**). Further UV irradiation and subsequent hydrogen abstraction can decompose the peroxides and generate alkoxy radicals (**G**) and hydroxides (**H**) (2).

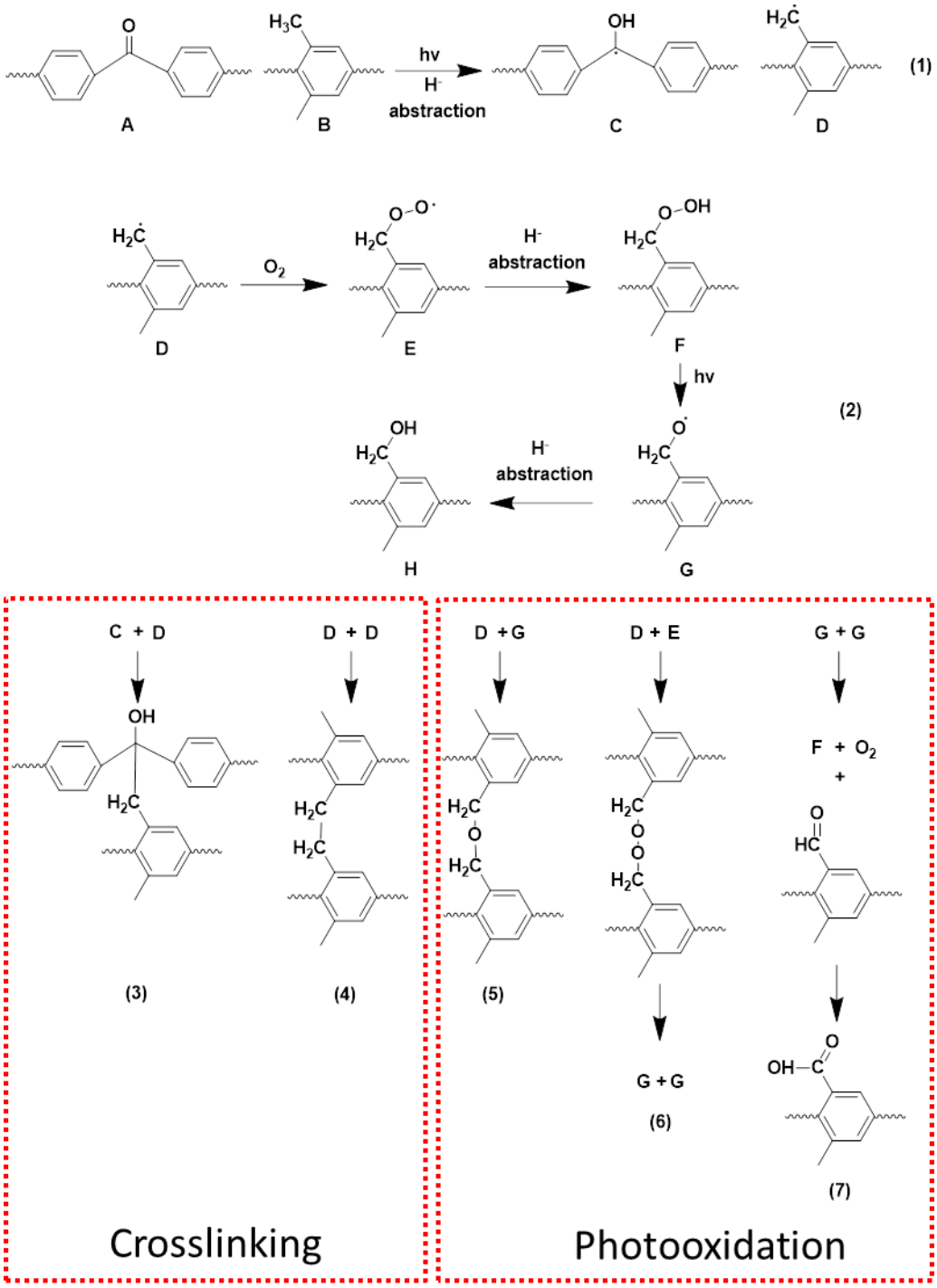

Fig. 3.3. Expected mechanism of UV-induced crosslinking and photooxidation.[23, 24, 46] (Figure used with permission from Elsevier).

Afterwards, radicals can couple according to either the crosslinking or photooxidation pathway, as outlined in Fig. 3.3. For crosslinking reactions,

benzylic radicals can couple with other carbon-centered radicals (reaction 3) or benzylic radicals (reaction 4) to form crosslinks between polymer chains. McCaig et al. speculated, based on CPK models, that steric hindrance can potentially limit the benzylic-carbon radical coupling (reaction 3).[22] Therefore, coupling between benzylic pendent groups (reaction 4) is a more likely scenario, although this has not been proven.

Photooxidation reactions can occur via coupling of oxidation intermediates, according to reactions 5-7. For example, benzylic radicals (**D**) can couple with either alkoxy (**G**) or peroxy (**E**) radicals to form aliphatic ethers (reaction 5) or peroxides (reaction 6), respectively. However, because peroxides are typically not stable, they tend to rapidly dissociate to yield more alkoxy radicals (reaction 6). Finally, alkoxy radicals (**G**) can couple with other alkoxy radicals (**G**) to form aldehydes, which can be subsequently oxidized to carboxylic acids (reaction 7). Interactions among these polar groups, e.g., hydrogen bonding, etc., can potentially increase interchain cohesion, thereby decreasing polymer free volume and increasing gas selectivity.[24]

3.3.3 FTIR Characterization

Figs 3.4 A-3.4 C present FTIR spectra of TMBPA-BP films before and after UV irradiation at different conditions. In all spectra, the peak at around 1650 cm^{-1} corresponds to the carbonyl group in the benzophenone moiety, and the peak near 1600 cm^{-1} is attributed to the stretching of substituted benzene moieties.[46, 47] The intensity of each spectrum was normalized using the peak at

1600 cm^{-1} as an internal reference, which was assumed to not change with UV irradiation. In Fig. 3.4 A and 3.4 B, the carbonyl peak intensity at 1650 cm^{-1} decreases with increasing UV irradiation time. Concomitantly, a broad band at around 3500 cm^{-1}, attributed to the stretching of hydroxyl groups generated via crosslinking and/or photooxidation,[25, 47] is formed and increases with increasing UV irradiation time. In the spectra of samples irradiated in air at 254 nm (Fig. 3.4 A and 3.4 C), a broad feature at ~1730 cm^{-1}, which corresponds to C=O stretching from aldehydes and carboxylic acids generated from photooxidation, emerges and increases in intensity with increasing irradiation time. Interestingly, this band was also observed in the spectra of certain N_2-irradiated samples (e.g., "20, N_2", Fig. 3.4 B). As described in the Experimental section, the glove box was purged with N_2 until the O_2 level was below 0.1% by volume. Low levels of residual oxygen in the predominantly N_2 atmosphere might have initiated low levels of photooxidation, especially for samples irradiated for relatively long times. Interestingly, as shown in Fig. 3.4 C, both air- and N_2-irradiated samples at 365 nm have similar IR spectra, so the irradiation environment may not significantly influence the polymer structure at this irradiation wavelength for the irradiation times considered.

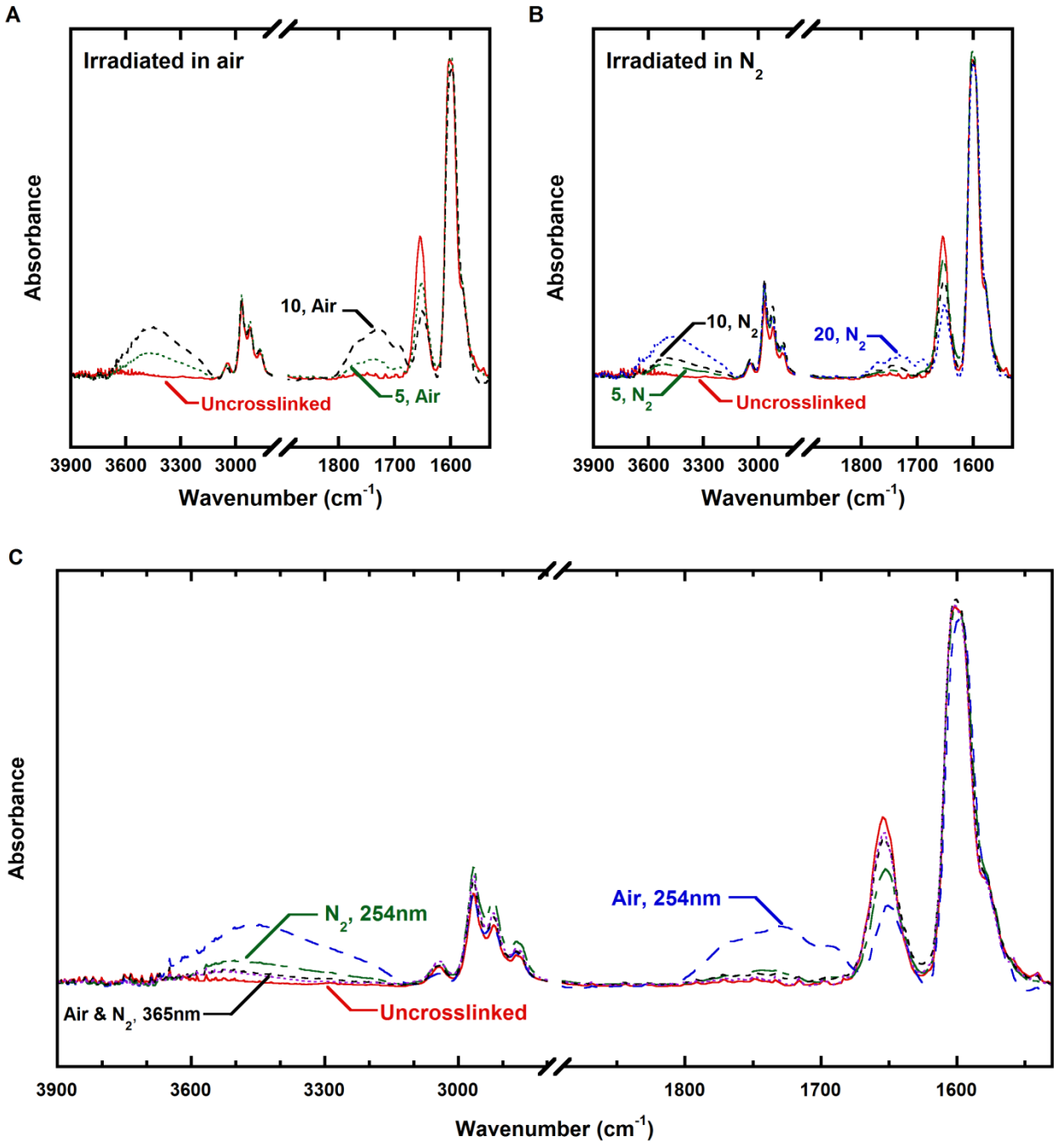

Fig. 3.4. FTIR spectra of TMBPA-BP films before and after UV irradiation. Samples in (A) and (B) were irradiated at 254 nm and are designated by the irrdiation time (in min) and the irrdiation environment. Samples in (C) were irradiated for 10 min (5 min/side) and are designated by the irradiation environment and irradiation wavelength. All samples were 150-170 nm thick. (Figure used with permission from Elsevier).

The progress of crosslinking and/or photooxidation can be monitored by tracking the benzophenone peak intensity (1650 cm^{-1}) decreases in the FTIR spectra with irradiation. Fig. 3.5 presents the relative BP intensity as a function of irradiation time. The relative intensity was calculated by dividing the BP intensities of irradiated samples by that of the uncrosslinked sample. As irradiation time increases, the relative BP intensity decreases as BP undergoes photoreactions to form crosslinks or photooxidative products. Because air-irradiated samples undergo photooxidation in addition to crosslinking, they experience a greater reduction in BP intensity than N_2-irradiated samples. For example, after irradiation at 254 nm for 10 min, the relative BP intensity of an air-irradiated sample is 33% lower than that of a N_2-irradiated sample. In addition, for a fixed irradiation environment and time, irradiating at 254 nm results in lower BP intensities than irradiating at 365 nm, suggesting that UV irradiation at 254 nm leads to a greater extent of crosslinking and/or photooxidation than irradiation at 365 nm. A more detailed discussion of effects of different irradiation wavelengths on properties is provided in Section 3.3.5.

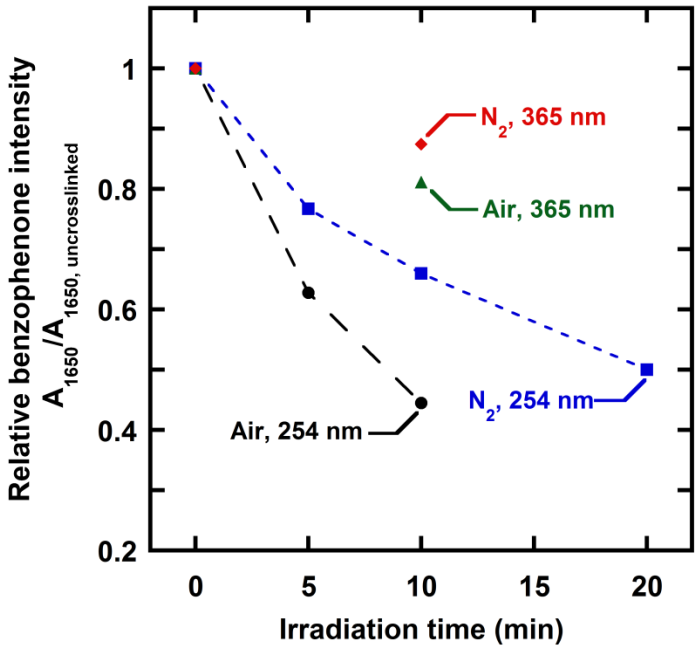

Fig. 3.5. Relative FTIR intensities of the benzophenone peak at 1650 cm^{-1} as a function of irradiation time, irradiation wavelength, and irradiation environment. The ratio of A_{1650} to A_{1600} for the uncrosslinked sample is normalized to unity. (Figure used with permission from Elsevier).

3.3.4 Influence of Irradiation Time and Environment on Physical Aging and Gas Transport Properties

Fig. 3.6 presents O_2 permeability (Fig. 3.6 A) and relative O_2 permeability (Fig. 3.6 B) as a function of aging time for uncrosslinked and irradiated TMBPA-BP films with thicknesses ranging from 150 to 170 nm. The relative O_2 permeability was calculated by dividing the O_2 permeability coefficient (P) at a given aging time by its initial value (P_0) at about 1 hour of aging. The irradiated samples were prepared using the crosslinker at 254 nm, and they are designated by the total irradiation time and environment. For example, "20, N_2" indicates a sample irradiated in N_2 at 254 nm for 20 min (10 min/side). The initial O_2

permeability of the uncrosslinked thin film is higher than that of the bulk film (cf., Table 3-1), indicating that additional free volume may have been captured in the thin film due to rapid quenching from above T_g.[3, 13, 14, 22] As aging time increases, free volume of glassy polymers typically decreases,[3] leading to permeability decreases. For example, the O_2 permeability of the uncrosslinked sample decreases by almost 50% after about 1000 h of aging.

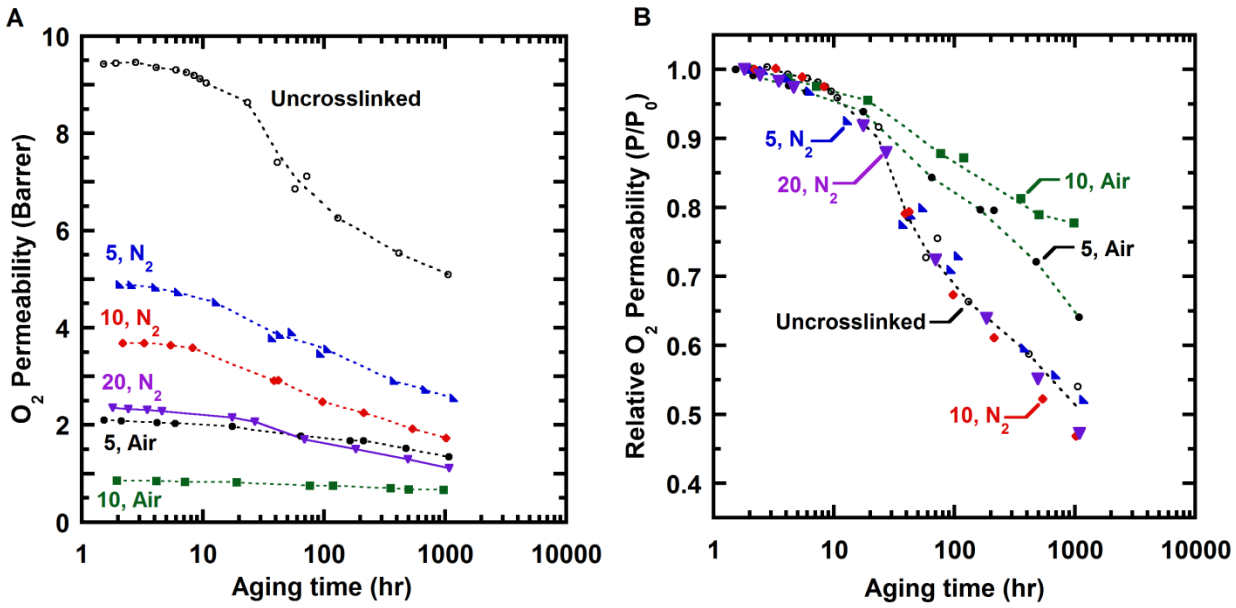

Fig. 3.6. Influence of physical aging on: (A) oxygen permeability and (B) normalized oxygen permeability of non-crosslinked and irradiated TMBPA-BP films. In (B), relative O_2 permeability was calculated by dividing the O_2 permeability (P) at a given aging time by its initial value (P_0) at ~1 hour of aging time. Samples were irradiated at 254 nm and they are designated by the total time (in min) and the environment of UV irradiation. Lines are drawn to guide the eye. (Figure used with permission from Elsevier).

The oxygen permeability also decreases with UV irradiation in either N_2 or air, which may be due to a loss in polymer free volume with crosslinking and/or photooxidation.[22, 25] Interestingly, as shown in Fig. 3.6 B, N_2-irradiated samples display similar rates of permeability loss as that of the uncrosslinked sample. Materials having different permeability coefficients yet similar aging rates have

been reported in earlier studies.[3, 5, 48] For example, Kim et al. observed that a chemically crosslinked thin polyimide film (281 nm thick) had a similar aging rate as its uncrosslinked analog (312 nm thick), even though the initial O_2 permeability of the crosslinked sample was 57% lower than that of the uncrosslinked film.[48] Similar observations were also reported for thin films of polysulfone (annealed vs. non-annealed)[5] and poly(2,6-dimethyl-1,4-phenylene oxide) (semicrystalline vs. amorphous).[3]

The aging rate, according to the self-retarding aging model developed by Struik, can be expressed as the ratio of the driving force, i.e., the displacement of the specific volume at time t away from that at equilibrium, to a characteristic relaxation time, τ, which is a function of the polymer's current free volume state, glass transition temperature, T_g, and experimental temperature:[2]

$$\text{Aging rate} \equiv \frac{dv}{dt} = \frac{-(v - v_\infty)}{\tau\,(v, T_g - T)} \qquad (3.3)$$

where v and v_∞ are the specific volumes of the polymer at time t and at equilibrium, respectively. One possible explanation for the similar aging rates of the uncrosslinked and N_2-irradiated samples is that the extent of decrease in polymer free volume due to crosslinking may not be significant enough to considerably impact the driving force, i.e., $v - v_\infty$, of aging. In addition, the distance between crosslinks in N_2-irradiated samples may be large enough that the polymer chain mobility is not affected much by crosslinking, leading to little or no change in τ. As a result, if changes in the driving force and the relaxation

time are small, and work in opposite directions, the overall aging rate may not be significantly affected.

For a fixed UV irradiation time, air-irradiated samples have lower O_2 permeability than N_2-irradiated samples. In addition to crosslinking, photooxidation can occur due to irradiation in air, which introduces polar groups into the polymer matrix (cf., Fig. 3.4 B). Interactions among these polar groups, such as hydrogen bonding, etc., can increase interchain cohesion, thereby lowering free volume and gas permeability.[23,24] Moreover, such interactions may also restrict polymer chain mobility, increasing its T_g, and according to Equation (3.3), increase the relaxation time, thereby decreasing the aging rate. Consistent with this hypothesis, as shown in Fig. 3.6 B, air-irradiated samples have lower aging rates than uncrosslinked and N_2-irradiated samples, and the aging rate of air-irradiated samples decreases as irradiation time increases.

In addition to the interactions described above, polar groups introduced by photooxidation can potentially increase polymer hydrophilicity.[49] Particularly in more hydrophilic polymers, water can influence their physical aging.[50] To explore the potential influence of water on physical aging of air-irradiated polymers considered in this study, two fresh thin film samples were prepared and irradiated in air for 10 min (5 min/side). One film was kept in a permeation apparatus for up to 1000 h. Except during permeation measurements, which used dry O_2 and N_2, that film was aged in vacuum at 35°C, and consequently, had minimal contact with water vapor. The other sample was aged in the ambient atmosphere, which had a relative humidity of about 25% at 35°C. After

each permeation measurement, the sample was immediately removed from the permeation apparatus and continued aging in the ambient atmosphere. The aging behavior of these samples is presented in Fig. 3.7. During the first 21 h, each sample was kept in its respective permeation apparatus, so the samples were not exposed to water vapor, and the initial change in relative O_2 permeability with time is essentially identical for both samples. After about 21 h, one sample was removed from its permeation system and aged in ambient environment, as described above. As shown in Fig. 3.7, the sample aged in the ambient environment, which contained water vapor at about 25% relative humidity, underwent accelerated aging relative to the sample aged in vacuum, which did not contain water.

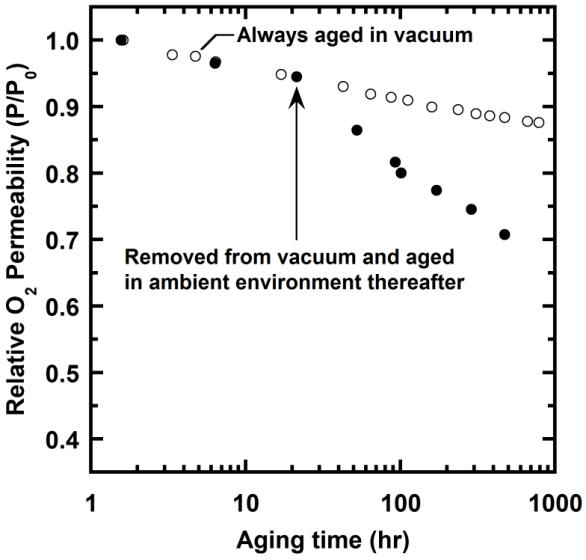

Fig. 3.7. Influence of aging environment on aging rate of air-irradiated TMBPA-BP thin films. Relative O_2 permeability was calculated by dividing the O_2 permeability (P) at a given aging time by its initial value (P_0) at ~ 1 h of aging time. The films were irradiated in air for 10 min (5 min/side) and were around 170 nm thick. One sample was aged in vacuum at 35°C, and the other sample was aged in vacuum for 21 hours before being subsequently aged in the

ambient environment, which had a relative humidity of about 25%, at 35°C. (Figure used with permission from Elsevier).

This accelerated aging in the presence of water is similar to a phenomenon reported by Horn et al., who investigated the influence of long term CO_2 exposure on aging behavior of thin Matrimid films (~200 nm).[33] For a fixed feed pressure and temperature, CO_2 permeability in Matrimid initially increases until a maximum is reached, then decreases for the remainder of the experiment. Initially, CO_2 plasticizes the polymer and increases gas permeability. As the polymer is plasticized, its free volume increases and T_g decreases, leading to an increase in the driving force for physical aging and a decrease in the relaxation time (cf., Equation (3.3)), which increases the aging rate. Consequently, the influence of aging on permeability becomes more important, resulting in a decrease in CO_2 permeability with time.[33] A similar interplay between plasticization and physical aging may also be at work in this study. Because water (T_c = 647 K[51]) is a more condensable penetrant than CO_2 (T_c = 304 K[51]), water can potentially plasticize the more hydrophilic air-irradiated samples, leading to accelerated aging process, as shown in Fig. 3.7. Of course, other components in the ambient environment, such as carbon dioxide or other species, may also have an impact on physical aging. A more detailed and controlled study of aging environment influence on aging behavior deserves further investigation but it is beyond the scope of this study. In any case, the observed dependence of aging rate on the aging environment highlights the importance of maintaining consistent aging conditions and reporting how

samples are stored in between gas permeation measurements during aging studies.

Fig. 3.8 presents the absolute (A) and relative (B) O_2/N_2 selectivity of uncrosslinked and irradiated samples as a function of aging time. Relative selectivity was determined by dividing selectivity at time t by the initial selectivity, which was measured after about 1 h of aging. The uncertainty for the 10 min, air-irradiated sample is presented, calculated based on uncertainties in permeability coefficients using propagation of errors.[52] The initial O_2/N_2 selectivity of the uncrosslinked sample is similar to that of the bulk film (cf., Table 3.1), indicating that the PDMS-coated thin film is essentially defect-free. Selectivity generally increases with irradiation time and aging time, although increases in selectivities from UV irradiation are greater. This increase in selectivity can be attributed to potential densification of the polymer accompanying UV irradiation and physical aging, which should reduce free volume and increase the size-sieving ability of the polymer.[22] At a fixed irradiation time, air-irradiated samples have higher O_2/N_2 selectivity than N_2-irradiated samples. As mentioned earlier, air-irradiated samples undergo both crosslinking and photooxidation, which can effectively lower polymer free volume, restrict chain mobility, and improve selectivity.[15, 23, 27] As a result of lower aging rates of air-irradiated samples (cf., Fig. 3.6 B), the O_2/N_2 selectivities of air-irradiated samples do not change much with aging time.

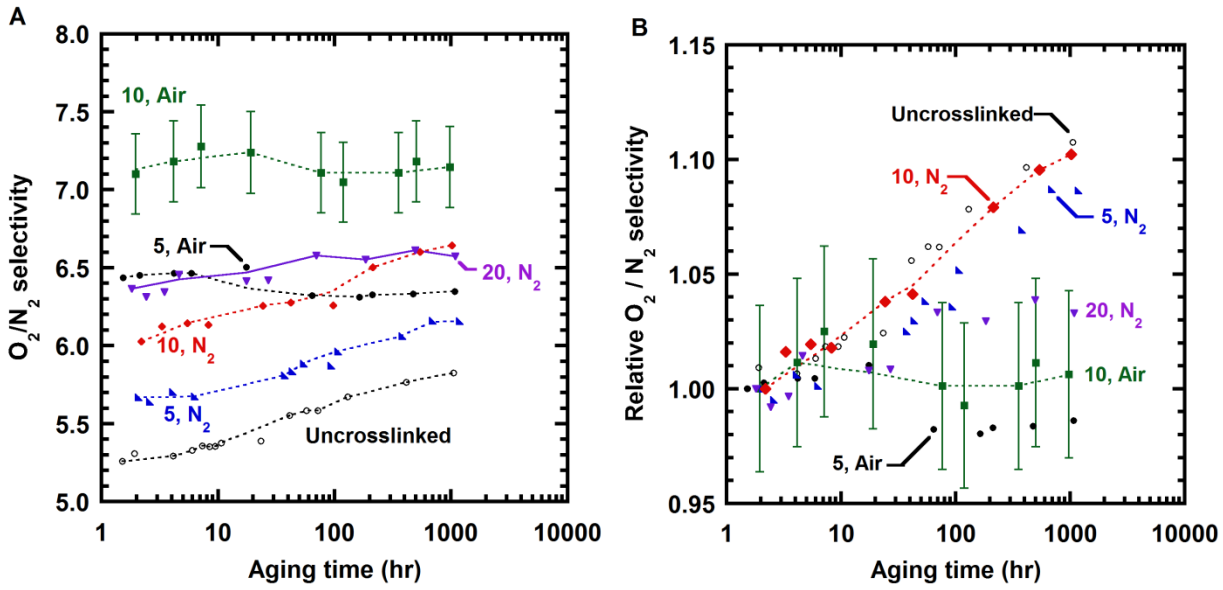

Fig. 3.8. Influence of physical aging on: (A) O2/N2 selectivity and (B) normalized O2/N2 selectivity of non-crosslinked and crosslinked TMBPA-BP films. In (B), data were normalized based on permeability at ~ 1 h of aging time. Samples were irradiated at 254 nm and they are designated by the total irradiation time (in min) and the irradiation environment. Lines are drawn to guide the eye. (Figure used with permission from Elsevier).

Fig. 3.9 presents the influence of UV irradiation and physical aging on O_2/N_2 separation performance of TMBPA-BP thin films relative to the upper bound.[53] Transport data of thin polysulfone (PSF) films (125 nm) are also included for comparison.[14] As polymers are UV-irradiated and undergo physical aging, the ensuing decrease in gas permeability and increase in selectivity move transport properties in a direction parallel to but slightly away from the upper bound. Similar trends were observed in previous studies of physical aging of uncrosslinked and non-irradiated glassy polymers.[3, 14, 38]

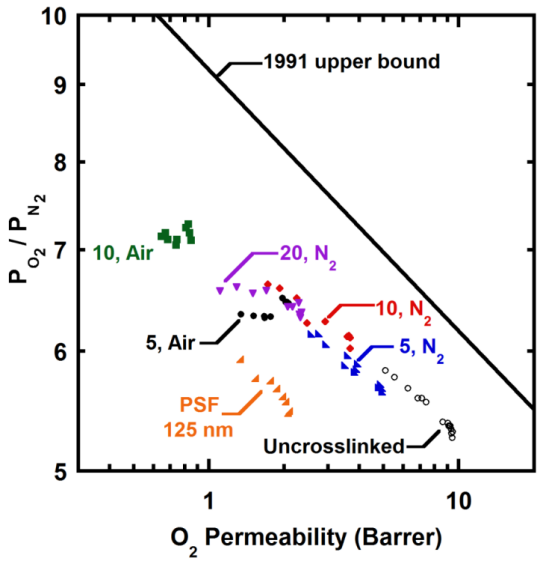

Fig. 3.9. Influence of physical aging and UV irradiation on O_2/N_2 separation performance of uncrosslinked and UV-irradiated TMBPA-BP samples relative to the 1991 upper bound.[53] Samples were irradiated at 254 nm. All samples were 150-170 nm thick. Transport data of ultra-thin polysulfone (125 nm thick) are also included for reference.[14] (Figure used with permission from Elsevier).

3.3.5 Influence of Irradiation Wavelength on Physical Aging and Gas Permeation Properties

Fig. 3.10 presents the influence of UV irradiation wavelength and environment on aging behavior of TMBPA-BP thin films. Each crosslinked sample was irradiated for 10 min total (5 min/side) and is designated by the irradiation environment and wavelength. Similar to transport properties observed for samples irradiated at 254 nm, the air-irradiated sample at 365 nm has lower O_2 permeability than the N_2-irradiated sample at 365 nm, presumably due to more extensive photooxidation in the air-irradiated sample, which can decrease the free volume. However, the extent of photooxidation in the air-irradiated sample at 365 nm is probably small (relative to that for samples

irradiated at 254 nm), as is evident from the similar FTIR spectra of air- and N_2-irradiated samples at 365 nm (cf., Fig. 3.4 C) and similar reductions in their benzophenone peak intensities after irradiation (cf., Fig. 3.5). Consequently, air- and N_2-irradiated films at 365 nm have similar O_2/N_2 selectivities, as shown in

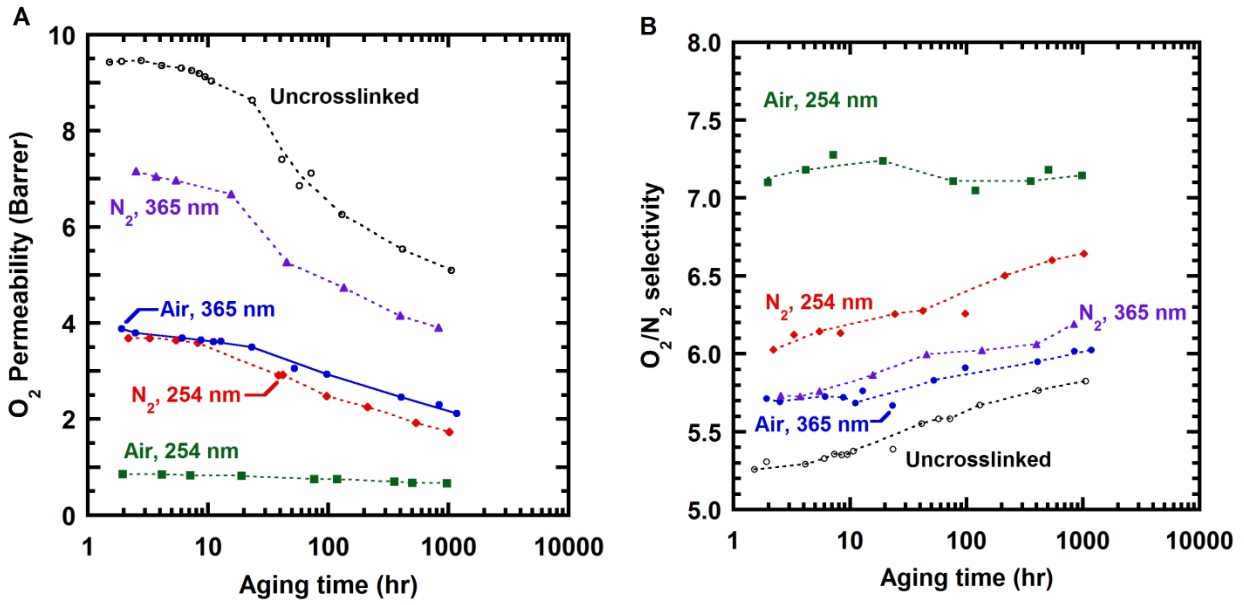

Fig. 3.10. Influence of crosslinking wavelength and environment on: (A) O_2 permeability and (B) O_2/N_2 selectivity of uncrosslinked and irradiated TMBPA-BP thin films. Each crosslinked sample was irradiated for 10 min total (5 min per side) and is designated by the irradiation environment and wavelength. All samples were 150-170 nm thick. Lines are drawn to guide the eye. (Figure used with permission from Elsevier).

Fig. 3.10 B.

In a fixed irradiation environment, samples irradiated at 254 nm have lower O_2 permeabilities and higher O_2/N_2 selectivities than samples irradiated at 365 nm. This difference in transport properties, as well as the lower benzophenone peak intensities for samples irradiated at 254 nm relative to those at 365 nm (cf., Fig. 3.5), indicate that irradiation at 254 nm has likely induced more crosslinking and/or photooxidation than irradiation at 365 nm. In general,

the amount of radicals generated via UV irradiation depends on the amount of UV energy absorbed by the polymer and the efficiency of converting absorbed energy to radicals.[18, 54] Table 3-2 characterizes the different UV irradiation methods considered in this study. After undergoing irradiation for 10 min, polymers irradiated at 254 nm (via UV crosslinker) absorbed more energy per unit area than those irradiated at 365 nm (via UV lamp). Moreover, because photons at 254 nm (472 kJ/mol) are more energetic than those at 365 nm (328 kJ/mol), photons at 254 nm are more likely to overcome the energy barrier (310 kJ/mol) required in promoting the n→π* transition of benzophenone (cf., Fig. 3.1),[55, 56] which leads to more radicals available for photochemical reactions. Consequently, due to greater UV energy absorption and a higher probability of radical formation, irradiation at 254 nm leads to more extensive crosslinking and/or photooxidation than irradiation at 365 nm.

Table 3-2. Characteristics of UV irradiation methods at 254 nm and 365 nm.

	UV Crosslinker (254 nm)	**UV Lamp** (365 nm)
Absorbance[a]	0.475	0.112
Bulb intensity (mW/cm^2)	6.55	16.7
Emitted energy per area	3900	10,000

after 10 min irradiation (mJ/cm^2)		
Absorbed energy per area after 10 min irradiation (mJ/cm^2)[b]	2600	2300

(Table used with permission from Elsevier).

[a] cf., Fig. 1

[b] determined using Equation (2)

Fig. 3.11 presents the influence of irradiation wavelength, irradiation environment, and physical aging on O_2/N_2 separation performance relative to the 1991 upper bound.[53] Each crosslinked sample was irradiated for 10 min (5 min per side). Transport properties of polysulfone as well as uncrosslinked and crosslinked (irradiated in N_2 at 365 nm for 7 min) tetramethyl bisphenol A benzophenone dicarboxylic acid (TMBPA-BnzDCA) are included for comparison.[14, 22] As shown in Fig. 3.11, at 365 nm, the properties of air-irradiated sample are somewhat farther away from the upper bound than those of the N_2-irradiated sample, because the air-irradiated sample has lower O_2 permeability coefficients yet similar O_2/N_2 selectivities to those of the N_2-irradiated sample. On the other hand, at 254 nm, the air-irradiated sample has

higher selectivities and lower O_2 permeabilities than the N_2-irradiated sample, presumably due to more extensive photooxidation at 254 nm. In addition, as observed earlier, physical aging and UV irradiation move transport properties to the upper-left direction on paths that are parallel to but slightly away from the upper bound.

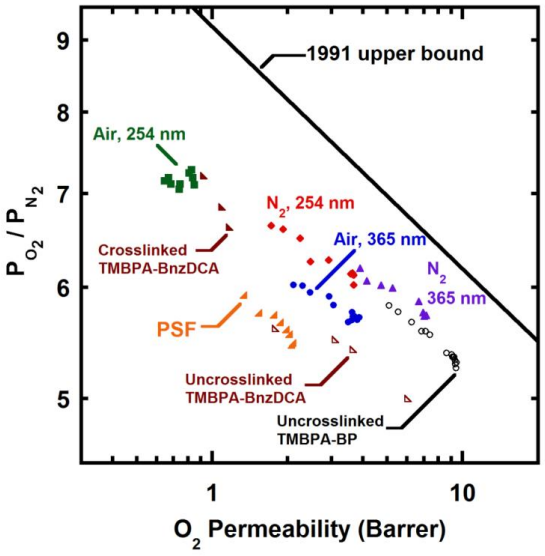

Fig. 3.11. Influence of irradiation wavelength, irradiation environment, and physical aging on O2/N2 separation performance of uncrosslinked and crosslinked TMBPA-BP samples relative to the 1991 upper bound.[53] All TMBPA-BP samples were 150-170 nm thick. Each crosslinked sample was irradiated for 10 min total (5 min per side) and is designated by the UV irradiation environment and wavelength. Physical aging of polysulfone (125 nm) [14] as well as non-crosslinked and crosslinked (irradiated in N_2 at 365 nm for 7 min) TMBPA-BnzDCA (380-860 nm thick) [22] are also included for comparison. (Figure used with permission from Elsevier).

3.4 Conclusions

The influence of UV irradiation and physical aging on O_2 and N_2 transport properties of thin TMBPA-BP films was explored at 35°C and a feed pressure of 2 atm. To investigate the influence of UV irradiation on the instrinsic polymer

properties, uniform crosslinking throughout the polymer is desired, which necessitates using very thin films. To balance the need for relatively uniform irradiation and practicality of making defect-free films, films of 150-170 nm were used for this study and were coated with PDMS to caulk any pinholes arising during the thin film casting process. The influence of the PDMS layer on UV irradiation uniformity is small.

Both UV irradiation and physical aging decrease gas permeability coefficients and increase O_2/N_2 selectivity. Changes in transport properties become more significant as irradiation time increases, likely due to a loss in polymer free volume associated with crosslinking and/or photooxidation. For samples irradiated at 254 nm for a fixed period of time, air-irradiated samples have lower permeability and higher selectivities than N_2-irradiated samples. FTIR spectra of air-irradiated samples at 254 nm showed peaks ascribed to carbonyl groups, which were believed to be photooxidation products that were generally absent in the spectra of N_2-irradiated samples. Interactions among these polar groups can potentially decrease polymer free volume, leading to further losses in permeability and gains in selectivity.

The influence of irradiation wavelength on transport properties was also explored. Samples were irradiated on both sides via either a UV crosslinker (254 nm) or a UV lamp (365 nm). In a fixed irradiation environment (air or N_2), samples irradiated at 254 nm were less permeable and more selective than those irradiated at 365 nm. This difference is attributed to greater UV absorption by the polymer and a higher probability of radical formation at 254 nm, both of

which contribute to greater extents of crosslinking and/or photooxidation than irradiation at 365 nm. Finally, comparisons to the upper bound established by Robeson showed that UV irradiation and physical aging moved the transport properties mainly parallel to but slightly away from the upper bound line, a trend similar to that reported in previous aging studies on non-irradiated polymer samples.

3.5 References

1. P. H. Pfromm and W. J. Koros, *Polymer*, 1995, **36**, 2379-2387.
2. L. C. E. Struik, *Physical aging in amorphous polymers and other materials*, Elsevier Scientific Pub. Co., Amsterdam; New York, 1978.
3. Y. Huang and D. R. Paul, *Polymer*, 2004, **45**, 8377-8393.
4. Y. Huang and D. R. Paul, *Journal of Membrane Science*, 2004, **244**, 167-178.
5. Y. Huang, X. Wang and D. R. Paul, *Journal of Membrane Science*, 2006, **277**, 219-229.
6. C. M. Laot, E. Marand, B. Schmittmann and R. K. P. Zia, *Macromolecules*, 2003, **36**, 8673-8684.
7. C.-C. Hu, Y.-J. Fu, S.-W. Hsiao, K.-R. Lee and J.-Y. Lai, *Journal of Membrane Science*, 2007, **303**, 29-36.
8. L. Starannikova, V. Khodzhaeva and Y. Yampolskii, *Journal of Membrane Science*, 2004, **244**, 183-191.
9. F. Alghunaimi, B. Ghanem, N. Alaslai, R. Swaidan, E. Litwiller and I. Pinnau, *Journal of Membrane Science*, 2015, **490**, 321-327.
10. R. W. Baker, *Industrial & Engineering Chemistry Research*, 2002, **41**, 1393-1411.
11. D. F. Sanders, Z. P. Smith, R. Guo, L. M. Robeson, J. E. McGrath, D. R. Paul and B. D. Freeman, *Polymer*, 2013, **54**, 4729-4761.
12. L. Cui, W. Qiu, D. R. Paul and W. J. Koros, *Polymer*, 2011, **52**, 3374-3380.
13. M. S. McCaig and D. R. Paul, *Polymer*, 2000, **41**, 629-637.
14. B. W. Rowe, B. D. Freeman and D. R. Paul, *Polymer*, 2009, **50**, 5565-5575.
15. H. Kita, T. Inada, K. Tanaka and K.-i. Okamoto, *Journal of Membrane Science*, 1994, **87**, 139-147.
16. G. Tillet, B. Boutevin and B. Ameduri, *Progress in Polymer Science*, 2011, **36**, 191-217.

17. J. D. Wind, C. Staudt-Bickel, D. R. Paul and W. J. Koros, *Macromolecules*, 2003, **36**, 1882-1888.
18. A. A. Lin, V. R. Sastri, G. Tesoro, A. Reiser and R. Eachus, *Macromolecules*, 1988, **21**, 1165-1169.
19. K. Vanherck, G. Koeckelberghs and I. F. J. Vankelecom, *Progress in Polymer Science*, 2013, **38**, 874-896.
20. C. T. Wright and D. R. Paul, *Journal of Membrane Science*, 1997, **124**, 161-174.
21. C. N. Dudley, B. Schöberl, G. K. Sturgill, H. W. Beckham and M. E. Rezac, *Journal of Membrane Science*, 2001, **191**, 1-11.
22. M. S. McCaig and D. R. Paul, *Polymer*, 1999, **40**, 7209-7225.
23. I. K. Meier and M. Langsam, *Journal of Polymer Science Part A: Polymer Chemistry*, 1993, **31**, 83-89.
24. I. K. Meier, M. Langsam and H. C. Klotz, *Journal of Membrane Science*, 1994, **94**, 195-212.
25. S. Matsui, T. Ishiguro, A. Higuchi and T. Nakagawa, *Journal of Polymer Science Part B: Polymer Physics*, 1997, **35**, 2259-2269.
26. S. Matsui, H. Sato and T. Nakagawa, *Journal of Membrane Science*, 1998, **141**, 31-43.
27. S. Matsui and T. Nakagawa, *Journal of Applied Polymer Science*, 1998, **67**, 49-60.
28. M. L. Chng, Y. Xiao, T. S. Chung, M. Toriida and S. Tamai, *Polymer*, 2007, **48**, 311-317.
29. S. K. Wu and J. F. Rabek, *Polymer Degradation and Stability*, 1988, **21**, 365-376.
30. J. C. Scaiano, J. C. Netto-Ferreira, A. F. Becknell and R. D. Small, *Polymer Engineering & Science*, 1989, **29**, 942-944.
31. B. J. Sundell, A. T. Shaver, Q. Liu, A. Nebipasagil, P. Pisipati, S. J. Mecham, J. S. Riffle, B. D. Freeman and J. E. McGrath, *Polymer*, 2014, **55**, 5623-5634.
32. R. R. Tiwari, Z. P. Smith, H. Lin, B. D. Freeman and D. R. Paul, *Polymer*, 2014, **55**, 5788-5800.
33. N. R. Horn and D. R. Paul, *Polymer*, 2011, **52**, 1619-1627.
34. J. M. S. Henis and M. K. Tripodi, *Separation Science and Technology*, 1980, **15**, 1059-1068.
35. *United States Pat.,* 1980.
36. J. M. S. Henis and M. K. Tripodi, *Journal of Membrane Science*, 1981, **8**, 233-246.
37. J. M. S. Henis and M. K. Tripodi, *Science*, 1983, **220**, 11-17.
38. T. M. Murphy, B. D. Freeman and D. R. Paul, *Polymer*, 2013, **54**, 873-880.
39. H. Lin and B. D. Freeman, *Springer Handbook of Materials Measurement Methods*, 2006, 371-387.
40. D. R. Paul, *Journal of Membrane Science*, 1984, **18**, 75-86.

41. in *Intermolecular and Surface Forces (Third Edition)*, Academic Press, San Diego, 2011, DOI: http://dx.doi.org/10.1016/B978-0-12-375182-9.10026-0, p. iv.
42. V.-M. Graubner, R. Jordan, O. Nuyken, B. Schnyder, T. Lippert, R. Kötz and A. Wokaun, *Macromolecules*, 2004, **37**, 5936-5943.
43. B. Schnyder, T. Lippert, R. Kötz, A. Wokaun, V.-M. Graubner and O. Nuyken, *Surface Science*, 2003, **532–535**, 1067-1071.
44. K. Efimenko, W. E. Wallace and J. Genzer, *Journal of Colloid and Interface Science*, 2002, **254**, 306-315.
45. V. Balzani, P. Ceroni and A. Juris, *Photochemistry and Photophysics: Concepts, Research, Applications*, Wiley, 2014.
46. S.-i. Kuroda and I. Mita, *European Polymer Journal*, 1989, **25**, 611-620.
47. R. M. Silverstein, F. X. Webster and D. Kiemle, *Spectrometric identification of organic compounds*, Wiley Global Education, Seventh edn., 2005.
48. J. H. Kim, W. J. Koros and D. R. Paul, *Journal of Membrane Science*, 2006, **282**, 32-43.
49. D. F. Sanders, R. Guo, Z. P. Smith, K. A. Stevens, Q. Liu, J. E. McGrath, D. R. Paul and B. D. Freeman, *Journal of Membrane Science*, 2014, **463**, 73-81.
50. B. W. Rowe, B. D. Freeman and D. R. Paul, *Macromolecules*, 2007, **40**, 2806-2813.
51. B. Poling, J. Prausnitz and J. O. Connell, *The properties of gases and liquids*, McGraw-Hill Education, Fifth edn., 2000.
52. P. R. Bevington and D. K. Robinson, *Data reduction and error analysis for the physical sciences*, McGraw-Hill, 3rd edn., 2003.
53. L. M. Robeson, *Journal of Membrane Science*, 1991, **62**, 165-185.
54. N. J. Turro, C. J. Dalton, K. Dawes, G. Farrington, R. Hautala, D. Morton, M. Niemczyk and N. Schore, *Accounts of Chemical Research*, 1972, **5**, 92-101.
55. W. Reusch, in *Virtual Textbook of Organic Chemistry*, 1999.
56. P. Atkins and J. dePaula, *Physical Chemistry*, W. H. Freeman, 2006.

Chapter 4: Poly(2,6-dimethyl-1,4-phenylene oxide) Blends with a Poly(arylene ether ketone) for Gas Separation Membranes

Andrew Shaver,[1] Joshua D. Moon,[2] Donald Savacool,[1] Wenrui Zhang,[1] Gurtej Narang,[1] Gregory Miller,[1] Britannia Vondrasek,[1] J. J. Lesko,[1] Benny D. Freeman,[2] J. S. Riffle,[1*] James E. McGrath[1]

[1]Macromolecules Innovation Institute, Virginia Tech, Blacksburg, VA

[2]Dept of Chemical Engineering, University of Texas, Austin, TX

Shaver, A.; Moon, J. D.; Savacool, D.; Zhang, W.; Narang, G.; Miller, G.; Vondrasek, B.; Lesko, J. J.; Freeman, B. D.; Riffle, J. S.; McGrath, J. E., Poly(2,6-dimethyl-1,4-phenylene oxide) blends with a poly(arylene ether ketone) for gas separation membranes. *Polymer* **2017,** *114*, 135-143.

4.1 Introduction

Gas separations via membranes have grown over approximately the past 50 years due to reduced energy consumption, equipment size, and waste generation relative to cryogenic distillation and absorption processes.[1-3] Currently, membranes are used to separate various gas pairs in applications including nitrogen enrichment, acid gas treatment, ammonia purge gas recovery, refinery gas purification, syngas ratio adjustment, and dehydration.[2-4] There are several challenges that need to be addressed within these areas such as low

selectivities, plasticization caused by CO_2 and other condensable gas absorption, physical aging, and thermal and mechanical stability of the membranes.[4]

Gas transport performance for non-porous gas separation membranes is primarily characterized in terms of permeability and selectivity. Permeability is the pressure- and thickness-normalized gas flux through the membrane, and selectivity is the permeability ratio of two gases of interest.[5, 6] The best performance occurs when the permeability and selectivity of the membrane are high.[5, 6] However, it is known that there is a tradeoff between permeability and selectivity which was described in terms of an upper bound by Robeson in 1991 and later theoretically explained by Freeman.[7-9]

Glassy polymers such as poly(arylene ether)s including polysulfones and poly(2,6-dimethyl-1,4-phenylene oxide), polycarbonates, polyimides, cellulose acetates, and aramids are all used as membrane materials and show great performance and processability for various applications.[4] This paper will focus on poly(2,6-dimethyl-1,4-phenylene oxide) (PPO) as a membrane material. PPO was first commercialized over 50 years ago by General Electric and it is now marketed by Sabic.[10] It gained interest as a material for gas separation membranes due to its aromatic ether structure. Its kinked ether linkages and benzylic methyl groups inhibit chain packing and lead to a high fractional free volume and consequently high permeabilities.[4, 11] However, the high free volume leads to reduced selectivities when compared to other commercial materials, and several research efforts have been undertaken to solve this problem.[12, 13]

Crosslinking is of great interest for dense-film gas separation membranes due to the potential to increase selectivity, decrease gas plasticization, and decrease the effect of physical aging.[4, 14] Crosslinking controllably reduces the mobility of polymer chains, which can improve the size sieving capability of glassy polymers and increase selectivity. Gas plasticization occurs when some sufficiently high concentration sorbs into a film and causes swelling that can decrease selectivity. Crosslinking inhibits this swelling and can reduce the overall effect of plasticization. Physical aging involves the gradual densification of a non-equilibrium glassy polymer over time towards its equilibrium state and decreases permeability and increases selectivity. By crosslinking the film, the aging rate may be reduced. Both crosslinking and aging increase selectivity. However, literature has reported that crosslinking has a more pronounced effect for UV-irradiated polyarylates.[14, 15]

The focus of this study has been to UV crosslink PPO to enhance its transport properties. A poly(arylene ether ketone) based on bisphenol A (BPA-PAEK) was blended with PPO to produce a UV crosslinkable material with improved selectivity. Structures are shown in Figure 1. The key crosslinking groups within the polymers are the benzophenone in the BPA-PAEK and the benzylic methyl groups on the PPO. UV light was used to excite a benzophenone moiety that could subsequently abstract a hydrogen radical from a benzylic methyl group. This creates two free radicals that can then combine to form a covalent crosslinked bond. Qiang et al. have extensively described this crosslinking reaction and explored the effect of thickness, atmosphere, and

aging.[15] Other systems have been studied utilizing this crosslinking reaction.[15-17] However, in the previous work, the two key components were within the same polymer by polymerizing tetramethylbisphenol A or tetramethylbisphenol F with 4'4-difluorobenzophenone.

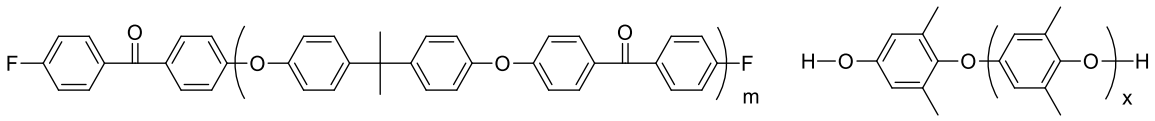

Figure 4.1. Bisphenol A poly(arylene ether ketone) and poly(2,6-dimethyl-1,4-phenylene oxide) (Figure used with permission from Elsevier).

In this study, blends were explored as a function of the molecular weight of the PPO. The 22,000 M_n PPO was used to study the effect of PPO/BPA-PAEK composition on the properties of the blended films. NMR, DSC, gel fractions, tensile and transport properties were used to characterize the films.

4.2 Experimental

4.2.1 Materials

N,N-Dimethylacetamide (DMAc), toluene, pyridine, and 2,6-dimethylphenol were purchased from Sigma Aldrich. DMAc was vacuum distilled from calcium hydride. Toluene, pyridine, and 2,6-dimethylphenol were used as received. 4,4'-Difluorobenzophenone and bisphenol A were kindly donated by Solvay and recrystallized from 2-propanol and toluene, respectively. Potassium carbonate was purchased from Fisher Scientific and dried at 150°C under vacuum. Copper(I) chloride was purchased from Alfa Aesar and used as received.

Hydrochloric acid and methanol were purchased from Spectrum Chemicals and used as received. Chloroform, purchased from Spectrum Chemicals, was stored over activated 3Å molecular sieves. Ultra-high purity (UHP) oxygen gas (99.993%) used for synthesis was purchased from Praxair, and UHP gases (99.999%) used for gas transport measurements were purchased from Airgas.

4.2.2 Synthesis of BPA-PAEK

Synthesis of the BPA-PAEK polymer was adapted from previous literature.[18-22] Bisphenol A (67.713 g, 296.6 mmol), 4,4'-difluorobenzophenone (65.643 g, 306.4 mmol), and DMAc (600 mL) were charged to a three-neck flask equipped with a N_2 inlet, mechanical stirrer, and Dean-Stark trap. Toluene (300 mL) and K_2CO_3 (48.352 g, 349.8 mmol) were added to the flask, and the Dean Stark trap was filled with toluene. The apparatus was placed in a silicone oil bath that was heated to 155°C to begin azeotropic removal of water. After 4 h, the toluene and water were removed from the Dean-Stark trap. The oil bath was maintained at 150°C for 12 h, then the reaction was allowed to cool to room temperature. The polymer solution was filtered to remove any excess K2CO3 or by-product salts. The polymer solution was precipitated into deionized water, then the polymer was stirred in deionized water at 80°C to further assist in the removal of salts and solvents. The white polymer was filtered and dried at 110°C under vacuum. Yield was 81%.

4.2.3 Synthesis of 6,000, 17,000 and 22,000 M_n poly(2,6-dimethyl-1,4-phenylene oxide)s

PPO synthesis was adapted from Hay et al.,[23] and the protocol for synthesizing an ~6,000 M_n oligomer is provided. A 500-mL, 4-neck, round bottom flask equipped with an overhead stirrer, oxygen inlet tube, and condenser was charged with 250 mL of pyridine and 0.5 g (0.005 moles) of copper(I) chloride. Oxygen gas (0.1 SCFH) was passed through the vigorously stirred solution for 30 min, and the solution became dark green. Then, 10 g (0.082 mole) of 2,6-dimethylphenol was added. The reaction mixture became dark orange and the temperature was increased from 25 to 45°C. Oxygen flow was terminated after 1 h and the reaction was stirred for 2 h. The solution became viscous and the color of the solution returned to dark green. The reaction mixture was cooled to room temperature and slowly added into 500 mL of methanol to precipitate the polymer, then the polymer was filtered and washed thoroughly with methanol containing a small amount of hydrochloric acid. The product was dissolved in chloroform, filtered and re-precipitated into methanol. After filtration, the faint yellow powder was dried at 110°C for 24 h under vacuum. Yield: 7.1 g, 71%. The structure was confirmed by ^{1}H-NMR.

For the 17,000 M_n PPO, a 1-L, 4-neck, round bottom flask was used and 800 mL of pyridine, 2.0 g (0.02 moles) of copper(I) chloride. Oxygen gas (0.1 SCFH) was passed through the vigorously stirred solution for 30 min, and then 30 g (0.246 mole) of 2,6-dimethylphenol was added. Oxygen flow was terminated after 3 h and the reaction was stirred for 2 h. The product (23.4 g, yield 78%)

was obtained and the structure was confirmed by ^{1}H-NMR. For the 22,000 M_n PPO, a 500-mL, 4-neck, round bottom flask was used and 250 mL of pyridine, 1.0 g (0.01 mole) of copper(I) chloride. Oxygen gas (0.1 SCFH) was passed through the vigorously stirred solution for 30 min, and then 10 g (0.082 mole) of 2,6-dimethylphenol was added. Oxygen flow was terminated after 4 h and the reaction was stirred for 2 h. The product (8.0 g, yield 80%) was obtained and the structure was confirmed by ^{1}H-NMR.

4.2.4. SEC of the PPO Polymer Series

SEC was conducted to measure molecular weights and distributions of the PPO polymers. The eluent was $CHCl_3$. The column set consisted of two Shodex KF-801 columns connected in series with a guard column having the same stationary phase. The columns and detectors were maintained at 35°C. An isocratic pump (Waters 515 HPLC Pump, Waters Technologies) and 717 Waters autosampler were used for mobile phase delivery and sample injection. Calibrations were performed using a set of nine Shodex polystyrene standards spanning the entire column molecular weight range. Molecular weights were calculated based on the polystyrene standards.

4.2.5. SEC of BPA-PAEK

SEC was conducted to measure the molecular weight and distribution of the BPA-PAEK. The mobile phase was DMAc distilled from CaH_2 containing dry LiCl (0.1 M). The column set consisted of 3 Agilent PLgel 10-µm Mixed B-LS columns 300 x 7.5 mm (polystyrene/divinylbenzene) connected in series with a

guard column having the same stationary phase. The columns and detectors were maintained at 50°C. An isocratic pump (Agilent 1260 infinity, Agilent Technologies) with an online degasser (Agilent 1260), autosampler and column oven were used for mobile phase delivery and sample injection. Multiple detectors connected in series were used for the analyses. A multi-angle laser light scattering detector (DAWN-HELEOS II, Wyatt Technology Corp.), operating at a wavelength of 658 nm, a viscometer detector (Viscostar, Wyatt Technology Corp.), and a refractive index detector operating at a wavelength of 658 nm (Optilab T-rEX, Wyatt Technology Corp.) provided online results. The system was corrected for interdetector delay and band broadening using a 21,000 g/mole polystyrene standard. Data acquisition and analysis were conducted using Astra 6 software from Wyatt Technology Corp. Validation of the system was performed by monitoring the molar mass of a known molecular weight polystyrene sample by light scattering. The accepted variance of the 21,000 g/mole polystyrene standard was defined as 2 standard deviations (11.5% for M_n and 9% for M_w) derived from a set of 34 runs. The specific refractive index value was calculated based on the assumption of 100% recovery. Molecular weights were calculated from the light scattering data.

4.2.6. Film-casting

The polymers (0.6 g) were weighed into a small glass vial with a magnetic stir bar at the desired wt/wt ratio. Chloroform (20 mL) was added to the vial. The solution was filtered through a 0.45-µm syringe filter into a clean glass vial. A 6" x 6" glass plate with the corners cut off (34 in^2 area) was placed in a base bath

for 30 min to clean the surface. The glass plate was rinsed and dried, then placed on a level surface for casting. The solution was poured onto the plate and the solution was spread to the edges of the plate until it covered the whole glass plate. A glass dome with 2 outlets was used to cover the plate. One outlet was fitted with a syringe filter to inhibit dust from entering the glass container and the other was connected to the house air stream running at 2 SCFH. The plate was left undisturbed for a minimum of 30 min, then transferred to an oven at 110°C for an additional 30 min. Once removed from the oven, the film was secured to the glass plate with clips and placed into a DI water bath for 1 min to assist with film removal. The free-standing films were then placed in a vacuum oven set at 110°C for 2 h without vacuum and then for 10 h with vacuum. The resulting films were between 20 and 30 μm thick.

4.2.7. Proton Nuclear Magnetic Resonance (NMR) Spectroscopy

The compositions of the blends were confirmed via NMR. ^{1}H-NMR analysis was performed on a Varian Inova spectrometer operating at 400 MHz. All spectra were obtained from 15% (w/v) 1-mL solutions in chloroform-d. The two peaks used in the calculation were from the three hydrogens on each benzylic methyl group (PPO) and from the four aromatic hydrogens nearest the ketone linkage (BPA-PAEK).

4.2.8. Thermogravimetric Analysis (TGA)

Thermal stabilities of the polymers were investigated using a TA Instruments TGA Q5000 under a N_2 atmosphere with a purge rate of 25 mL min^{-1}. The heating rate was 10°C min^{-1} from room temperature to 700°C.

4.2.9. Differential Scanning Calorimetry (DSC)

The thermal properties were investigated with a TA Instruments DSC Q2000. The polymers were heated under N_2 at 60 mL/min to ensure an inert atmosphere. The heating rate was 10°C min^{-1} to 350°C, then the sample was cooled to 0°C at 10°C min^{-1}. It was heated once more to 350°C at 10°C min^{-1} and the reported DSC thermograms are from the second scans. Reported T_g's were measured at the midpoint.

4.2.10. UV Spectroscopy

UV spectra of the bulk polymers and the blends were collected using a Shimadzu Corp. UV – 1601 UV analyzer. Solutions (0.05 mg/mL) of the samples in chloroform were analyzed in quartz cuvettes placed in the sample cell with chloroform in a similar cuvette in the reference cell. A 50 W Tungsten bulb (from 1100 to 340.8 nm) and a deuterium bulb (340.8 to 190 nm) were used as the light sources. Scans were conducted in 'Spectrum Mode' sweeping wavelengths from 700 to 190 nm.

4.2.11 UV Crosslinking

The polymer membranes were placed between an upper quartz and a lower glass plate. The setup was passed under a Heraeus UV Fusion "H+" bulb (200 to 450 nm wavelength range) via a conveyor belt set at 6 ft/min. This procedure was repeated until the film was exposed to the desired amount of radiation. A UV Power Puck was used to measure the amount of energy that the sample was exposed to, and this was multiplied by the number of passes.

4.2.12 Gel Fraction Measurements

Crosslinked films were dried at 120°C under vacuum overnight. Then 0.1-0.2 g of the crosslinked film was placed in a 20-mL scintillation vial filled with chloroform and stirred overnight. The remaining solid was filtered through a Buchner funnel having a pre-weighed filter paper. The filter paper with the gelled polymer on it were dried at 120°C under vacuum overnight, then weighed once more to obtain the final weight. Gel fractions were calculated by Equation 4.1.

$$Gel\ Fraction\ (\%) = \frac{W_{final}}{W_{initial}} \times 100 \qquad (4.1)$$

4.2.13 Gas Permeability Measurements

The pure gas permeabilities for a series of light gases (H_2, CH_4, N_2, O_2, CO_2) were measured at 35°C in a constant-volume, variable-pressure apparatus as described elsewhere.[1-2] The membrane sample, after being epoxied to a brass support disk, was loaded into a stainless steel Millipore filter holder (Millipore,

Billerica, MA, USA) inside a temperature-regulated water bath. The downstream pressure was measured with a MKS Baratron 626B transducer (MKS, Andover, MA, USA) with a max pressure of 10 Torr, and the pressure in the upstream was measured using a Honeywell Super TJE transducer (Honeywell Sensotec, Columbus, Ohio, USA) with a max pressure of 1500 psig. The feed pressure of each gas was varied between 3 and 17 atm, and both the upstream and downstream pressures were recorded in a custom Python application using National Instruments. Each sample was degassed overnight prior to measuring transport of the gas, and the stainless steel upstream line connected to the feed gas cylinder was flushed and degassed for a minimum of 45 min prior to each test to prevent contamination from other gases.

4.2.14 Tensile Properties

Tensile samples were cut from solvent cast films using a Cricut Explore One™ computer controlled cutting machine. The resulting samples were consistent with sample Type V described in ASTM D638-14. Nine samples produced by the cutter were inspected for any visible flaws, defects, or inclusions that arose during the casting process. The six highest quality samples were selected for testing. The sample thickness was measured at both ends of the narrow section using a Mitutoyo digimatic micrometer model MDC-1"SXF. Uniaxial load tests were performed using an Instron ElectroPuls E1000 testing machine equipped with a 250-N Dynacell load cell. The crosshead displacement rate was 5 mm min^{-1} and the initial grip separation was 25 mm. Nominal strain was calculated by dividing the change in grip separation by the initial grip

separation. Tensile strength was calculated by dividing the load by the average cross-sectional area of the narrow section, which was based on the average of the two sample thickness measurements and a sample width of 3.18 mm.

4.3 Results and Discussion

NMR and SEC were used to characterize the PPO and BPA-PAEK molecular weights and the results are shown in Table 1 and Figure 2. The PPO nomenclature is based on the M_n's from SEC. PPO oligomers with a series of molecular weights were produced to investigate structure-property behavior as a function of the molecular weights of the PPO component.

Table 4-1. Molecular weights of the polymers

	M_n (kDa) NMR	M_n (kDa) SEC	M_w (kDa) SEC	PDI SEC
BPA-PAEK	-	52	78	1.5
2k PPO	1.0	2	3.2	1.7
6k PPO	4.0	6	11.8	2.0
17k PPO	13	17	50.2	3.0
19k PPO	33	19	55.8	2.9
22k PPO	19	22	109	5.0

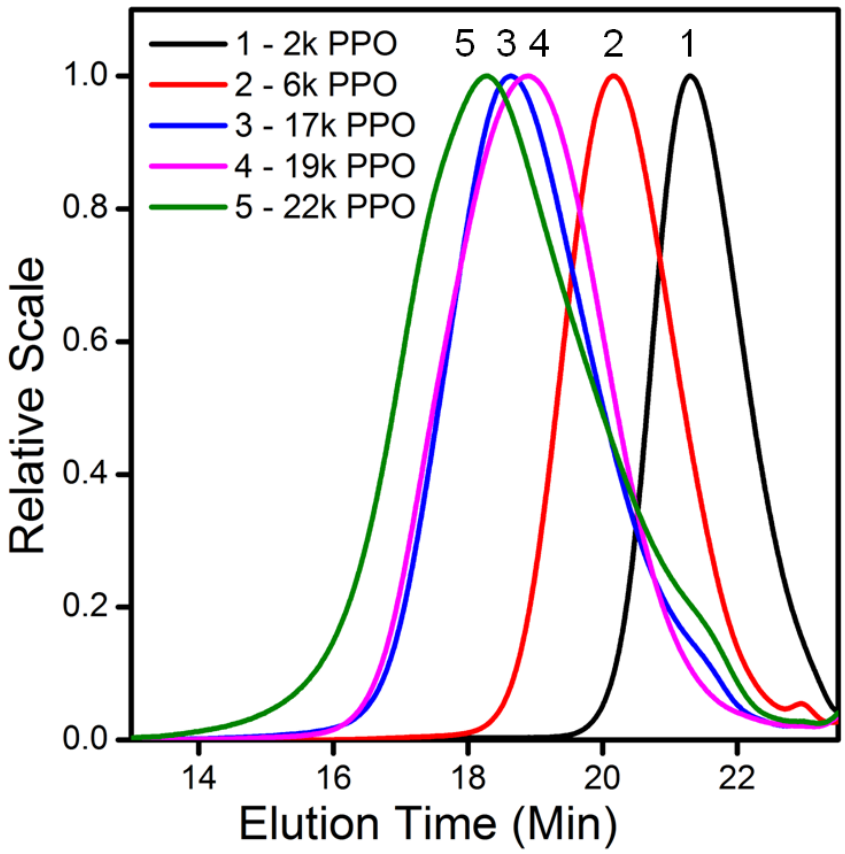

Figure 4.2. SEC refractive index curves of the PPO oligomers (Figure used with permission from Elsevier).

DSC thermograms of the films are shown in Figure 4.3. Figure 4.3A compares two films of blends with different PPO molecular weights of 2,000 and 22,000 g/mole at a wt/wt composition of 33/67 PPO/BPA-PAEK relative to their controls. Thermogram 2 shows the 2,000 g/mole PPO/BPA-PAEK blend with a T_g of 149°C. This T_g is located between the two control T_gs, curves 1 and 3, which suggests that the 2,000 g/mole PPO is miscible with BPA-PAEK at those compositions. Curve 4.4 shows the thermogram of a high molecular weight 22,000 g/mole PPO/BPA-PAEK blend that produced two T_gs, one at 152 and another at 213°C. These two T_gs correspond with the control T_gs in curves 3 and

5 which indicates that the 22,000 M_n PPO produced an immiscible blend with BPA-PAEK at those compositions. The T_gs of the blend are slightly reduced in comparison to the respective control polymers. A definite reason for this behavior is unclear, but it does occur consistently. This can be observed in Figure 3B with the lower T_gs corresponding to the BPA-PAEK in blends with the 6,000, 17,000, 19,000 and 22,000 PPO.

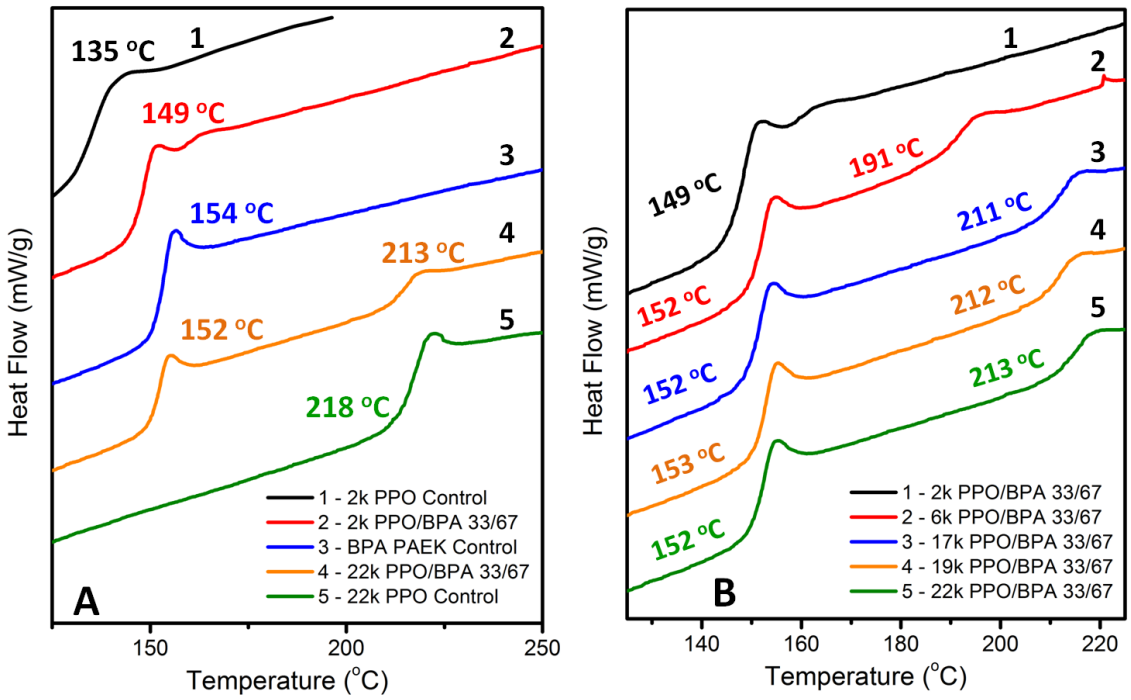

Figure 4.3. A) DSC thermograms of the 2,000 g/mole PPO/BPA-PAEK 33/67 wt/wt and the 22,000 g/mole PPO/BPA-PAEK 33/67 wt/wt blends with their respective controls. B) comparison of each of the PPO molecular weights blended with BPA-PAEK at the 33/67 wt/wt composition of PPO/BPA-PAEK (Figure used with permission from Elsevier).

Figure 4.3 B compares blends with the five PPO polymers with different molecular weights with 67 wt% of BPA-PAEK. Thermogram 1 shows the single T_g for the 2,000 g/mole PPO/BPA-PAEK blend. Once the molecular weight of the

PPO in the blends was increased to 6,000 M_n, two clear T_gs emerged, and this was also true as the molecular weight was increased further, thus indicating the presence of two phases. The upper T_g in the 6,000 M_n PPO/BPA-PAEK blend, which correlates to the PPO phase, is lower than the 17,000, 19,000, and 22,000 upper PPO T_g's in the blends. This is expected since T_g is a function of molecular weight.[24] In Figure 4.4, the 6,000 M_n PPO non-crosslinked blend (curve 2) is compared to its BPA-PAEK control (curve 1), the 6,000 PPO control (curve 4), and the crosslinked blend (curve 3). The PPO T_g in the non-crosslinked blend correlates with the control 6,000 M_n PPO T_g. Once crosslinked, at least the upper T_g was slightly raised, and this was attributed to reduced mobility, particularly of the PPO chains.[25]

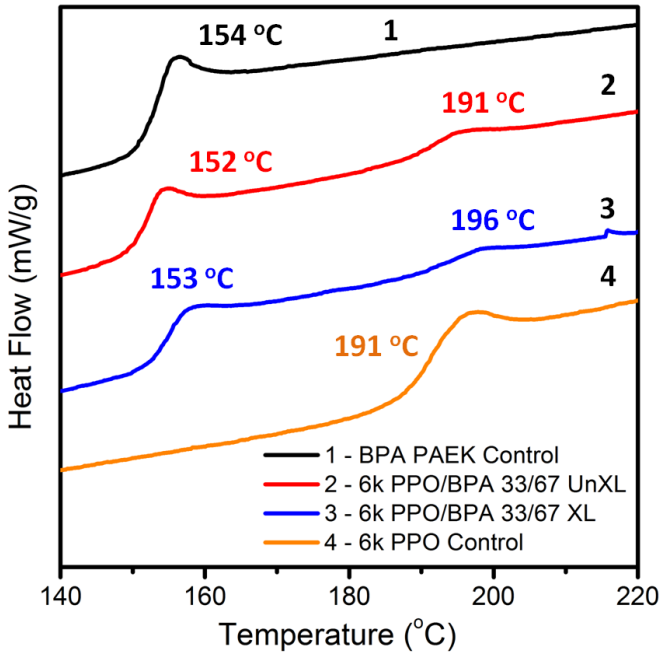

Figure 4.4. DSC thermograms of 6,000 g/mole PPO/BPA-PAEK 33/67 wt/wt non-crosslinked and crosslinked blends with the controls (Figure used with permission from Elsevier).

The crosslinking reaction is activated via UV light and occurs between the activated ketone carbon and benzylic radical. Figure 4.5 shows the solution UV absorbance spectra of the six control polymers. At a given concentration, the PPO absorbs significantly less light than BPA-PAEK in the wavelength range of interest (200 to 450 nm). The absorbance of the BPA-PAEK results in ketone excitation from the nonbonding to the antibonding state.[26] Therefore, in later discussions regarding the gel fractions as a function of PPO weight composition, it will be important to remember that blends containing a greater PPO content will not absorb as much light as blends with higher compositions of the BPA-PAEK. This is beneficial because the UV light will penetrate further into the film to crosslink more polymer chains.

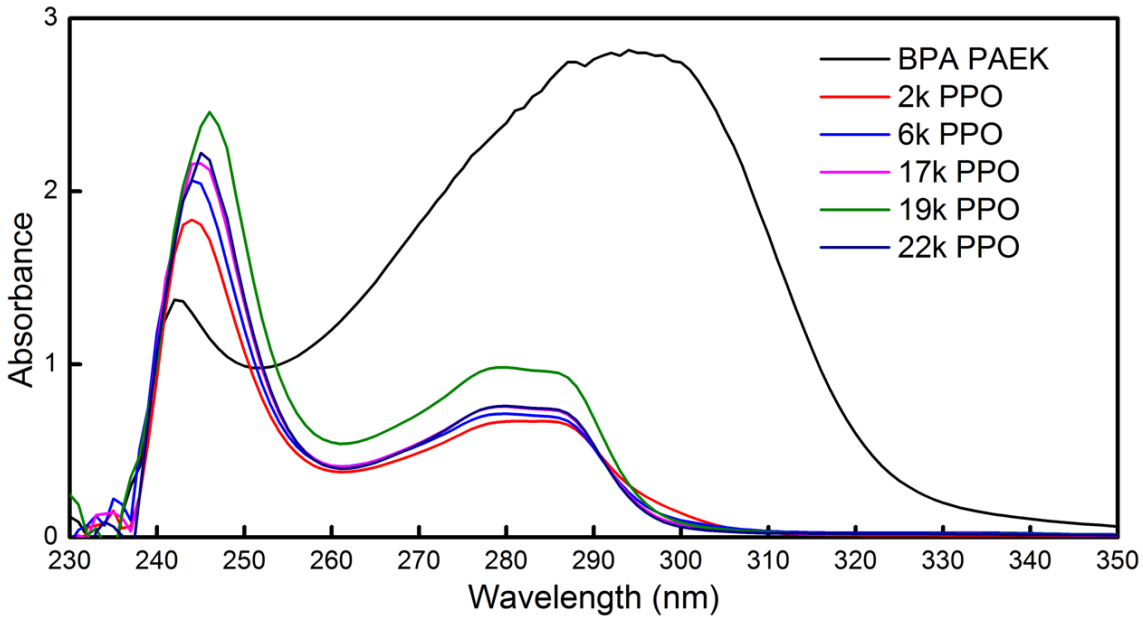

Figure 4.5. Solution UV absorption spectra of the PPO and BPA-PAEK (Figure used with permission from Elsevier).

The extent of crosslinking was explored by measuring gel fractions. The set of gel fractions shown in Figure 4.6 compares the five PPO molecular weights blended with BPA-PAEK along with those for the 19,000 g/mole PPO homopolymer. The films were exposed to 11, 23, or 34 J/cm^2 of energy in efforts to optimize the UV exposure. The higher exposure resulted in increased gel fractions in the blended films but not in the PPO homopolymer control. The control PPO film did not undergo significant crosslinking which showed the importance of the ketone group to the crosslinking reaction. The blend with the 2,000 PPO/BPA-PAEK 33/67 wt/wt composition only reached gel fractions a little above 20%, and this was much lower than the gel fractions obtained with blends having higher molecular weight PPOs. This was attributed to the fact that higher molecular weight PPO contains more benzylic crosslinkable methyl groups per mole (i.e., higher functionality), and thus requires fewer crosslinks to reach gelation.

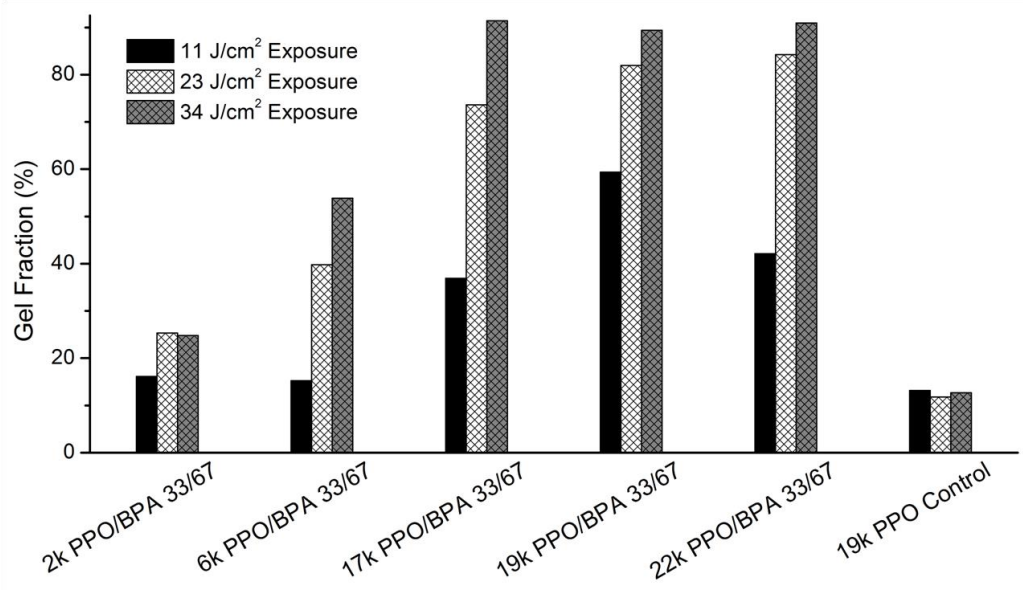

Figure 4.6. Gel fractions after UV crosslinking of PPO/BPA-PAEK blends over a range of PPO molecular weights (Figure used with permission from Elsevier).

The 22,000 M_n PPO was used to explore gel fractions and gas separation properties in these blends as a function of PPO composition. Figure 4.7 compares the gel fractions of four blend compositions. Unexpectedly, there was not a significant change in gel fraction as a function of composition. This is likely a result of several competing factors. One is that the amount of crosslinks may have decreased with less BPA-PAEK content simply because fewer ketone groups that participate in the crosslinking reaction were present. Secondly, the UV light should penetrate more deeply into the film with increased PPO content since the PPO absorbs less light relative to the BPA-PAEK. These factors produce results that are counter to each other, so this may lead to the insignificant change shown in Figure 4.7.

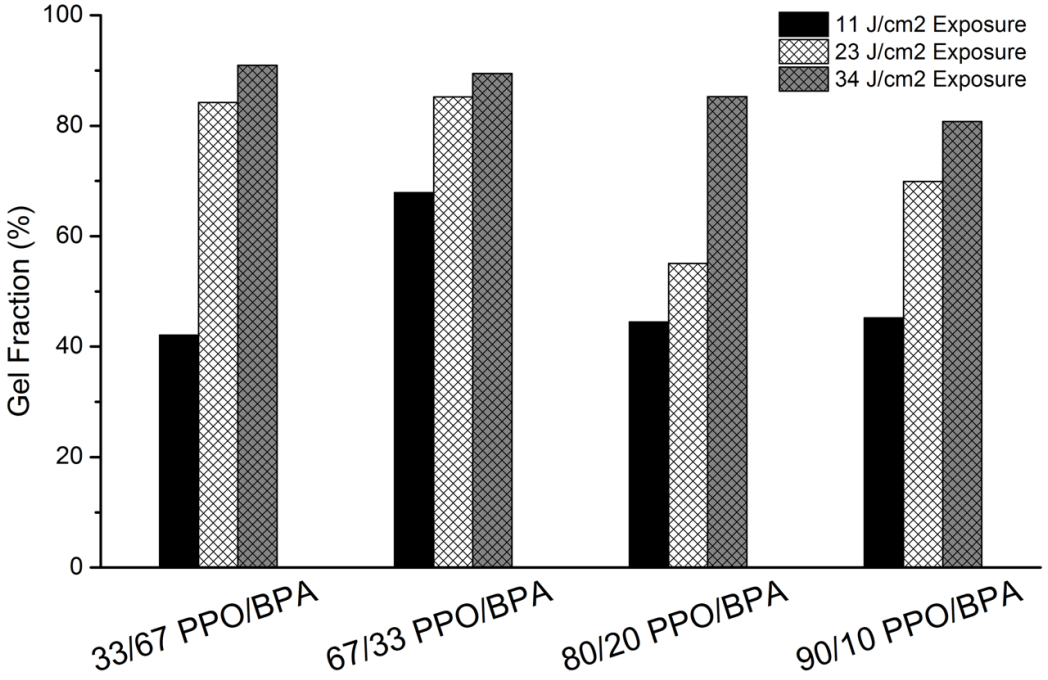

Figure 4.7. Gel fractions after UV crosslinking of blends of 22,000 M_n PPO with BPA-PAEK over a range of compositions (Figure used with permission from Elsevier).

It is expected that the phase structure of the blends is also a contributing factor. The DSC thermograms in Figures 4.3-4.4 show two T_gs for all of the PPO molecular weights except for the very low 2000 M_n polymer, thus strongly suggesting that two phases are present. However, high gel fractions were obtained after crosslinking blends of the 22,000 M_n PPO/BPA-PAEK, and it is postulated that this can only occur when the benzylic methyl groups are in the same phase as the ketone groups. This suggests some level of miscibility within the system. It is believed that there are two phases within the blends and that each contain both PPO and BPA-PAEK. Referring back to Figure 4.4 where T_gs measured by DSC are reported for blends of the PBA-PAEK with the 6,000 M_n PPO, the T_g of the phase that contains the higher volume fraction of PPO increases upon crosslinking. This suggests a decrease in molecular mobility after crosslinking. While it is reasoned that crosslinking may increase compatibility (or the level of miscibility), we are cognizant of the fact that these films were crosslinked in the solid state well below either T_g, and also that T_g would reflect both any change in miscibility but also changes in mobility. The morphology of the blends was not explored in this study but would provide information regarding the unique behavior of this system.

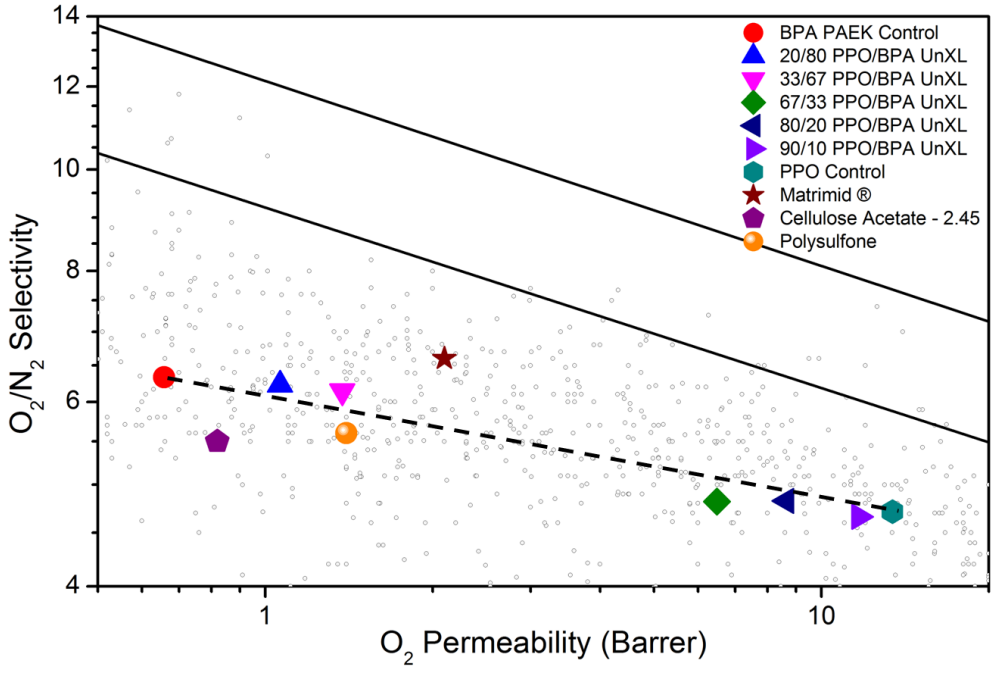

Figure 4.8. Comparison of oxygen and nitrogen transport in blends of the 22,000 Mn PPO/BPA-PAEK at different compositions and the controls. The dashed line represents linear behavior.[4, 7, 8] (Figure used with permission from Elsevier).

The permeabilities and ideal selectivities for the 22,000 g/mole PPO/BPA-PAEK films with different compositions are shown in Table 4-2, and a graph showing their placement on the O_2/N_2 upper bound is given in Figure 4.8. The linear dashed line in Figure 4.8 represents the transport properties that would be expected for miscible blends.[27, 28] As would be expected in these multiphase blends, the membranes with high compositions of PPO have higher permeabilities and lower selectivities and this is attributed to the high free volume of PPO. A few commercial polymers are included in Figure 4.8, and the 33/67 22,000 M_n PPO/BPA-PAEK showed better selectivity than either polysulfone or cellulose acetate.

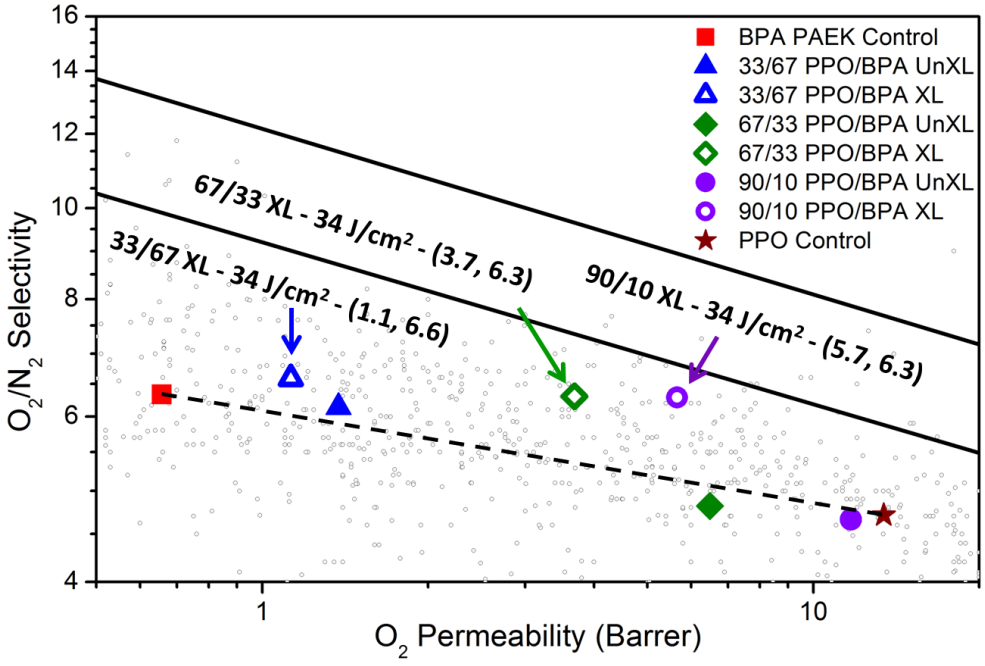

Figure 4.9. Comparison of 22,000 Mn PPO/BPA PAEK non-crosslinked and crosslinked blends at different compositions relative to the controls. The dashed line represents the linear behavior and the numbers on the graph are permeabilities and selectivities with the format (x,y).[7, 8] (Figure used with permission from Elsevier).

The 33/67, 67/33, and 90/10 22,000 M_n PPO/BPA-PAEK films were crosslinked via exposure to UV radiation and the results are provided in Figure 4.9 along with the bulk and non-crosslinked controls. The 90/10 22,000 M_n PPO/BPA-PAEK crosslinked membrane exhibited good selectivity and permeability for O_2/N_2 separation in a film that was comprised largely of a readily available commercial polymer. As discussed previously, the UV light was able to penetrate further into this film to crosslink more polymer and therefore increase the selectivity substantially. Secondly, the UV exposure created a gradient of crosslinked material through the thickness of the film. Therefore, the highly

crosslinked surface likely contributed to the high selectivity while the lightly crosslinked center of the film likely contributed to the high permeability.[15,17]

Table 4-2. Transport properties of BPA-PAEK blends with PPO at 35 °C and 3 atm

	O_2 (Barrer)	N_2 (Barrer)	O_2/N_2 Selectivity	H_2 (Barrer)	CH_4 (Barrer)	CO_2 (Barrer)
BPA-PAEK Control	0.66	0.1	6.3	8.2	0.12	2.7
20/80 22k PPO/BPA-PAEK NonXL	1.1	0.17	6.2	13	0.19	4.5
33/67 22k PPO/BPA-PAEK NonXL	1.4	0.22	6.1	16	0.24	5.8
33/67 22k PPO/BPA-PAEK XL	1.1	0.17	6.6	16	0.15	4.5
67/33 22k PPO/BPA-PAEK NonXL	6.5	1.3	4.8	54	1.5	28
67/33 22k PPO/BPA-PAEK XL	3.7	0.58	6.3	45	0.47	14
80/20 22k PPO/BPA-PAEK NonXL	8.6	1.8	4.8	70	2.1	36
90/10 22k PPO/BPA-PAEK NonXL	11.7	2.5	4.7	90	2.9	50
90/10 22k PPO/BPA-PAEK XL	5.7	0.9	6.3	68	0.71	22
22k PPO Control	13.4	2.8	4.7	105	3.3	57
Matrimid® *	2.1	0.32	6.6	18	0.28	10
Cellulose Acetate - 2.45 *	0.82	0.15	5.5	12	0.15	4.8
Polysulfone *	1.4	0.25	5.6	14	0.25	5.6

(Table used with permission from Elsevier).

* Values are from Sanders et al.[4]

Pure 22,000 g/mole PPO has suitable mechanical properties for application in gas separation membranes. Therefore, the tensile properties of the non-crosslinked blends at all blend ratios were compared to those of pure PPO films. Steel with control nonparametric multiple comparisons analysis[29] (conducted using a 95% confidence interval and 100% PPO as the control data

set) shows no statistical differences between the modulus data sets or the tensile strength at yield data sets for any of the samples. Using the same type of analysis for the elongation and strength at break data sets, the only blends that showed a statistical difference were those comprised of 20 and 33% PPO (Figure 4.10). Thus, even though these are two-phase blends, the mechanical properties remain consistent with those of pure PPO over a wide range of PPO-rich blend ratios. For BPA-PAEK-rich blends (33% PPO or less) the properties of BPA-PAEK dominate the mechanical responses, which result in higher strength and elongation at break.

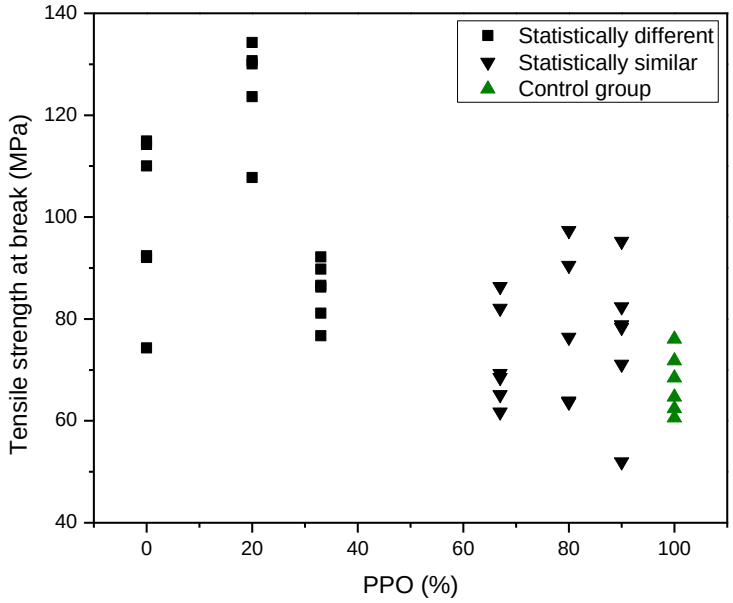

Figure 4.10. Tensile strength at break data. Only the 0, 20, and 33% PPO data sets are statistically different from the 100% PPO control data set. (Figure used with permission from Elsevier).

Blends containing 33 wt% PPO and 67 wt% of BPA-PAEK of varying molecular weights were also tested in tension. Despite the higher fraction of BPA-

PAEK, the molecular weight of the PPO had a significant impact on the mechanics of the films. Films containing the 2,000 and 6,000 g/mole PPO exhibited a brittle failure mechanism with little to no yielding (Figure 4.11-A) while films containing higher molecular weight PPO displayed yielding and drawing behavior (Figure 4.11-B). This result confirms that the mechanics of the blends are highly dependent on the molecular weight of the PPO, even when the

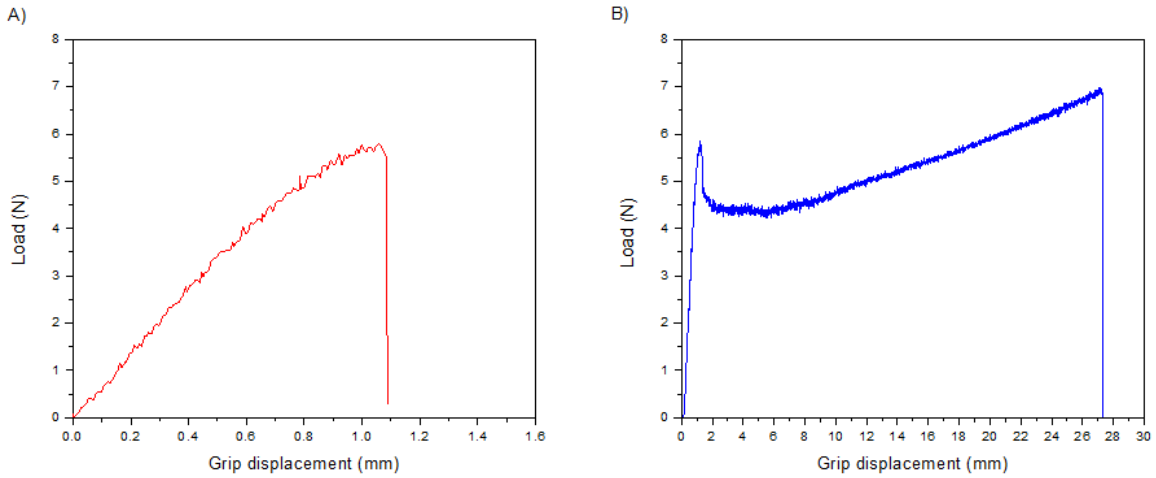

Figure 4.11. Representative load-displacement curves for A) 67% BPA-PAEK blended with 33% 6,000 g/mole PPO (shows brittle failure mode), B) 67% BPA-PAEK blended with 33% 22,000 g/mole PPO (shows yielding, drawing, and strain hardening behavior) (Figure used with permission from Elsevier).

BPA-PAEK is the dominant phase.

4.4 Conclusions

PPO and BPA-PAEK were blended to form membranes that were phase separated except for the samples with the very low M_n PPO. The DSC results showed that the 6000, 17,000, 19,000, and 22,000 blended films had two T_gs that closely correlated with the corresponding homopolymer T_gs, suggesting that

they had a two-phase nature. Despite the immiscibility of these films, the gel fractions showed significant insolubility after UV exposure. Gel fractions as a function of the 22,000 M_n PPO composition were explored and did not show any significant change. This is likely a result of several competing factors. One trend is that as the PPO composition is increased, there is a lower ketone content which participates in the crosslinking reaction. Counter to that is that with increased PPO content, UV light can penetrate further into the film and crosslink more chains. This is because PPO absorbs significantly less UV light than the BPA-PAEK as shown via solution UV absorbance spectra.

The 33/67 wt/wt PPO/BPA-PAEK demonstrated the best permselectivity performance with respect to the linear behavior due to its increased permeability with little decrease in selectivity. However, with respect to the upper bound, the 90/10 PPO/BPA-PAEK had the best performance due to PPO's high permeability. Between the three crosslinked blended films, the 90/10 PPO/BPA-PAEK gained the most selectivity and maintained a larger amount of its permeability. This can be attributed to a greater degree of UV light penetration into the film to crosslink more polymer chains due to PPO's lower absorbance. Another reason is that the UV exposure created a gradient of crosslinked material that created a selective surface and a permeable center.

Overall, we were able to blend a small amount of BPA-PAEK with the commercially used PPO to create mechanically robust crosslinkable polymer films. In comparison to commercial gas separation polymers, the 33/67 wt/wt 22,000 PPO/BPA-PAEK blend outperformed polysulfone and cellulose acetate

without any crosslinking. In the future, such systems might be able to crosslink substantially with even less of the ketone-containing polymer. Additionally, PPO could be blended with other materials to focus on other gas pairs and applications.

4.5 References

1. P. Bernardo, E. Drioli and G. Golemme, *Industrial & Engineering Chemistry Research*, 2009, **48**, 4638-4663.
2. R. W. Baker, *Industrial & Engineering Chemistry Research*, 2002, **41**, 1393-1411.
3. R. W. Baker and B. T. Low, *Macromolecules*, 2014, **47**, 6999-7013.
4. D. F. Sanders, Z. P. Smith, R. Guo, L. M. Robeson, J. E. McGrath, D. R. Paul and B. D. Freeman, *Polymer*, 2013, **54**, 4729-4761.
5. Y. Yampolskii, *Macromolecules*, 2012, **45**, 3298-3311.
6. B. D. Freeman and I. Pinnau, in *Polymer Membranes for Gas and Vapor Separation*, American Chemical Society, 1999, vol. 733, ch. 1, pp. 1-27.
7. L. M. Robeson, *Journal of Membrane Science*, 1991, **62**, 165-185.
8. L. M. Robeson, *Journal of Membrane Science*, 2008, **320**, 390-400.
9. B. D. Freeman, *Macromolecules*, 1999, **32**, 375-380.
10. US3306875, 1967.
11. M. Aguilar-Vega and D. R. Paul, *Journal of Polymer Science Part B: Polymer Physics*, 1993, **31**, 1599-1610.
12. K. Ghosal and R. T. Chern, *Journal of Membrane Science*, 1992, **72**, 91-97.
13. S. Sridhar, B. Smitha, M. Ramakrishna and T. M. Aminabhavi, *Journal of Membrane Science*, 2006, **280**, 202-209.
14. M. S. McCaig and D. R. Paul, *Polymer*, 1999, **40**, 7209-7225.
15. Q. Liu, A. T. Shaver, Y. Chen, G. Miller, D. R. Paul, J. S. Riffle, J. E. McGrath and B. D. Freeman, *Polymer*, 2016, DOI: http://dx.doi.org/10.1016/j.polymer.2016.01.075, 202-214.
16. B. J. Sundell, A. T. Shaver, Q. Liu, A. Nebipasagil, P. Pisipati, S. J. Mecham, J. S. Riffle, B. D. Freeman and J. E. McGrath, *Polymer*, 2014, **55**, 5623-5634.

17. J. R. Rowlett, Q. Liu, W. Zhang, J. D. Moon, M. E. Dose, J. S. Riffle, B. D. Freeman and J. E. McGrath, *Journal of Materials Chemistry A*, 2016, **4**, 16047-16056.
18. S. A. Srinivasan and J. E. McGrath, *High Performance Polymers*, 1993, **5**, 259-274.
19. T. P. Bender, R. A. Burt, G. K. Hamer, C. DeVisser, P. F. Smith and M. Saban, *Organic Process Research & Development*, 2002, **6**, 714-720.
20. G. D. Lyle, H. Grubbs, C. Tchatchoua and J. E. McGrath, *Polymeric Materials Science and Engineering*, 1993, **69**, 238-239.
21. Y. Chen, R. Guo, C. H. Lee, M. Lee and J. E. McGrath, *International Journal of Hydrogen Energy*, 2012, **37**, 6132-6139.
22. G. D. Lyle, J. S. Senger, D. H. Chen, S. Kilic, S. D. Wu, D. K. Mohanty and J. E. McGrath, *Polymer*, 1989, **30**, 978-985.
23. A. S. Hay, *Journal of Polymer Science*, 1962, **58**, 581-591.
24. T. G. Fox and P. J. Flory, *Journal of Polymer Science*, 1954, **14**, 315-319.
25. C. T. Wright and D. R. Paul, *Journal of Membrane Science*, 1997, **124**, 161-174.
26. H. Morawetz, *Journal of Polymer Science Part C: Polymer Letters*, 1988, **26**, 243-244.
27. H. B. Hopfenberg and D. R. Paul, in *Polymer Blends*, ed. D. R. N. Paul, S. , Academic Press, New York, 1978, pp. 445-489.
28. A. E. Barnabeo, W. S. Creasy and L. M. Robeson, *Journal of Polymer Science: Polymer Chemistry Edition*, 1975, **13**, 1979-1986.
29. R. G. D. Steel, *Biometrics*, 1959, **15**, 560-572.

Chapter 5: Synthesis and Membrane Properties of Sulfonated Poly(arylene ether sulfone) Statistical Copolymers for Electrolysis of Water: Influence of meta and para-Substituted Comonomers

Amin Daryaei,[1] Gregory C. Miller,[1] Jason Willey,[3] Britannia Vondrasek,[2] Shreya Roy Choudhury,[1] Dana Kazerooni,[1] Matt Burtner,[2] Cortney Mittelsteadt,[3] John J. Lesko,[2] Judy S. Riffle,[1*] James E. McGrath[1]

[1] Department of Chemistry and Macromolecular Innovation Institute, Virginia Tech, Blacksburg, VA 24061

[2] College of Engineering, Virginia Tech, Blacksburg, VA 24061

[3]Giner Inc. Newton, MA 02466

5.1 Introduction

Hydrogen gas as a green fuel is a high energy molecule that can be used in fuel cells to generate electricity for the grid and automobiles.[1] Among different commercial pathways for hydrogen gas production,[2-5] electrolysis of water using proton exchange membranes has attracted much attention as a result of positive aspects such as producing high purity product,[6] high current density[7, 8] and fast kinetics at elevated temperatures.[9] The electrolyzers can also be coupled to renewable energy sources such as wind turbines or solar cells as environmentally friendly electricity producers. Hydrogen produced by electrolysis can be directly used in a fuel cell to provide a potential alternative to fossil fuels for generating electricity.

The state-of-the-art PEM for electrolysis of water is DuPont's perfluorosulfonic acid membrane, Nafion™. Nafion™ is a good proton conductor and it is highly chemically resistant and mechanically robust at temperatures below its T_g. However,

it has drawbacks including high gas permeability and poor mechanical stability above the α relaxation temperature of ~80°C and at the high operating pressure of the electrolyzer. Such operating conditions eventually result in loss of mechanical strength and reduced proton conductivity.[10-12] Sulfonated random and block copolymers such as polyimides,[13, 14] poly(arylene ether ketones),[15] poly(arylene ether sulfones)[16-19] and polybenzimidazoles[20] have been intensively investigated as PEMs in fuel cells. Fuel cells and electrolyzers have similar requirements regarding membrane properties. Both systems operate under highly acidic conditions and this places special stability requirements on the membranes for extended use. High temperature water electrolyzers are operated under harsher conditions than fuel cells including a higher pressure and fully hydrated environment and this requires a robust membrane to withstand any reactive radicals that may form as well as hydrolysis reactions.[8, 21, 22] However, in the literature, there are not as many studies on potential alternatives for Nafion™ for electrolysis of water. Creating a PEM that has decreased gas permeability to minimize gas crossover and superior conductive properties relative to perfluorosulfonic acid membranes is a challenge that needs to be addressed.

Smith et al.[23] prepared a poly(ether ketone) via step growth polymerization and post sulfonated this polymer in concentrated sulfuric acid at elevated temperatures. In comparison with Nafion™, this copolymer had comparable proton conductivity, lower gas permeability and better mechanical stability for use in electrolysis of water with higher efficiencies, most likely as a result of its microphase separated structure. Albert et al.[24] grafted styrene and acrylonitrile and a crosslinker onto an ethylene tetrafluoroethylene film using radiation, then post-sulfonated the styrenic rings. This synthesis method resulted in a cost effective membrane with better mechanical

properties than Nafion™, but using aliphatic chains in PEMs can lead to lower chemical resistance under harsh electrochemical conditions.[25] Moreover, inhomogeneous sulfonic acid distribution across the membranes resulted in high membrane area resistance. High membrane resistance could also be at least partially attributed to the presence of non-conductive hydrophobic polymer on the membrane surface that acts as a water (mass) transfer inhibitor as suggested by Takimoto *et al.*[26] It is known that a direct synthesis route to disulfonated polysulfones using pre-disulfonated comonomers allows control over factors including random distribution of the sulfonic acid groups, ion exchange capacity (IEC) of the membrane, morphology and proton conductivity and it can also avoid crosslinking of the membrane.[16, 27-29]

In this work, gas permeability and proton conductivity in PEMs were investigated in two series of sulfonated poly(arylene ether sulfone) statistical copolymers. These series were synthesized based on the difference between phenolic monomers and their ratio in the polymer backbone. One series contains solely hydroquinone (HQ) as a *para*-substituted comonomer. The second series contains 25 mole % of resorcinol (RSC) as a *meta*-substituted phenolic comonomer, co-reacted into a HQ-based linear copolymer. Both series of copolymers were synthesized by direct synthesis of disulfonated dichlorodiphenyl sulfone via step-growth polymerization. Fundamental properties of the PEMs for high temperature water electrolysis systems such as water uptake of the membranes in liquid water at room and elevated temperatures, H_2 gas permeability, mechanical stability, and the ratio of $\frac{Proton\ conductivity}{Gas\ permeability}$ from room temperature to 100°C were established and compared with Nafion™.

5.2 Experimental

5.2.1 Materials

Toluene was purchased from Sigma-Aldrich and was used as received. 1,4-Benzenediol (hydroquinone, HQ) was provided by Eastman Chemical Company. 4,4'-Dichlorodiphenylsulfone (DCDPS) was provided by Solvay Advanced Polymers. 1,3-Benzenediol, resorcinol (RSC, >99%), was purchased from Sigma-Aldrich. DCDPS, HQ, and RSC were recrystallized from toluene and dried under vacuum at 120°C prior to use. *N,N*-Dimethylacetamide (DMAc) was purchased from Sigma-Aldrich and distilled from calcium hydride before use. Calcium hydride (90−95%) was purchased from Alfa Aesar. 2-Propanol was obtained from Fisher Scientific and used as received. Sulfuric acid (H_2SO_4, 98%) was purchased from Spectrum Chemical and used as received. Potassium carbonate (K_2CO_3) was purchased from Aldrich and dried under vacuum at 180°C prior to use. 3,3'-Disulfonated-4,4' dichlorodiphenylsulfone (sDCDPS, >99%) was purchased from Akron Polymer Systems and was dried at 180°C prior to use. DuPont's Nafion™ 212 was provided by Giner Electrochemical Systems.

5.2.2 Synthesis of Statistical Copolymers

Aromatic nucleophilic substitution step copolymerization was used to synthesize both series of disulfonated poly(arylene ether sulfone) copolymers. A typical HQS-20 with 20% of the repeat units disulfonated was synthesized as follows. HQ (36.33 mmol, 4.00 g), DCDPS (29.06 mmol, 8.3451 g), SDCDPS (7.265 mmol, 3.57 g), and DMAc (55 mL) were charged into a 250-mL three neck round bottom flask equipped with a mechanical stirrer, condenser, nitrogen inlet, and Dean-Stark trap filled with toluene. The mixture was stirred in an oil bath at 150°C until all the monomers completely

dissolved. K_2CO_3 (47.22 mmol, 6.52 g), and toluene (25 mL) were added into the flask. The reaction was refluxed for 4 h to azeotropically remove water from the system. Toluene was drained from the Dean-Stark trap, and the oil bath temperature was raised to 180°C to remove residual toluene from the reaction. The reaction solution was stirred for 48 h to complete polymerization, then allowed to cool to room temperature. After dilution of the resulting solution with DMAc (150 mL), it was filtered to remove the salt. The transparent solution was precipitated by addition into isopropanol with vigorous stirring. The white fibers were filtered and then stirred in boiling DI water for 4 h to remove any residual DMAc. The copolymer was filtered and dried at 120°C under reduced pressure in a vacuum oven. Yield of this copolymer synthesis was 94% copolymer.

Synthesis of $HQ_{0.75}RSC_{0.25}$-XX copolymers: A typical $HQ_{0.75}RSC_{0.25}$-19 with 19 of the repeat units disulfonated was synthesized as follows. HQ (27.24 mmol, 3.00 g), RSC (9.08 mmol, 1.00 g), DCDPS (28.33 mmol, 8.137 g), SDCDPS (8.0 mmol, 3.93 g), and DMAc (55 mL) were charged into a 250-mL three neck round bottom flask equipped with a mechanical stirrer, condenser, nitrogen inlet, and Dean-Stark apparatus filled with toluene. The mixture was stirred in an oil bath at 150°C until the monomers completely dissolved. K_2CO_3 (47.22 mmol, 6.52 g), and toluene (25 mL) were added into the flask. The reaction was refluxed for 4 h, the toluene was drained from the Dean-Stark apparatus, then the oil bath temperature was raised to 180°C to remove residual toluene from the reaction. The solution was stirred for 48 h at 180°C, then cooled to room temperature. The solution was diluted with DMAc (150 mL), the filtered to remove the salt. The transparent solution was precipitated into isopropanol. The white fibers were filtered and stirred in boiling DI water for 4 h. The copolymer

was then filtered and dried at 120°C under reduced pressure in a vacuum oven. Yield of this copolymer synthesis was 94% copolymer.

5.2.3. Nuclear Magnetic Resonance Spectroscopy (NMR)

^{1}H NMR analysis of the statistical copolymers was conducted on a Varian Unity Plus spectrometer operating at 400 MHz. The spectra of the copolymers were obtained from a 10% (w/v) solution in DMSO-d_6.

5.2.4 Size Exclusion Chromatography (SEC)

Molecular weights and polydispersities of the polymers were measured using SEC. The mobile phase was DMAc distilled from CaH_2 containing dry LiCl (0.1 M). The column set consisted of 3 Agilent PLgel 10-mm Mixed B-LS columns 300 * 7.5 mm (polystyrene/divinylbenzene) connected in series with a guard column having the same stationary phase. The columns and detectors were maintained at 50°C. An isocratic pump (Agilent 1260 infinity, Agilent Technologies) with an online degasser (Agilent 1260), autosampler and column oven were used for mobile phase delivery and sample injection. A system of multiple detectors connected in series was used for the analyses. A multi-angle laser light scattering detector (DAWN-HELEOS II, Wyatt Technology Corp.), operating at a wavelength of 658 nm, a viscometer detector (Viscostar, Wyatt Technology Corp.), and a refractive index detector operating at a wavelength of 658 nm (Optilab T-rEX, Wyatt Technology Corp.) provided online results. The system was corrected for interdetector delay and band broadening using a 21,000 g/mole polystyrene standard. Data acquisition and analysis were conducted using Astra 6 software from Wyatt Technology Corp. Validation of the system was performed by monitoring the molar mass of a known molecular weight polystyrene sample by light

scattering. The accepted variance of the 21,000 g/mole polystyrene standard was defined as 2 standard deviations (11.5% for M_n and 9% for M_w) derived from a set of 34 runs. Specific refractive index values were calculated based on the assumption of 100% recovery.

5.2.5 Membrane casting and characterization

The copolymers in their salt form were dissolved in DMAc (~6% w/v), and then filtered through a 0.45 μm Teflon syringe filter. The solutions were cast onto clean glass substrates and dried under an infrared lamp at 50-60°C for 8 h. Afterwards, the membranes were placed in a vacuum oven under reduced pressure at 120-140°C for 4 h. The membranes were soaked in water for an additional 24 h to remove residual solvent and to delaminate them from the glass plates. The membranes were converted to their acid form by boiling in 0.1 M H_2SO_4 for 2 h and they were then boiled in DI water for 2 h to remove residual acid.

5.2.6 Ion Exchange Capacity (IEC)

Dry membranes in their acid form were weighed, then soaked in 1 M NaCl solution for 48 h to convert them to their salt form and eliminate HCl. Each membrane solution was titrated with 0.1 N NaOH solution. The IEC of each membrane in units of mequiv/g of dry membrane was calculated from equation 5.1:

$$IEC = \frac{V*N}{M}\ x\ 1000 \qquad (5.1)$$

Where V is volume of NaOH, N is NaOH normality, and M is the mass of the dry membrane.

5.2.7 Water Uptake at Room and Elevated Temperatures

The water uptakes of the membranes were determined gravimetrically. First, the membranes in their acid form were dried at 120°C under vacuum for 24 h and weighed. These membranes were soaked in water at room temperature for 48 h. Wet membranes were removed from the liquid water, blotted dry to remove surface droplets, and quickly weighed. For high temperature water uptake, the previously wet membranes were placed in boiling water for at least 4 h. Then the hot, wet membranes were removed from the boiling water, immediately blotted dry to remove surface droplets, and quickly weighed. The water uptake of the membranes was calculated according to equation 5.2, where mass dry and mass wet refer to the masses of the dry and the wet membranes, respectively.

$$\text{Water Uptake (\%)} = \frac{Mass_{wet} - Mass_{dry}}{Mass_{dry}} \times 100 \qquad (5.2)$$

5.2.9 Differential Scanning Calorimetry (DSC)

The glass transition temperatures (T_gs) of the copolymers were investigated using a TA Instruments DSC Q200. For dry samples, standard aluminum hermetic pans were used, and for hydrated samples, high volume DSC pans were used. The samples were hydrated by immersion in deionized water for 24h prior to loading into the DSC pans. The polymers were heated under nitrogen at a rate of 10 °C min^{-1} to 200 °C, cooled at a rate of 10 °C min^{-1} to 0 °C, and heated again at a rate of 10 °C min^{-1} to 240 °C. The T_g's of the samples were determined from the second heat by finding the inflection point of the W/g vs. temperature curve with the aid of TA Universal Analysis software.

5.2.10 Tensile Tests

Tensile samples were cut from hydrated solvent cast films using a Cricut Explore One™ computer controlled cutting machine. Nafion™ samples were prepared in the same manner from Nafion™ 212. The resulting dogbone shaped samples were consistent with sample Type V described in ASTM D638-14. The sample films were inspected for any visible flaws, defects, or inclusions that may have arisen during the casting process. The seven highest quality samples were selected for testing. The sample thickness was measured at five points along the narrow section using a Mitutoyo digimatic micrometer model MDC-1"SXF. Uniaxial load tests were performed using an Instron ElectroPuls E1000 testing machine equipped with a 250 N Dynacell load cell. The instrument was fitted with a water bath and the samples were completely immersed in deionized water. The samples were allowed to equilibrate in the water for at least 3 minutes before testing to obtain fully hydrated mechanical data. For high temperature hydrated tests, the tank was fitted with an immersion heater and was well insulated to maintain the water at the target temperature of 80°C. For all mechanical tests, the crosshead displacement rate was 10 mm/min and the initial grip separation was 25 mm.

Young's moduli were calculated from the slope of the initial linear region of the loading curve. The yield point was considered to be the intersection of the load curve with a 1% offset of this modulus line. This offset was chosen because it correlated with the yield point for lower IEC samples, some of which showed a distinct yield point in the load-displacement curve. Nominal strain at yield was calculated by dividing the change in grip separation by the initial grip separation. Tensile strength at yield was calculated by dividing the load by the average cross-sectional area of the narrow

section, which was based on a sample width of 3.18 mm and the average of the five sample thickness measurements. Since the instrument's stroke was limited to around 5 cm (200% strain for this sample geometry) and some of the samples did not fail within this range, the ultimate properties of the polymer are not presented here. However, because most samples failed above 60% strain and above 20 MPa stress, we consider these polymers to have suitable ultimate properties for separation applications.

5.2.11 H_2 Gas Permeability (P)

A membrane was loaded into a Fuel Cell Technologies standard fuel cell hardware set. This set-up was installed inside a TestEquity environmental chamber with both heating and cooling capabilities. All flows were controlled or measured with Alicat mass flow controllers and meters. A flow of carrier gas was established on one side of the cell and the humidified permeant gas to the other. For these tests, over-humidified (condensing) permeant gas was used to simulate the flooded membrane of the electrolyzer. The permeant diffuses through the membrane, and a slipstream of the carrier gas is sent to an Agilent microGC for analysis of the permeant. The amount of permeant in the carrier gas was used to calculate the permeation rate of that gas through the membrane at that specific temperature according to equation 5.3. Then the temperature was changed and the process repeated.

$$P = \frac{DT}{tA\Pi} \qquad \textbf{(5.3)}$$

5.2.12 Proton Conductivity (σ)

The conductivity test stand consisted of a house-made four-point probe assembly with platinum electrodes and a Wayne-Kerr LCR meter. The membrane was clamped between the probe assembly and placed in the water bath at room temperature. The water bath was heated steadily to 100°C and AC impedance measurements were taken at intervals of 10°C as the assembly was heated and cooled. Using the dimensions of the membrane, the conductivity of the ionomer was calculated based on equation 5.4:

$$\sigma = \frac{l}{RA} \qquad \textbf{(5.4)}$$

5.2.13 Performance

The ratio of $\frac{\sigma}{P}$ was calculated for selected membranes at temperatures of 30, 60, 90 and 100°C. The performance of each copolymer was calculated by normalizing the $\frac{\sigma}{P}$ to that of Nafion at each temperature based on equation 5.5:

$$\textbf{Performance} = \frac{\frac{\sigma_{polymer}}{P_{polymer}}}{\frac{\sigma_{Nafion}}{P_{Nafion}}} \qquad \textbf{(5.5)}$$

where $\sigma_{polymer}/P_{polymer}$ are the ratio of proton conductivity to H_2 gas permeability for each copolymer and $\sigma_{Nafion}/P_{Nafion}$ are the ratio of proton conductivity to H_2 gas permeability through Nafion™, respectively.

5.3 Results and Discussion

5.3.1. Synthesis and Characterization of Statistical Copolymers

Synthesis of sulfonated poly(arylene ether sulfone) random and block copolymers have been intensively studied by many research groups.[30-34] In this study, two series of random copolymers were synthesized via step-growth polymerization based on the reaction shown in Scheme 5.1. It is noteworthy that as more resorcinol (the *meta*-substituted bisphenol) was incorporated into such copolymers, this detracted from the mechanical properties. Thus, only copolymers with 25 mole % of resorcinol together with 75 mole % of hydroquinone, where the mechanical properties were considered to be good, were pursued in this study.

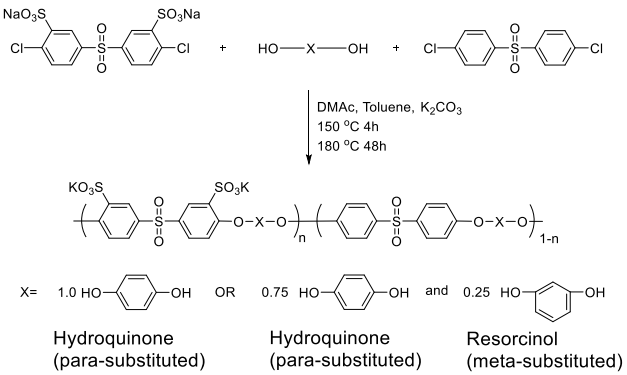

Figure 5.1. Random copolymer synthesis of a 100% *para*-substituted phenolic HQ-based copolymer or a 75% *para*- and 25% *meta*-substituted phenolic HQRSC copolymer

Reactions were designed so that the IEC of a copolymer in the hydroquinone-based series would match with one in the $HQ_{0.75}RSC_{0.25}$ series. SEC confirmed that the molecular weight of each copolymer was well above the threshold entanglement point which is ~10,000 g/mole,[35, 36] and therefore was suitable for these investigations. Representative ^1H NMR spectra of HQ 16 and HQRSC 17 in Figure 5.1 confirm the

structures of these random copolymers. The molecular weights and IECs of the membranes are shown in Table 5-1.

Table 5-1. Degree of disulfonation, IEC per gram of dry copolymer, and molecular weights of the copolymers

Copolymer-Degree of disulfonation	IEC (meq/g)	M_w (kDa)
HQRSC 17	0.95	107
HQRSC 19	1.08	108
HQRSC 24	1.33	70
HQRSC 25	1.36	92
HQRSC 32	1.63	104
HQ 16	0.93	153
HQ 20	1.12	199
HQ 23	1.29	80
HQ 25	1.39	101
HQ 30	1.59	91

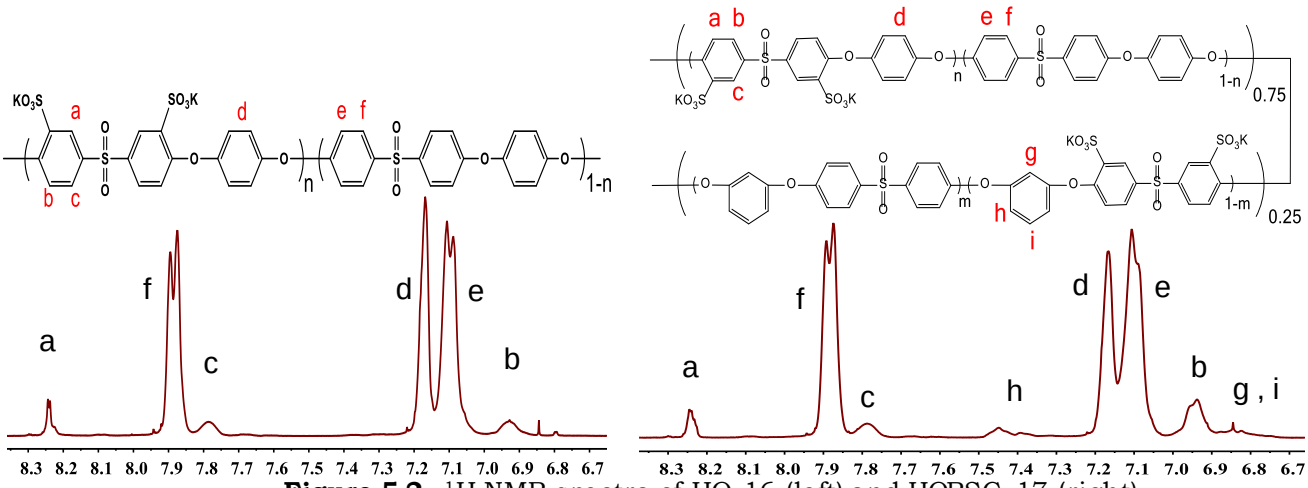

Figure 5.2. ^{1}H NMR spectra of HQ 16 (left) and HQRSC 17 (right)

5.3.2 Membrane Water Uptake

In general, an increase in water uptake correlates with a large increase in the proton conductivity of PEMs. This has been attributed to water molecules weakening the electrostatic interaction between H^+ ions and the polymer backbone fixed SO_3^- groups, thus resulting in faster H^+ ion transfer.[37] However, high water uptake directly correlates to a decrease in mechanical properties of the membrane in an electrochemical device.[21, 38, 39] Figure 5.2 shows the weight percent of water uptake at room temperature and ~80°C for both series of copolymers.

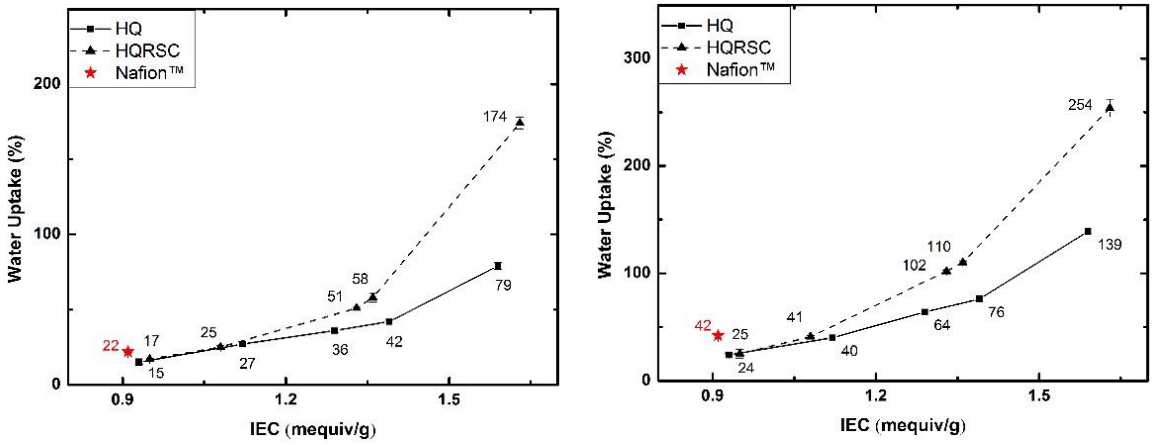

Figure 5.3. Water uptake of the membranes at room temperature (Left) and high temperature (Right).

As expected, water uptake increases with IEC and the degree of disulfonation in both series. For cases of polysulfones without sulfonate groups and with varying *meta* versus *para* orientation of the backbone rings, it has been shown that polymers with *meta*-substituted rings in the dry state pack more tightly, have lower free volume, and generally have lower gas permeabilities.[40] The anticipated decrease in gas permeability with incorporation of the resorcinol was indeed one of our prime motivations for undertaking this study. The present case, however, is much more complicated than studying polymers in their dry state since the fixed sulfonate groups lead to significant water uptake. Figure 5.2 clearly shows a large increase in water uptake in the disulfonated copolymers that contain some resorcinol relative to those containing only the *para*-substituted bisphenol. However, this is only prominent above the IECs that are of most interest for electrolysis (IEC ~0.9 and ~1.1 in meq/g of dry polymer). Figure 5.2 also shows increased water uptake at elevated temperatures relative to ambient temperature, but there is little difference in water uptake at the two temperatures at the lower IEC points of most interest.

5.3.3 Membrane Thermal Properties

As shown in Figure 5.3, the glass transition temperatures of these copolymers in the dry state are high and they increase with increasing IEC for both the HQ and HQRSC copolymers. As the number of sulfonate groups are increased in the backbone, the chains stiffen and therefore are less mobile and unable to explore various conformations at low temperatures. Furthermore, the 100% HQ copolymers have higher T_g's at each comparable IEC than their HQRSC analogues in the dry state. This can also be explained by the chain stiffness. As confirmed by the modulus data that is discussed in this paper, the *para*-substituted hydroquinone moiety leads to a more

rigid chain than the *meta*-substituted resorcinol moiety. This also follows the trend noted with *para* versus *meta*-substituted rings without the added sulfonate groups.[41]

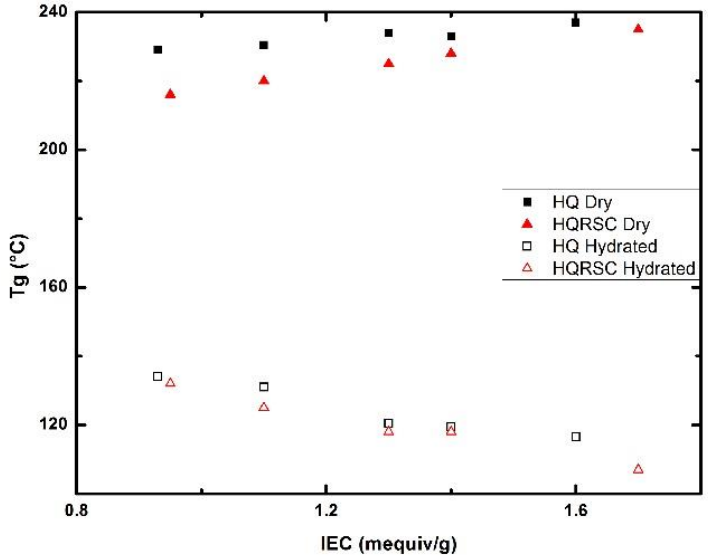

Figure 5.4. T_gs of the random copolymers in their dry and hydrated states.

In the hydrated state, HQ and HQRSC copolymers both show decreasing T_gs with increasing IEC. This is expected because as the number of sulfonic acids increases, the water uptake increases, leading to increased plasticization of the polymers. It is known that hydration of the membranes causes plasticization, resulting in decreased glass transition temperatures.[41, 42] Interestingly, the HQ and HQRSC copolymers show a slight difference in T_g from one another at comparable IECs in the hydrated state. Figure 5.4 shows T_g vs water uptake for the HQ and HQRSC copolymers. Two morphological regimes are suggested with the transition between regimes occurring at water uptakes of 40-60%, where the slopes of the curves appear to change. This transition is consistent with a transition from localized hydrophilic clusters to a percolating network of hydrated polymer, as presented elsewhere.[43]

The distinction between the two morphological regimes may be explained by the way in which the copolymers interact with water. As described by Roy et al. in reference

45, ~ 9 moles of water per sulfonic acid group are non-freezable, while additional water was characterized as "loosely bound" to the sulfonic acid groups or "free water".[44] A morphological transition was suggested with the rise in "free water" that occurred at an IEC of 1.2-1.4 meq/g and that corresponded to ~40-50% by weight of water uptake. The present paper expands such correlations for both hydroquinone and resorcinol-containing random copolymers. HQ 20 and HQ 23 have IECs and water uptakes of 1.12 meq/g and 27 % uptake and 1.29 meq/g and 36 % water uptake, respectively. By correlating these materials with those described earlier,[44] this correlates with 9 moles of non-freezable water and 5 and 7 moles of freezable water, respectively. In agreement with earlier suggestions, Figure 5.4 shows an abrupt change in the slope of T_g with water uptake at ~40-50% water. We believe this also signifies a change in morphology at these compositions. Above approximately 50% water uptake, the hydrated regimes reach a percolation threshold, and a dominant amount of the water is considered to be free or unbound to the hydrophilic segments, and therefore does not lead to a strong plasticization effect.[44,45] At this point and above, the non-freezing water remains constant at 9 moles and freezing water content starts to rise from approximately 5 moles in HQ 20 to 19 moles of water in HQ 30.

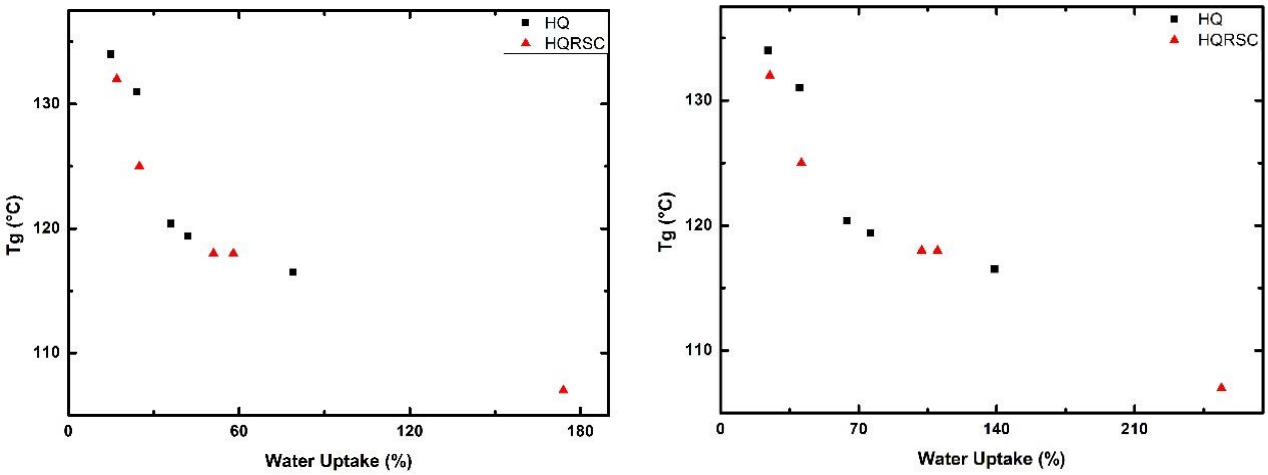

Figure 5.5. T_g vs room and high temperature water uptake for HQ and HQRSC copolymers.

5.3.4 Mechanical Properties

As shown in Figure 5.3, all of these hydrated copolymers are in the glassy state at both ambient temperature and 80°C, but the copolymers with IEC's greater than 1.1 mequiv/g are fairly close to T_g at 80°C. The moduli displayed in Figure 5 are typical for glassy polymers (~10^9 Pa) at ambient temperature for those of most interest with IEC's of 0.9 and 1.1 mequiv/g, even in their fully hydrated state. Consistent with the decrease in T_g as IEC is increased to ~1.2 and higher, with the concomitant large increase in water uptake, the hydrated moduli drop drastically. Figure 6 shows the large drops in moduli at low water uptake (and low IECs), with a leveling out of moduli at high water uptakes. This also correlates well with the suggestion that there is a change in hydrated morphology at approximately 40-60% water uptake. While such a change in morphology has been suggested earlier, we believe this is the first time that the hydrated mechanical properties have been correlated with such changes. For copolymers with high water uptakes, we expect to have high free water content and a percolating network morphology,[44] and this is accompanied by a decrease in mechanical properties.

Even for the high IEC disulfonated polysulfone copolymers, both the strengths at yield and the elastic moduli are notably higher than for Nafion under similar hydration conditions. For lower IEC disulfonated random copolymers at room temperature and in the hydrated condition, the strength at yield is between 20 and 30 MPa and the modulus is between 800 and 1200 MPa. This result indicates that these copolymers are significantly more mechanically robust in the hydrated state than the current state of the art material, Nafion, due to the robustness of the aromatic backbone.

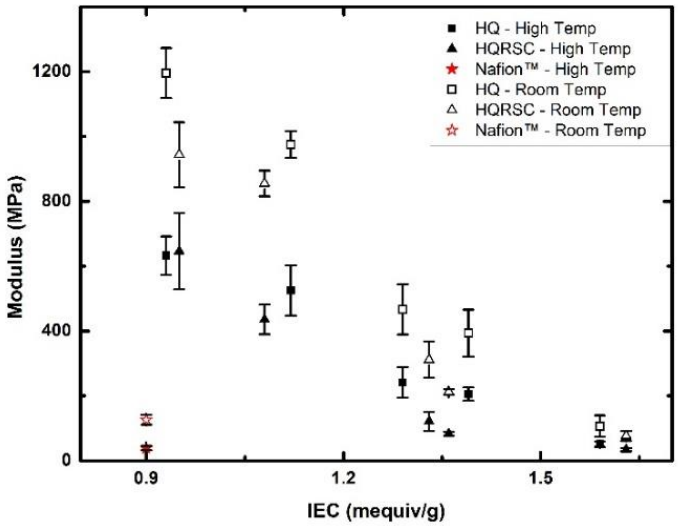

Figure 5.6. Young's moduli vs. IEC for polymer films in the fully hydrated state at room and high temperatures.

The aromatic copolymer membranes with fully *para*-substituted comonomers (HQ series) have consistently higher moduli at a given IEC than partially *meta*-substituted copolymers (HQRSC series), even in the fully hydrated state (Figure 5.5). The trend in the modulus vs. water uptake plot shown in Figure 6 is remarkably similar to the T_g data presented in Figure 5.4. It similarly shows two distinct regimes, with the transition between regimes occurring near 50% water uptake. The consistency of the trend in mechanical properties and thermal properties supports the occurrence of a

morphological transition in these random copolymer systems as the degree of disulfonation is increased.

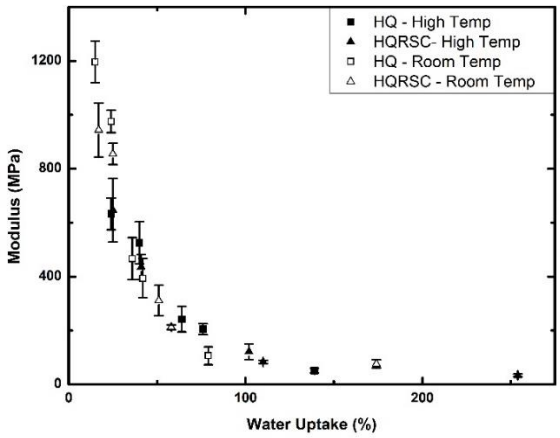

Figure 5.7. Transition between morphological regimes shown by Young's moduli vs. water uptake for hydrated membranes.

5.3.5 Proton Conductivity

In this study, the proton conductivities of the copolymer membranes and Nafion were measured in liquid water at four temperatures: 30, 60, 90, and 100°C. In each hydrocarbon-based copolymer series, two polymers with IEC=0.9 and 1.1 meq/g were emphasized due to their reasonable water uptakes and superior mechanical properties. Copolymers with the lower IECs (HQ 16 and HQRSC 17) have similar IECs to Nafion. Copolymers with IEC=1.1 meq/g (HQ 20 and HQRSC 19) showed comparable water uptakes at elevated temperatures to that of Nafion (40-42%). Table 5-2 shows the copolymers of interest and their relative proton conductivity at four temperatures.

Table 5-2. Relative proton conductivity of the selected copolymers compared with Nafion in liquid water

Temperature (°C)	Conductivity				
	HQ 16 (S/cm)	HQRSC 17 (S/cm)	HQ 20 (S/cm)	HQRSC 19 (S/cm)	Nafion (S/cm)
30	0.03	0.06	0.06	0.08	0.08
60	0.06	0.08	0.09	0.12	0.13
90	0.07	0.11	0.12	0.16	0.21
100	0.08	0.12	0.13	0.18	0.23

Increasing temperature from 30 to 100°C results in improved proton conductivity in all of these membranes including Nafion.[46] This can be attributed to increased water uptake at higher temperatures.[47] Comparison of proton conductivities in two hydrocarbon-based copolymers at a given IEC revealed that copolymers containing the RSC comonomer have slightly higher proton conductivity than those of the solely HQ containing copolymers. The difference in proton conductivity becomes more pronounced when temperature is increased from 30 to 100°C. This remarkable difference is correlated with increased chain flexibility in the RSC containing copolymers that have lower T_gs in liquid water. In addition, it is hypothesized that the RSC comonomers decrease the rigidity relative to the HQ-based copolymers and allow for more mobility in the presence of water.

When IEC is increased in a series of copolymers, proton conductivity increases as expected.[47] Increasing the number of sulfonic acid groups on the backbone brings more water molecules into the membrane and improves proton transfer. Similar results are obtained when the *m*-substituted phenolic comonomer is incorporated into

the polymer backbone. This may allow for increased chain movement and water uptake by increasing the volume and chain spacing. The higher proton conductivity of Nafion at any given temperature may be due to its lower pK_a than hydrocarbon-based copolymers.[48]

5.3.6 H_2 Gas Permeability in Saturated Water Conditions

Decreasing gas permeability (i.e., crossover) in PEMs is an important factor for increasing efficiency of an electrolysis cell and safety.[49] Like proton conductivity and mechanical properties, H_2 gas permeability is highly dependent on water content in the PEM which acts as a plasticizer in the membrane by reducing the T_g.[50] Figure 5.7 shows H_2 gas permeability through these PEMs in saturated water at various temperatures.

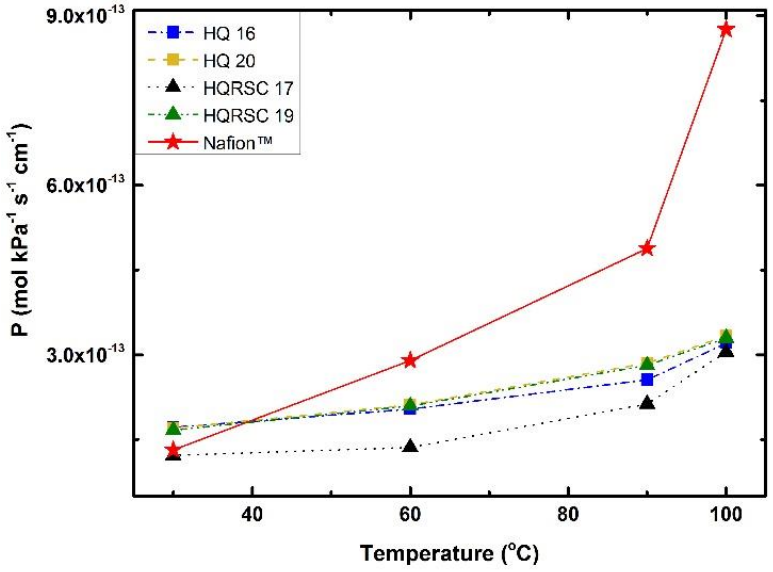

Figure 5.8. H_2 gas permeability, P, through selected membranes in saturated water vapor at various temperatures

Comparison of gas permeability in hydrocarbon-based copolymers and Nafion shows two main regions and trends. At low temperature below 40°C, H_2 gas

permeability of the Nafion membrane is slightly lower than that of the poly(arylene ether) copolymers, while with increasing temperature, the opposite is observed. Increasing temperature results in undesirable increased gas permeability in the Nafion membrane, such that above 60°C a sharp increment is observed. However, gas permeability in the disulfonated copolymers only increases slowly and steadily. This behavior in PEMs is related to their T_gs. As shown in the bottom of Figure 5.3, the T_gs of all of these copolymers where the gas permeabilities were measured are above the measurement temperatures, so they are all in the glassy state. Nafion has a significantly lower T_g relative to those of the aromatic copolymers.[45, 51, 52] When Nafion is plasticized by water, its T_g decreases further to lower temperatures.[47] The drastic increase in gas permeability in the water at 60°C and above is due to the low polymer T_g.

Unlike Nafion that has a low T_g, these disulfonated copolymers with higher wet T_gs show low gas permeabilities due to their aromatic rings and increased chain rigidity. Investigation of the effect of symmetric and asymmetric aromatic comonomers on gas permeability of glassy copolymers confirms that *meta*-substituted comonomers act as a good gas barrier in the copolymer, even in the hydrated state.[40] As expected, Figure 5.5 shows that incorporation of the *meta*-substituted RSC comonomer into these HQ-based copolymers resulted in lower gas permeabilities in this temperature range.

5.3.7 Performance

The ratio of proton conductivity (σ) and gas permeability (P), defined as $\frac{\sigma}{P}$ gives better insight regarding the performance of a membrane in the water electrolysis cell.

Performance of each selected copolymer, normalized to that of Nafion, (equation 5.4) over the range of 30-100°C are shown in Figure 5.8.

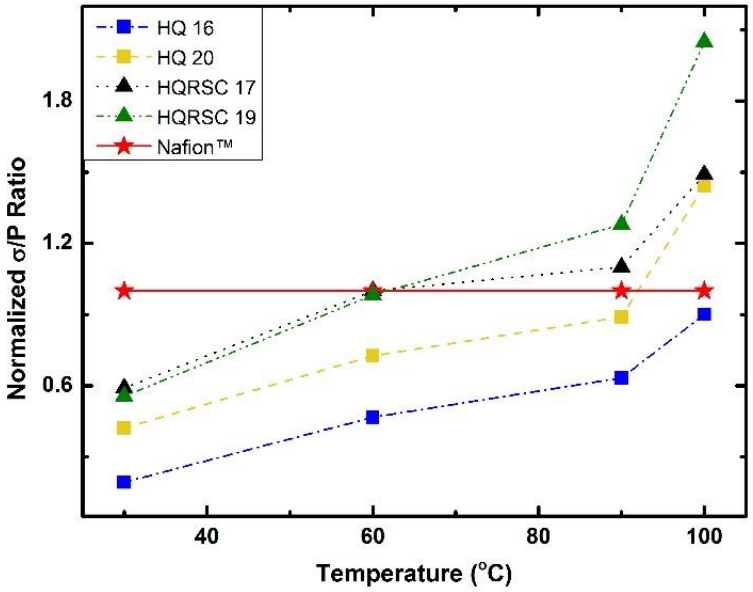

Figure 5.9. Performance of the selected copolymers at various temperatures

At low temperature where the proton conductivity of Nafion is higher than for the disulfonated copolymers and gas permeability is comparable, Nafion shows better performance. However, at the mid-temperature of 60°C, due to increased conductivity for the disulfonated copolymers, and slow gas permeabilities, their performance is comparable to that of the Nafion. The σ/P parameter at high temperature such as at 100°C, where Nafion shows the highest conductivity, shows an opposite trend. Under these conditions, the disulfonated copolymers show significantly better results. This is due to improved conductivity at the higher temperature, but with controlled gas permeability in the disulfonated copolymers while Nafion shows much higher undesirable gas permeability.

5.4 Conclusions

Two series of hydrocarbon copolymers, based on completely *para*-substituted and partially *meta*-substituted compositions, were synthesized for high temperature water electrolyzers. Addition of resorcinol, the *meta*-substituted comonomer, to the *para*-substituted copolymer structure results in decreased chain stiffness (decreased hydrated moduli with *meta*-substitution) and increased water absorption. These factors are reflected in the increased proton conductivities of the *meta*-substituted copolymers in the hydrated state.

Despite the slightly lower proton conductivities of the selected hydrocarbon-based copolymers in comparison to Nafion, they showed remarkably lower H_2 gas permeabilities, particularly at elevated temperatures. This is attributed to their much higher T_gs in their hydrated form relative to the perfluorinated polymer. In fact, Nafion has such a high gas permeability that having exceptional proton conductivity at elevated temperature was not sufficient to elicit reasonable performance. In addition to gas permeability, mechanical properties of this ionomer near 100°C are unsatisfactory for long term performance as a high temperature electrolysis membrane. In contrast, the aromatic HQ 17 and HQRSC 19 copolymers showed good proton conductivity, excellent mechanical properties, and good σ/P performance ratios at elevated temperatures in their hydrated state.

5.5 References

1. A. Ursua, L. M. Gandia and P. Sanchis, *Proceedings of the IEEE*, 2012, **100**, 410-426.
2. P. Lv, J. Chang, T. Wang, Y. Fu and Y. Chen, *Energy & Fuels*, 2004, **18**, 228-233.
3. U. Amjad, A. Vita, C. Galletti, L. Pino and S. Specchia, *Industrial & Engineering Chemistry Research*, 2013, **52**, 15428–15436.
4. Zeng Kai and Z. Dongke, *Progress in Energy and Combustion Science*, 2010, **36**, 307-326.

5. J. A. Turner, *Science*, 1999, **285**, 687.
6. M. Carmo, D. L. Fritz, J. Mergel and D. Stolten, *International Journal of Hydrogen Energy*, 2013, **38**, 4901-4934.
7. S. Siracusano, V. Baglio, A. Stassi, L. Merlo, E. Moukheiber and A. S. Arico', *Journal of Membrane Science 466 (2014) 1–7*, 2014, **466**, 1–7
8. P. Millet, D. Dragoe, S. Grigoriev, V. Fateev and C. Etievant, *International Journal of Hydrogen Energy*, 2009, **34**, 4974-4982.
9. C. A. Linkous, H. R. Anderson, R. W. Kopitzke and G. L. Nelson, *International Journal of Hydrogen Energy*, 1998, **23**.
10. M. A. Navarra, F. Croce and B. Scrosati, *Journal of Materials Chemistry*, 2007, **17**, 3210–3215.
11. M. Schalenbach, M. Carmo, D. L. Fritz, J. Mergel and D. Stolten, *International Journal of Hydrogen Energy*, 2013, **38**, 14921-14933.
12. M. Schalenbach, T. Hoefner, P. Paciok, M. Carmo, W. Lueke and D. Stolten, *J. Phys. Chem. C*, 2015, **119**, 25145−25155.
13. K. Miyatake, H. Zhou, T. Matsuo, H. Uchida and M. Watanabe, *Macromolecules*, 2004, **37**, 4961-4966.
14. P. Sarkar, A. K. Mohanty, P. Bandyopadhyay, S. Chattopadhyay and S. Banerjee, *RSC advance*, 2014, **4**, 11848.
15. Y. Gao, G. P. Robertson, M. D. Guiver, S. D. Mikhailenko, X. Li and S. Kaliaguine, *Macromolecules*, 2004, **37**, 6748-6754.
16. Q. Li, Y. Chen, J. R. Rowlett, J. E. McGrath, N. H. Mack and Y. S. Kim, *ACS Appl. Mater. Interfaces*, 2014, **6**, 5779−5788.
17. A. S. Badami, O. Lane, H. S. Lee, A. Roy and J. E. McGrath, *Journal of Membrane Science*, 2009, **333**, 333.
18. T. Higashihara, K. Matsumoto and M. Ueda, *Polymer*, 2009, **50**, 5341–5357.
19. C. H. Lee, S. Y. Lee, Y. M. Lee, S. Y. Lee, J. W. Rhim, O. Lane and J. E. McGrath, *ACS Appl. Mater. Interfaces*, 2009, **1**, 1113–1121
20. S. Yuan, X. Guo, D. Aili, C. Pan, Q. Li and J. Fang, *journal of Membrane Science*, 2014, **454**, 351-358.
21. N. W. Li and M. D. Guiver, *Macromolecules*, 2014, **47**, 2175-2198.
22. M. Danilczuk, S. Schlick and F. D. Coms, *Macromolecules*, 2013, **46**, 6110-6117.
23. D. W. Smith, F.O. Oladoyinbo, W. A. Mortimore, H. M. Colquhoun, M. S. Thomassen, A. Ødegård, N. Guillet, E. Mayousse, T. Klicpera and W. Hayes, *Macromolecules*, 2013, **46**, 1504-1511.
24. A. Albert, B. O. Alejandro, M. S. Thomassen, T. J. Schmidt and L. Gubler, *ACS Appl. Mater. Interfaces*, 2015, **7**, 22203−22212.
25. H. Zhang and P. K. Shen, *Chemical Society Reviews*, 2012, **41**, 2382–2394.

26. N. Takimoto, S. Takamuku, M. Abe, A. Ohira, H. S. Lee and J. E. McGrath, *Journal of Power Sources*, 2009, **194**, 662-667.
27. Maria Gil, Xiangling Ji, Xianfeng Li, Hui Nab, J. Eric Hampsey and Y. Lu, *Journal of Membrane Science*, 2004, **234**, 75–81.
28. Feng Wang, Michael Hickner, Yu Seung Kima, Thomas A. Zawodzinski and J. E. McGrath, *journal of Membrane Science*, 2002, **197**, 231–242.
29. K. Krajinovic, T. Kaz, T. Haering, V. Gogel and J. Kerres, *FUEL CELLS*, 2011, **11**, 787–800.
30. J. Kerres, A. Ullrich and M. Hein, *Journal of Polymer Science Part A: Polymer Chemistry*, 2001, **39**, 2874-2888.
31. H. Ghassemi, J. E. McGrath and T. A. Zawodzinski, *Polymer*, 2006, **47**, 4132-4139.
32. K. Krajinovic, T. Kaz, T. Haering, V. Gogel and J. Kerres, *Fuel Cells*, 2011, **11**, 787-800.
33. H. S. Lee, A. Roy, O. Lane, M. Lee and J. E. McGrath, *J Polym Sci Pol Chem*, 2010, **48**, 214-222.
34. F. Wang, M. Hickner, Q. Ji, W. Harrison, J. Mecham, T. A. Zawodzinski and J. E. McGrath, *Macromolecular Symposia*, 2001, **175**, 387-396.
35. H. J. Oh, B. D. Freeman, J. E. McGrath, C. J. Ellison, S. Mecham, K. S. Lee and D. R. Paul, *Polymer*, 2014, **55**, 1574-1582.
36. J. Roovers, P. M. Toporowski and R. Ethier, *High Performance Polymers*, 1990, **2**, 165-179.
37. N. Hu, R. Chen and A. Hsu, *Polym. Int.*, 2006, **55**, 872-882.
38. J. Choi, K. M. Lee, R. Wycisk, P. N. Pintauro and P. T. Mather, *Macromolecules*, 2008, **41**, 4569-4572.
39. B. R. Einsla, Y. S. Kim, M. A. Hickner, Y. T. Hong, M. L. Hill, B. S. Pivovar and J. E. McGrath, *J Membrane Sci*, 2005, **255**, 141-148.
40. C. L. Aitken, W. J. Koros and D. R. Paul, *Macromolecules*, 1992, **25**, 3424-3434.
41. W. Xie, H. Ju, G. M. Geise, B. D. Freeman, J. I. Mardel, A. J. Hill and J. E. McGrath, *Macromolecules*, 2011, **44**, 4428-4438.
42. E. H. Immergut and H. F. Mark, in *Plasticization and Plasticizer Processes*, American Chemical Society, 1965, vol. 48, ch. 1, pp. 1-26.
43. Kim Y. S., F. Wang, M. A. Hickner, S. McCartney, Y. T. Hong, W. Harrison, T. A. Zawodzinski and J. E. McGrath, *J. Polym. Sci., Part B: Polym. Phys.*, 2003, **41**, 2816–2828.
44. A. Roy, M. A. Hickner, H.-S. Lee, T. Glass, M. Paul, A. Badami, J. S. Riffle and J. E. McGrath, *Polymer*, 2017, **111**, 297-306.
45. Y. S. Kim, L. M. Dong, M. A. Hickner, T. E. Glass, V. Webb and J. E. McGrath, *Macromolecules*, 2003, **36**, 6281-6285.
46. M. Saito, K. Hayamizu and T. Okada, *J. Phys. Chem. B*, 2005, **109**, 3112-3119.
47. W. L. Harrison, M. A. Hickner, Y. S. Kim and J. E. McGrath, *Fuel Cells*, 2005, **5**, 201-212.

48. F. Wang, M. Hickner, Y. S. Kim, T. A. Zawodzinski and J. E. McGrath, *J Membrane Sci*, 2002, **197**, 231-242.
49. H. F. Mohamed, Y. Kobayashi, C. S. Kuroda and A. Ohira, *J. Phys. Chem. B*, 2009, **113**, 2247-2252.
50. T. Sakai, H. Takenaka, N. Wakabayashi, Y. Kawami and E. Torikai, *J Electrochem Soc*, 1985, **132**, 1328-1332.
51. S. J. Osborn, M. K. Hassan, G. M. Divoux, D. W. Rhoades, K. A. Mauritz and R. B. Moore, *Macromolecules*, 2007, **40**, 3886-3890.
52. H. Y. Jung and J. W. Kim, *Int J Hydrogen Energ*, 2012, **37**, 12580-12585.

Chapter 6: Recommended Future Work

6.1 Future Work Towards Melt-spinnable Polyacrylonitrile Copolymer Precursors for Carbon Fibers

The most obvious future recommendation would be to investigate the melt-extrusion of the PAN-MA/modifier mixtures that performed well in the rheological studies detailed in this chapter, and to optimize the precursor fiber properties that could be derived from a melt process. If the extrusion is successful, the resulting precursor fibers should be characterized by scanning electron microscopy, mechanical analysis, and carbon fiber conversion. A full characterization of the resulting carbon fibers should be performed, with a particular emphasis on the mechanical analysis.

It would be interesting to determine interrelationships among the mechanical properties of the carbon fibers relative to those of the melt-extruded PAN-MA precursor fibers, and to compare these properties to commercial carbon fibers. It would also be interesting to determine the effect of each particular PAN-MA modifier composition on the potential precursor fiber properties, and to relate that to the resulting carbon fiber mechanical properties. The author suspects that precursor fibers produced using a composition containing adiponitrile could have improved mechanical properties relative to precursor fibers produced from solution spinning. Adiponitrile acts as physical crosslinking agent between neighboring PAN-MA chains which should result in increased orientation of the chains therefore increasing the modulus of the system. These improved mechanical properties should carry over to the resulting carbon fibers.

Another possible future study may include the exploration of additional melting point modifying agents and combinations of modifiers. One example would be the application of tertiary modifier compositions to decrease the amount of water that is needed. Preliminary exploration into this possibility has shown promising results for PAN-MA/ACN/DMF/H_2O 75:5:5:15 wt:wt:wt:wt as shown in Figure 6.1. The analysis indicated that the tertiary mixture had two T_gs and a T_m near 142°C.

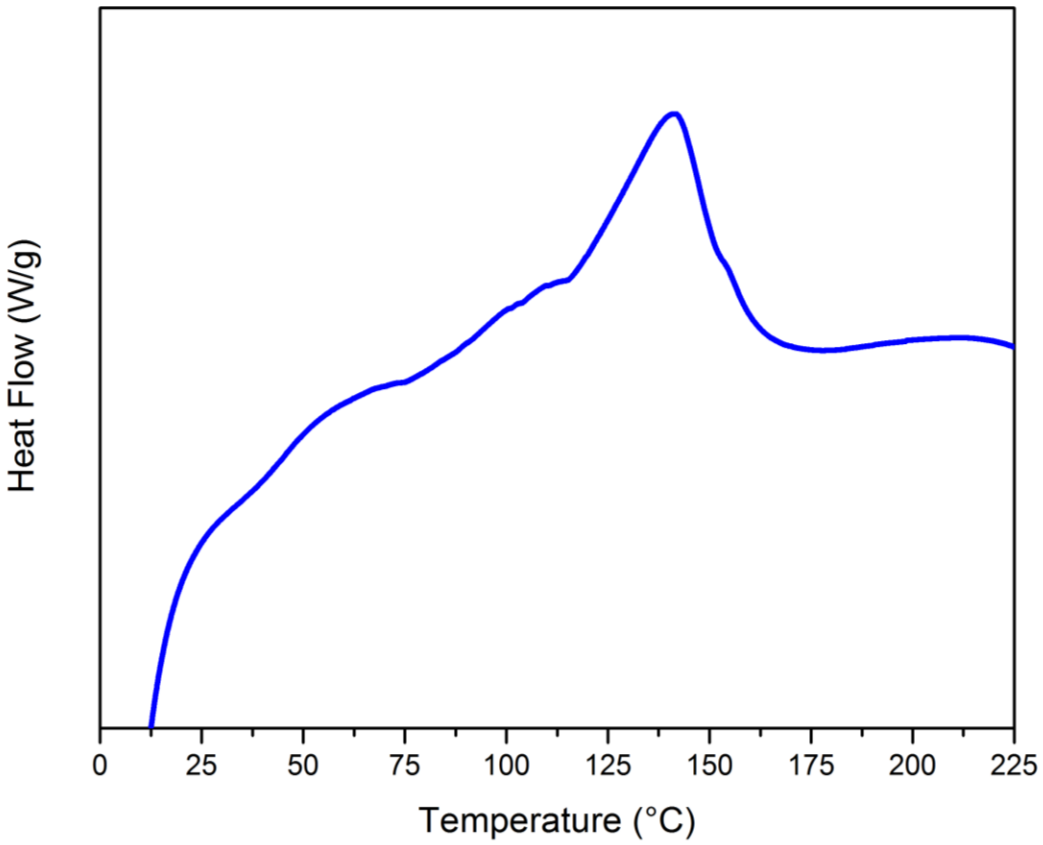

Figure 6.1. DSC Thermogram for PAN-MA/ACN/DMF/H_2O 75:5:5:15 wt:wt:wt:wt.

Recently the author has made an interesting discovery. PAN-MA was dissolved in ADPN at ~100°C to make a 5 wt% solution. Upon cooling, the solution produced a very firm gel, which is reversible upon re-heating. The results are shown in Figure 6.2.

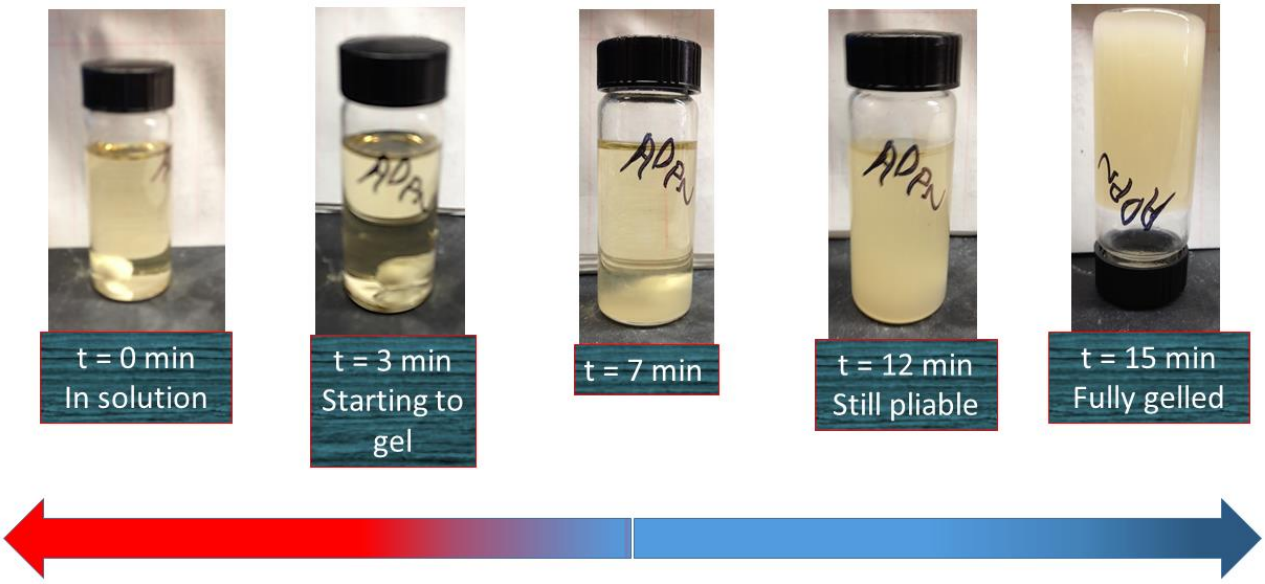

Figure 6.2. Sol-gel formation from 5 wt% solution of PAN-MA dissolved in adiponitrile at ~100°C.

The phenomenon of PAN-based sol-gels is not a novel discovery, but prior work in the area required precursor mixtures to be of a much higher concentration to produce fairly firm gels (≥ 20 wt %).[1] The author believes the physical crosslinking between the nitriles along the PAN-MA chain and adiponitrile allows gelation at much lower concentrations. Extensive research into the rheological characteristics of PAN-based sol-gels produced from various solvents has been performed,[1-4] but this research has not been applied to solutions produced from difunctional modifiers such as adiponitrile. Potential applications for PAN-based sol-gels include precursors to electrospun nanofiber mats[5] and ion conducting polymeric gels for batteries.[6]

6.2 References

1. M. Bercea, S. Morariu and C. E. Brunchi, *International Journal of Thermophysics*, 2009, **30**, 1411-1422.

2. L. Tan, H. Chen, D. Pan and N. Pan, *European Polymer Journal*, 2009, **45**, 1617-1624.

3. L. Tan, D. Pan and N. Pan, *Journal of Polymer Research*, 2009, **16**, 341-350.
4. Y. Eom and B. C. Kim, *European Polymer Journal*, 2016, **85**, 341-353.
5. D. K. Sharma, J. Shen and F. Li, *RSC Advances*, 2014, **4**, 39110-39117.
6. N. Krishna Jyothi, K. Vijaya Kumar, G. Sunita Sundari and P. Narayana Murthy, *Indian Journal of Physics*, 2016, **90**, 289-296.